Anteroposterior polarity and elongation in the absence of extraembryonic tissues and spatially localised signalling in *Gastruloids*, mammalian embryonic organoids

Turner D.A.[1], Girgin, M.[2], Alonso-Crisostomo L.[1], Trivedi V.[1], Baillie-Johnson, P.[1], Glodowski C.R.[1], Hayward P.C[1], Collignon J.[3], Gustavsen, C.[4], Serup P.[4], Steventon B.[1], Lutolf, M.[2] and Martinez Arias A.[1]*

[1]Department of Genetics, University of Cambridge, Downing Street, Cambridge CB23EH

[2]Laboratory of Stem Cell Bioengineering, Institute of Bioengineering, Ecole Polytechnique Fédérale de Lausanne, 1015 Lausanne, Switzerland

[3]Université Paris-Diderot, CNRS, Institut Jacques Monod, UMR 7592, Development and Neurobiology Programme, F-75013 Paris, France

[4]Danish Stem Cell Center, University of Copenhagen, DK-2200 Copenhagen, Denmark

*To whom correspondence is to be addressed: ama11@cam.ac.uk

Key Words:

Gastruloids, axial organisation, organoids, symmetry-breaking

Summary Statement:

We investigate the signalling requirements for early *Gastruloid* patterning, and demonstrate the development of the embryonic axes in *Gastruloids* in the absence of extraembryonic tissues.

Abstract:

The establishment of the anteroposterior (AP) axis is a critical step during animal embryo development. In mammals, genetic studies have shown that this process relies on signals spatiotemporally deployed in the extraembryonic tissues that locate the position of the head and the onset of gastrulation, marked by *T/Brachyury* (*T/Bra*) at the posterior of the embryo. Here, we use *Gastruloids*, mESC-based organoids, as a model system to study this process. We find that *Gastruloids* localise *T/Bra* expression to one end and undergo elongation similar to the posterior region of the embryo suggesting that they develop an AP axis. This process relies on precisely timed interactions between Wnt/β-Catenin and Nodal signalling, whereas BMP signalling is dispensable. Additionally, polarised *T/Bra* expression occurs in the absence of extraembryonic tissues or localised sources of signals. We suggest that the role of extraembryonic tissues in the mammalian embryo might not be to induce the axes but to bias an intrinsic ability of the embryo to initially break symmetry. Furthermore, we suggest that Wnt signalling has a separable activity involved in the elongation of the axis.

Introduction:

The establishment of the anteroposterior (AP) and dorsoventral (DV) axes during the early stages of animal development is a fundamental patterning event that guides the spatial organisation of tissues and organs. Although this process differs from one organism to another, in all cases it involves a break in an initial molecular or cellular symmetry resulting in the precise positioning of signalling centres that will drive subsequent patterning events (Meinhardt, 2006). Dipteran and avian embryos provide extreme examples of the strategies associated with these processes. For example, in *Drosophila*, the symmetry is broken before fertilisation within a single cell, the oocyte, which acquires information for both the AP and DV axes. This occurs through interactions with surrounding support cells that control processes of RNA and protein localisation which then serve as references for the rapid patterning of the embryo as the zygote turns into a multicellular system (Riechmann and Ephrussi, 2001; Roth and Lynch, 2009). On the other hand, in chickens the processes take place in the developing embryo, within a homogeneous multicellular system that lacks external references (Bertocchini and Stern, 2002; Stern, 2006). In mammalian embryos the axes are also established within a homogeneous cellular system, the epiblast, but in this case they are under the influence of an initial symmetry breaking event that takes place within the

extraembryonic tissues which is then transferred to the developing embryo (Rivera-Pérez and Hadjantonakis, 2015; Rossant and Tam, 2009; Stern, 2006; Takaoka and Hamada, 2012).

Efforts to understand the molecular mechanisms that pattern early embryos have relied on genetic approaches such as perturbation through genetic mutations and a correlation between specific processes and molecular events as highlighted by the activity of particular genes (Anderson, 2000; St Johnston, 2002). Although successful, these approaches have limitations as they often conflate correlation and causation and, importantly, cannot probe the role of mechanical forces that have been shown to play a role in the early events (Hamada, 2015; Hiramatsu et al., 2013). This suggests a need for a complementary experimental system in which, for example, rather than removing components we attempt to build tissues and organs from cells and learn what the minimal conditions are that allow this (Sasai et al., 2012). We have recently established a non-adherent culture system for mouse Embryonic Stem Cells (ESCs) in which small aggregates of defined numbers of cells undergo symmetry breaking, polarisation of gene expression and axial development in a reproducible manner that mirrors events in embryos (Turner et al., 2016b; Turner et al., 2014a; van den Brink et al., 2014). We call these polarised aggregates *Gastruloids* and believe that they provide a versatile and useful system to analyse the mechanisms that mediate cell fate assignments and pattern formation in mammalian embryos (Simunovic and Brivanlou, 2017).

Here, we show that *Gastruloids* become polarised along two axes that resemble the AP and DV axes of the mouse embryo in the absence of extraembryonic tissues. We focus on the AP polarity and find that, unlike the embryo, in *Gastruloids* this process does not require BMP signalling but relies on interactions between Nodal and Wnt signalling that are recorded in the expression of the transcription factor T/Brachyury (T/Bra) at one end of the *Gastruloid*. Furthermore we show that localisation of Nodal, which is widely held as essential for the establishment of the AP axis, is not required for the polarisation of T/Bra expression. Our results contrast with a recent report that the trophoectoderm is required for the expression and localisation of T/Bra in aggregates of ESCs (Harrison et al., 2017) and suggest that a spontaneous symmetry breaking event may occur in the embryo where the function of the extraembryonic tissues might to bias, rather than to induce, this event to ensure its reproducible location at the initial site of gastrulation.

Results:

Gastruloids exhibit anteroposterior and dorsoventral organisation in the elongating domain

Our previous studies using *Gastruloids* revealed a longitudinal polarisation with the expression of T/Bra located towards one end that will lead an elongation process (Baillie-Johnson et al., 2015; Turner et al., 2014a; van den Brink et al., 2014). This generates an axis reminiscent of the AP axis of early mammalian embryos. To follow these observations and determine whether other markers of the embryonic axis are present in the emerging structures we cultured *Gastruloids* for 120h and mapped the expression domain of reporters for three major signalling pathways involved in axial organisation in the embryo: Wnt/β-catenin , Nodal and BMP as well as for Cdx2, which identifies the posterior of the embryo (**Fig. 1** and **fig. S1** and Materials and Methods). At 120h After Aggregation (AA), *Gastruloids* which have been exposed to the Wnt signalling agonist CHI99201 (Chi) between 48 and 72h AA, are polarised, with localised expression of T/Bra (**Fig. 1A,C, fig. S1A,C**) and Cdx2 (**Fig. 1A**, **fig. S1B**) at one end of the protruding tip. They also exhibit a shallow gradient of Wnt signalling away from the T/Bra expressing region (**Fig. 1C**, **fig. S1E**) but no detectible BMP signalling activity (**Fig. 1D**; **fig. S1C**). This arrangement suggests that the elongating domain of the *Gastruloid* is similar to the tail bud of an embryo (Beddington et al., 1992; Herrmann, 1991; Wilkinson et al., 1990) supporting our previous observations that *Gastruloids* have AP axial organisation.

The extension of the *Gastruloids* is characterised by the expression of neural progenitor markers (Turner et al., 2014a; van den Brink et al., 2014). When we correlate the expression of T/Bra, Cdx2, Sox2 and a Sox1::GFP reporter (Ying et al., 2003) (**Fig. 1A,B, fig. S1A**), we observe an organisation perpendicular to the AP one in which high levels of expression of the neural markers Sox1, Sox2 and Cdx2 extend away from the T/Bra-expressing tip on one side of the *Gastruloid* and a weak Cdx2 expression domain directly opposite and just anterior to the T/Bra expressing cells (**Fig. 1A,B**; **fig. S1A**). This organisation of gene expression is reminiscent of the DV organisation of the embryonic Caudal Lateral Epiblast (CLE) at around E8.5 (see fig. 4 in (Kanai-Azuma et al., 2002) and various figures in (Zhao et al., 2014)). Furthermore, at this stage in the embryo some ventral endodermal cells express Sox17 (see figure 1 in (Choi et al., 2012) and fig. 2 in (Saund et al., 2012)) and we observe such domain here (**Fig. 1B**, **fig. S3**).

Taken together, these results suggest that by 120h AA, Chiron treated *Gastruloids* have an organisation reminiscent of that of the postoccipital region of the embryo. The lack of Sox1 expression in the anterior to the domain suggests that *Gastruloids* lack brain and head structures

(van den Brink et al., 2014); in this sense, they are very similar to gain-of-function β-Catenin mutants (Fossat et al., 2012; Fossat et al., 2011; Tam and Loebel, 2007), consistent with their being exposed to high levels of Wnt signalling during their early development.

Wnt/β-catenin signalling provides robustness to the polarisation of T/Bra expression

To understand the emergence of the AP polarisation in *Gastruloids*, we monitored the temporal expression of a T/Bra::GFP reporter line (Fehling et al., 2003) from their aggregation, as well as the patterns of Wnt, Nodal expression (using the Nodal::YFP reporter mentioned above) and activity (using an AR8::mCherry line to report on nodal signalling transduction (Serup et al., 2012)), and BMP signalling (IBRE::Cerulean (Serup et al., 2012)). We also assessed the transition from pluripotency towards differentiation using the *miR-290-mCherry/mir-302-eGFP* (DRC; **Fig. 2A,A'**) which marks distinct stages of pluripotency based on the expression of reporters for *mir-290* (E3.5-6.75) and *mir-302* (E4.75-E8.0) (Parchem et al., 2014), and a reporter for Nanog expression (TNGA; **Fig. 2B** (Chambers et al., 2007).

Analysis of *Gastruloids* grown in N2B27 24h AA revealed that, at this time, they are mostly positive for *mir-290* (**Fig. 2A,A'**, red) with a small proportion of cells within the *Gastruloid* expressing *mir-302* (**Fig. 2A,A'**, Green) (Parchem et al., 2014), express Nanog heterogeneously at low levels (**Fig. 2B**), and exhibit weak, heterogeneous expression of *T/Bra* with a proportion of *Gastruloids* already displaying signs of bias towards one pole (**Fig. 3A**, **table S1**). By 48h AA the levels of T/Bra::GFP had risen uniformly across the population and exhibited a more prominent polarisation (**Fig. 3A**) and continued culture in N2B27 resulted in variations in both the level of expression and the precision of its polarisation across individual *Gastruloids* and within experiments (**Fig. 3A**; DMSO). At this stage *Gastruloids* exhibit reduced levels of expression of *mir*-290 (**Fig. 2A**, red) and increased *mir*-302 (**Fig. 2A,A'**, green) (Parchem et al., 2014), with Nanog expression completely abolished (**Fig. 2B**). During this period we also observed expression of both the Wnt (TLC2; **Fig 2C**) and Nodal::YFP reporters (**Fig. 2D**) but no detectible BMP activity (**Fig. 2F**), suggesting that the cells are producing ligands for Wnt and Nodal signalling, a contention supported by the observation that inhibitors of these pathways suppress the expression of the reporters (not shown) and gene expression (See **Fig. 4**). Similar to T/Bra::GFP, TLC2 expression is well defined and polarised (**Fig. 2C**). Nodal signalling exhibits weak, non-polarised expression at 24h with a slight bias towards one region of the *Gastruloid* (**Fig. 2E**).

Addition of Chi or Wnt3a to the medium between 48 and 72h resulted in enhanced levels of T/Bra::GFP expression by 72h AA compared to the vehicle controls (**Fig. 3A,B**) which is maintained in all *Gastruloids* at the posterior tip at higher levels than the control (**Fig. 3A**). Similarly, Nodal expression is greatly enhanced following the Chi pulse and is expressed across the whole *Gastruloid* (**Fig. 2D**), although Nodal signalling reporter is not activated as strongly (**Fig. 2E**). This is consistent with the role of Wnt signalling in controlling Nodal expression in the postimplantation epiblast. *Gastruloids* also alter the expression of the miRNA reporters, down-regulating *mir*-290 and greatly up-regulating *mir*-302 (**Fig. 2A,A'**).

To garner an understanding of the heterogeneities in T/Bra::GFP expression over time, we quantified the fluorescence levels of the reporter in a posterior to anterior direction along the spine of the *Gastruloids* (**Fig. 3B,C,D**; **fig. S2A,B**; see Materials and Methods and (Baillie-Johnson et al., 2015)). We notice that the changes in shape and patterns of gene expression are highly reproducible and have used this feature to extract quantitative information about gene expression and morphogenesis at single-time-points or at regular intervals over time. Exposure of *Gastruloids* to Chi during 48 and 72h AA results in a tighter distribution of all the measured variables and a higher level of sustained fluorescence than when they are exposed to DMSO (**Fig. 3B,C,D**; **fig. S2A**; $p < 0.001$ at 72h and $p < 0.01$ at 120h). Stimulation with Wnt3a is able to substitute for Chi and results in similar fluorescence expression profiles over time with a similar rate of acquisition of an elongated morphology (**Fig. 3B,C,D**; **fig. S2B**; $p > 0.05$).

Live imaging of the T/Bra::GFP reporter throughout the process confirms that Chi enhances its intrinsically polarised expression but also reveals a global transient response to the Chi pulse throughout the *Gastruloid* which relaxes to the original position after the pulse (**Fig. 3E; Movies 1,2**). Using a Sox17:GFP line (Niakan et al., 2010) which reveals endodermal progenitors, we observe the initial expression in the anterior pole of the aggregate followed by a complex migration of some of the expressing cells towards the posterior region. At 120h, Sox17::GFP-expressing cells localise anterior to the T/Bra expression domain following the Chi pulse (**fig. S3**). The final patterning of the reporter showed some heterogeneity, examples of which are shown in **fig. S1C**.

Taken together, these results suggest that during the first 48h AA *Gastruloids* undergo an intrinsic symmetry breaking ability that is reflected in an AP axis made robust and stable by Wnt/β-catenin signalling.

Extraembryonic tissues are not required for Axial organisation in *Gastruloids*.

In the embryo, the spatial restriction of T/Bra is concomitant with the establishment of the AP axis and the onset of gastrulation at the posterior end of the embryo (Rivera-Pérez and Hadjantonakis, 2015; Tam and Gad, 2004). Genetic analysis has shown that this pattern arises from interactions between signalling systems asymmetrically deployed in the extraembryonic tissues (Rossant and Tam, 2009).

To determine the mechanism whereby *Gastruloids* are patterned along the AP axis and to compare the process with that taking place in embryos, we first analysed the expression of several genes involved in the AP patterning at 48h AA, when we first observe signs of polarisation in gene expression (**Fig. 4**). At this stage, *Gastruloids* expressed *Fgf4*, *Fgf5*, *Axin2*, *Wnt3*, *Nodal*, and *Cripto*, all of which are expressed in the epiblast in the embryo (**Fig. 4**). We also detect low levels of *Lefty1* (**Fig. 4**), which in the embryo is expressed mainly in the extraembryonic tissues but also in the epiblast as gastrulation begins. On the other hand, we do not detect significant expression of genes associated with extraembryonic tissues e.g. *BMP4*, *Dkk*, *Furin*, *Lrp2* and *Dab*, with very low levels of *Cerberus* (**Fig. 4**). By 72h AA in N2B27 we observed increases in expression of *Nodal*, *Lefty1* and *Fgf5*, decreases in *Fgf4* and the emergence, at low levels, of *Wnt3a* (**Fig. 4**). Some of these patterns are Wnt/β-Catenin signalling dependent as exposure to Chi during 48 to 72h AA leads to a clear increase in *Nodal*, *Lefty1* and *Wnt3a* as well as of the Wnt/β-catenin targets *Axin2*, *Dkk and Cripto* (**Fig. 4**).

These observations support the original contention that *Gastruloids* are made up exclusively of embryonic cells. This conclusion is reinforced by the absence of detectible BMP expression or signalling during the first 48h AA, when the polarisation of T/Bra expression is taking place as previously described (**Fig. 2F**, right). Additionally the lack of *GATA6* expression during the first 72h of culture also supports the embryonic composition of the *Gastruloids* (**fig. S4**), which, before implantation in the early embryo is associated with the Visceral Endoderm and in the *Gastruloids* is first expressed around 96h AA in a domain of cells at the opposite end of the T/Bra expression.

The patterns of gene expression at different times AA, together with the timing of the cell behaviours associated with gastrulation that we have described before (Baillie-Johnson et al., 2015; Turner et al., 2014a; Turner et al., 2016b; van den Brink et al., 2014), provide landmarks to correlate the development of *Gastruloids* with that of embryos. They suggest that 48h AA corresponds to the onset of gastrulation in the E6.0 embryo and 72h AA is an approximation to the E7.0. Precise timing will require more detailed and extensive expression analysis.

Nodal signalling promotes T/Bra expression.

The expression of signalling reporters suggests that by 48h AA, *Gastruloids* are being patterned through an intrinsic mechanism which relies on Nodal and Wnt signalling (**Fig. 3, 4**). To gain insights into this process we exposed *Gastruloids* to agonists and antagonists of both signalling pathways before or at the time of exposure to Chi. Treatment with the Nodal ALK4 receptor inhibitor SB431542 (SB43 (Inman et al., 2002)) between 48-72h AA in the absence of Chi abolished both the expression of T/Bra::GFP and the elongation, with *Gastruloids* remaining essentially spherical (**Fig. 5**, **fig. S5**). Co-treatment with Chi and SB43 (48-72h) severely reduced the levels of fluorescence and greatly impacted the ability of the *Gastruloids* to elongate in a typical manner, with a large degree of variation between experimental replicates (**Fig. 5, fig. S5**; $p < 0.001$ from 72h-120h). These results indicate an absolute requirement for Nodal signalling in the expression of T/Bra. To identify a temporal element to this requirement, we pre-treated *Gastruloids* with SB43 between 24 and 48h before pulsing them with Chi (48-72h). These *Gastruloids* are delayed in expressing T/Bra::GFP and the levels, generally low, exhibit a high degree of variation in the location and expression of *T/Bra* within individuals (**Fig. 5, fig. S6**; $p < 0.01$ for 72-120h); however their ability to elongate is not affected and occasionally enhanced relative to the Chi control (**Fig. 5, fig. S6**). These results confirm a requirement for Nodal in the expression of *T/Bra* and suggest that it is possible to separate the axial elongation from *T/Bra* expression.

Addition of Nodal, alone or together with Chi during 48 and 72h AA results in an increase in T/Bra expression similar to that observed with Chi alone (**Fig. 5, fig. S5,6;** $p > 0.05$ at all time-points except Nodal+Chi at 96h, where $p < 0.05$), however the elongation is severely reduced with respect to Chi alone, with *Gastruloids* tending to remain spheroid or ovoid (**Fig. 5, fig. S5,6**). This suggests a synergy between the two signalling events. To test this further we tried to rescue the effects of Nodal inhibition during 24 and 48hrs on *T/Bra* expression. The maximum average expression of Bra::GFP in *Gastruloids* treated with SB43 between 24-48hAA, followed by Chi and Nodal co-stimulation between 48-72h AA was not to the same extent as Chi and Nodal co-stimulation at 48 and 72h AA. Although the levels of expression at 96h were enhanced compared to Chi and Nodal co-stimulation with less variation (**Fig. 5, fig. S6**; $p < 0.01$), the *Gastruloids* were less polarised and peak expression was shifted anteriorly; the expression was maintained at higher levels at 120h however (**Fig. 5, fig. S6**). Additionally, the increased elongation that was observed with SB43 (24-48h) and Chi (48-72h) treatment is suppressed in this condition, and *Gastruloids*

tended to stay more spherical indicating that increased Nodal signalling at this period negatively impacts the elongation, similar to single Nodal stimulation (48-72h; **Fig. 5, fig. S6**).

These results demonstrate an absolute requirement for Nodal signalling in the expression of *T/Bra* and its requirement for precise modulation of its levels at specific phases for the elongation. Furthermore, they suggest a negative impact of Nodal signalling on axial elongation.

Wnt signalling promotes T/Bra expression and axial elongation in *Gastruloids*.

To test the role of Wnt signalling on the patterning process, *Gastruloids* were treated in different regimes with either recombinant Wnt3a or its antagonist Dkk1, as well as with small molecule inhibitors of Wnt signalling (IWP2 that affects secretion of all Wnt proteins (Chen et al., 2009) and XAV939 that increases β-Catenin degradation through Tankyrase inhibition (Huang et al., 2009); **Fig. 6, fig. S7**). As demonstrated above, Wnt3a is able to substitute for Chi during the 48-72h AA period with no significant difference in the normalised fluorescence traces at any time point (**Figs. 3B,C, 6A,B**; $p > 0.05$). Pre-treatment with Wnt3a prior to a pulse of Chi enhanced the expression of T/Bra::GFP ($p < 0.05$ at 48h and 120h), reduced expression heterogeneity at later time-points (shown in **Fig. S8**, lower panel, by the *normalised root square distance*), and generated an elongated phenotype more rapidly than controls (**Fig. 6, fig. S7**). By contrast, pre-treatment with Dkk1, XAV939 or IWP2 before Chi exposure results in a significantly delayed and variable expression of *T/Bra* (**Fig. 6** and **fig. S7,8**; see significance matrix in **fig. S7,8**); however we observe differences in the response to Dkk1 and IWP2, which target Wnt expression and receptor binding, compared to XAV939, that targets active β-catenin (**Fig. 6,** and **fig. S7,8**). This suggests a requirement for non-canonical Wnt signalling in T/Bra::GFP maintenance as reductions in Wnt expression (IWP2) or receptor interaction (Dkk1) have a more dramatic effect than reductions in β-Catenin activity (XAV939) (**Fig. 6, fig. S7,8**). These results reveal that Wnt signalling is essential and the primary signal required for the elongation of *Gastruloids* but that it cooperates with Nodal in the control of T/Bra expression and polarisation.

A synergy between Nodal and Wnt signalling during axial organisation has been reported in other organisms (Crease et al., 1998; Skromne and Stern, 2001; Steinbeisser et al., 1993) and is supported by our results which, in addition, suggest different roles for each signalling system. While Nodal is essential for the onset of T/Bra expression, Wnt/β-catenin signalling provides amplification and robustness to the response, promotes Nodal expression in a positive feedback for the process and mediates axial elongation..

Wnt/β-catenin can generate multiple axes in a Nodal dependent manner.

To further delimit the requirements for Wnt/β-Catenin signalling, we exposed aggregates for 24h at different periods between 24 and 72h AA and analysed elongation and T/Bra expression (**Fig. 7, fig. S9**; DAT and AMA: manuscript in preparation). The experiments reveal that the 48-72h period is critical for both the elongation and correct patterning of the Gastruloids. While in all cases there is localised T/Bra::GFP expression and tissue elongation, exposure during the 48-72h period elicits this behaviour most effectively (**Fig. 7A,B, fig. S9**). In the course of these experiments we observed that long exposures to Wnt signalling between 24-72h AA, led to *Gastruloids* with more than one focus of elongation and T/Bra::GFP expression which was significantly different from the 48-72h control (**Fig. 7A,B, fig. S9**, $p < 0.05$). In contrast, exposure between 48 and 96h AA tends to abolish the focussed polarisation of T/Bra::GFP expression and the *Gastruloids* are wider, resulting in a less slender elongation phenotype; the fluorescence traces along the spine of the *Gastruloids*, however are similar to the control 48-72h Chi pulse (**Fig. 7A,B, fig. S9**; $p > 0.05$).

These results reveal two overlapping events in the patterning of the *Gastruloids* centred around the 48h AA time that we have mapped to approximately E6.0 in the embryo. Between 24 and 48h AA there is autonomous axial organisation from within the *Gastruloid* which is stabilised through Wnt/β-Catenin signalling but critically dependent on Nodal signalling. Following this period (after 48h), it is essential that Nodal signalling is tightly regulated as it negatively impacts the elongation potential of the *Gastruloid* and long exposures abolish elongation without altering the expression localisation of T/Bra::GFP. This highlights the period between 24 and 48h as critical for axial establishment, which is then consolidated in the period after 48h AA.

BMP promotes T/Bra expression but not axial elongation

In the embryo the expression of Nodal and Wnt3 is thought to be modulated by BMP signalling (Rossant and Tam, 2009; Stern, 2006; Takaoka and Hamada, 2012) and it has been suggested that this is also the case in vitro (Harrison et al., 2017). As described above, a reporter for BMP signalling does not exhibit any detectible expression in the early stages of patterning (**Fig. 2E, Fig. 8A,B, fig. S10**). Consistent with this, exposure of the *Gastruloids* to DorsomorphinH1 (DMH1 (Neely et al., 2012)), a small molecule inhibitor of BMP signalling, prior to the Chi pulse did not significantly alter expression pattern of Bra::GFP or the morphology (length and roundness) of the

Gastruloids up to 96h AA (**Fig. 8A,B, fig. S10**; $p > 0.05$). Addition of BMP between 24-48h AA followed by a Chi pulse resulted in a more focused expression of T/Bra::GFP at 120h and, although the length of the *Gastruloids* was broadly similar to that of the control there was a clear effect on the elongation process *(***Fig. 8A,B, fig.S10**) On the other hand, when BMP is applied instead of Chi between 48 and 72hrs AA, although the majority of *Gastruloids* express the BMP reporter (~88%) albeit at a much lower level than in the Chi treated control, only half of these exhibit polarisation. Additionally, the frequency of elongation is greatly reduced when compared with Chi (~31% elongated; **Fig. 8C**). This suggests that, in our in vitro system, BMP cannot substitute for Chiron. Application of BMP between 24 and 48hrs AA leads to a weak focus of expression which is not consistently plated at the elongating tip, and no elongation is observed (**Fig. 8B, fig. S10**).

Altogether, these results suggest that BMP signalling does not play a significant role in the patterning or progression of *Gastruloids*.

A polarised source of Nodal signalling is not required for *Gastruloid* patterning.

Exposure of *Gastruloids* to Nodal during 48-72h AA does not lead to overall expression of T/Bra (**Fig. 5**) suggesting that, like Wnt signalling, a localised source of Nodal may not be required for its effect. We tested this hypothesis using *Nodal* mutant mESCs (Collignon et al., 1996) (**Fig. 9, fig. S11**). When aggregated in standard conditions and grown in N2B27 supplemented with the appropriate vehicle controls, *Nodal* mutant *Gastruloids* remain spherical or ovoid, exhibit a number of protrusions and by 120h AA a large proportion (~90%) have developed small bulbous structures at varying locations (**Fig. 9A,B, fig. S11**). These data confirm the absolute requirement for Nodal in symmetry breaking. We then attempted to rescue these *Gastruloids* with various signalling regimes. Addition of Nodal (24-48h AA) reduces the frequency of protrusions but the number is not significantly different from the control (**Fig. 9B**). Treatment with Chi (48-72h) leads to an increase in the proportion of elongated *Gastruloids* (~50%) supporting a role for Wnt signalling in elongation (**Fig. 9A**). However the average number of protrusions was similar to controls, with some showing four or more protrusions; the size of the protrusions was also increased relative to the control, but not statistically significant (**Fig. 9B, fig. S11**). Application of Nodal (24-48h) followed by Chi (48-72h) drastically increased the proportion of *Gastruloids* displaying an elongated, non-protrusion phenotype (0 to 50%) and the number of protrusions was greatly reduced, but not eliminated, compared with the Vehicle to Chi and Vehicle to DMSO controls. Immunofluorescence revealed that Nodal mutant *Gastruloids* treated with Chi were

unable to up-regulate the posterior markers T/Bra and Cdx2 compared with previous observations (**Fig. 1**). However, addition of Nodal prior to the Chi pulse rescued the patterning and location of the reporters (**Fig. 9C**).

To assess whether the timing and duration of Nodal addition are important for the rescue of the Nodal mutant phenotype, Nodal was applied between 48-72, 72-96 and 24-72h AA, in addition to Chi between 48 and 72h AA and *Gastruloid* morphology assessed at 120h AA (**Fig. 9B; fig. S11**). Although there was some variation between experimental replicates, applying Nodal at later time points reduced the 'no protrusion-elongated' phenotype whilst increasing the 'No protrusions, no elongation' morphology (**Fig. 9B; fig. S11**) compared with the 24-48h Nodal to 48-72h Chi condition. A longer duration of Nodal signalling did not result in effects different from those obtained for 72-96h Nodal.

These data reveal the absolute requirement for Nodal signalling for the symmetry-breaking event, and that tight control of Nodal signalling is necessary for proper *Gastruloid* elongation.

Discussion:

We find that *Gastruloids*, mouse embryonic organoids, develop an embryo-like AP organisation characteristic of the tail domain of the embryo in the absence of external patterned influences. Significantly they organise an AP axis in the absence of extraembryonic tissues, which have been shown to drive axial organisation during embryogenesis (Rossant and Tam, 2009; Stern, 2006; Takaoka and Hamada, 2012). This observation extends our previous finding (van den Brink et al., 2014) and leads us to suggest that *in vivo*, the role of the extraembryonic tissues might not be to induce axial organisation but rather to bias an intrinsically driven symmetry breaking event similar to the one we report here that occurs in the embryo (Turner et al., 2016b; Turner et al., 2017). The deployment of signalling centres around the embryo thus provides a robust source of spatial information that positions the onset of gastrulation in a defined and reproducible location. If the symmetry breaking were stochastic, it would be difficult to link gastrulation to the interactions of the emerging mesoderm cells with extraembryonic tissues in a reproducible manner. Our suggestion is supported by the observation that in the absence of extraembryonic signals, the embryo still exhibits a degree of patterning and axial organisation, though somewhat variable (Perea-Gomez et al., 2002; Yamamoto et al., 2004) and also by a recent report that Trophectoderm Stem cells appear to impose a polarisation on T/Bra expression in aggregates of ESCs (Harrison et al., 2017) that, as in our case (van den Brink et al., 2014), lack visceral endoderm.

However, this report suggests a strict requirement for extraembryonic tissues, specifically Trophoectoderm, for the expression of T/Bra which is at odds with observations that the expression and localisation of T/Bra occurs in over 90% of the extraembryonic-free aggregates (Baillie-Johnson et al., 2015; Turner et al., 2016b; Turner et al., 2017; van den Brink et al., 2014) and with previous reports which also showed T/Bra polarisation in Embryoid bodies (Berge et al., 2008; Marikawa et al., 2009). There are a number of explanations for this discrepancy. It may be that the, interaction between extraembryonic and embryonic tissues raises the threshold of the patterning events and creates interdependencies for relative spatial biases (*see also* (Turner et al., 2016a) *for a discussion of related matters*). Alternatively it might be that the spatial confinement of the TSCs, and/or receptor-ligand interactions of ESCs with Matrigel components, creates conditions that affect the rate and the frequency of the symmetry breaking events that we observe in our experiments. The resolution of these discrepancies will require further experiments in both systems. In our case we have shown that the transition from the pluripotent to the primed state follows a pattern similar to that of the embryo and it will be interesting to see if this is also the case when the ESCs are confined in matrigel.

A most important consequence of the symmetry breaking event in the embryo is the polarised onset of *T/Bra* (Rivera-Pérez and Magnuson, 2005; Yoon et al., 2015). A connection between the expression of T/Bra and Wnt signalling had been reported in assorted EBs (Berge et al., 2008) but the reproducibility and precision of this process in *Gastruloids* allows us to investigate its origin. In *Gastruloids* the joint action of Nodal and Wnt signalling promotes the expression and localisation of *T/Bra* expression between 24 and 48h AA but the stabilisation of this pattern requires a burst of Wnt signalling between 48 and 72h AA. An interpretation of our results is that Nodal provides the initial input on the expression of *T/Bra* and the organisation of an AP axis but that these effects are enhanced and consolidated by Wnt/β-catenin signalling. This possibility is supported by the observation that in the embryo *T/Bra* expression is initiated and localised in the absence of Wnt signalling, though this pattern is not robust (Tortelote and Hernández-Hernández, 2012). Similar interactions between Nodal and Wnt/β-catenin signalling have been described in chick and frog embryos (Crease et al., 1998; Skromne and Stern, 2001; Steinbeisser et al., 1993) and we have also shown them to occur in an adherent culture system of Primitive Streak formation (Turner et al., 2014b). It is therefore likely that they also occur in the mammalian embryo. At the molecular level this synergy is supported by reports of molecular interactions between Smad2,3 and β-Catenin in the regulatory regions of genes expressed in the Primitive Streak and specifically of *Nodal* and *T/Bra* (Dahle et al., 2010; Estarás et al., 2015; Funa et al., 2015).

Mechanisms to explain how Nodal leads to symmetry breaking during AP axis formation often invoke Reaction-Diffusion mechanisms (Juan and Hamada, 2001; Marcon et al., 2016; Müller et al., 2012). Accordingly, interactions between Nodal and its inhibitor and downstream target Lefty, lead to the asymmetric localisation of both and to the asymmetric expression of target genes e.g. *T/Bra*. Surprisingly we observe that ubiquitous exposure of *Gastruloids* to Nodal leads to polarisation of *T/Bra* expression and, moreover, that this will occur when high ubiquitous concentrations of Nodal are provided to a *Nodal* mutant *Gastruloid*. This observation challenges many of our current notions about patterning driven by Nodal and demonstrates that Nodal needs not be localised to generate an axis. One possible explanation for this observation that is consistent with our results is that Nodal signalling initiates the expression of *T/Bra* but that it is not involved in its refinement and maintenance which depends on a positive feedback between Wnt/β-catenin signalling and T/Bra (Turner et al., 2014b). Indeed, several Wnt genes are known to be downstream targets of T/Bra (Evans et al., 2012) which, in turn, is a target of Wnt/β-catenin signalling thus providing the elements for a positive feedback loop that could be involved in the patterning and localisation of T/Bra and its downstream targets. In agreement with this we observe a spatial correlation between the pattern of Wnt signalling and of T/Bra expression (**Fig. 1C,D**).

Our results also highlight that, in addition to, and independently of, its role in T/Bra expression and of its interactions with Nodal/Smad2,3 signalling, Wnt/β-catenin signalling is central to axial elongation. This provides an independent proof of this well established phylogenetic relationship (Petersen and Reddien, 2009). Timing of exposure suggests two different phases to this involvement. Long exposures to Wnt signalling early (24-72h AA; E5.0-E7.0 in the embryo) can lead to multiple axes, only some of which express T/Bra; this mirrors situations with gain of function of Wnt signalling (Merrill et al., 2004; Pöpperl et al., 1997). Increased activity later on (48-96h AA; E6.0-E8.0) results in abolition of the polarity and ubiquitous expression of T/Bra. These observations highlight two temporally separate activities of Wnt: a first one in the establishment and enhancement of the AP axis, probably together with Nodal signalling, followed by a second phase of stabilisation of T/Bra expression and axial elongation. As in the case of Nodal but in a more manifest manner, the observation that a localised source of Wnt/β-catenin activity is not necessary for the polarisation of T/Bra expression and the elongation of the *Gastruloid*, questions the widespread notion for a role of Wnt signalling gradients in pattern formation and supports views in which the function of Wnt signalling is to control the signal to noise ratio of events induced by other means (Martinez Arias and Hayward, 2006; Mateus et al., 2009).

A remarkable feature of *Gastruloids* is the degree to which their spatial organisation resembles the posterior region of an E8.5 embryo. However this structure though coherent is partial e.g *Gastruloids* lack the most anterior structures (van den Brink et al., 2014). In this regard they resemble Dkk (Fossat et al., 2011) or some Smad2,3 (Dunn et al., 2004) mutants and show that it is possible to orientate an axis without an identifiable head or brain. A likely cause for this deficiency is a combination of the exposure to high levels of Wnt signalling between 48 and 72h AA, which will suppress anterior development (Arkell et al., 2013; Pöpperl et al., 1997) and the lack of a prechordal plate and anterior mesendoderm which are essential for anterior neural induction (Andoniadou and Martinez-Barbera, 2013). Thus while signalling from the extraembryonic tissues might not be strictly necessary for the establishment of an AP axis, it might be essential not only for the reliable positioning of the initiation of gastrulation but also for the location of the brain at the opposite pole.

Over the last few years a number of experimental systems have emerged in which ESCs become spatially patterned and each of them can make a contribution to our understanding of the connection between cell fate assignments and the polarisation of the embryo (Bauwens et al., 2008; Desbaillets et al., 2000; Etoc et al., 2016; Harrison et al., 2017; Warmflash et al., 2014). The system that we have developed has some advantages, in particular its 3D self organisation, reproducibility and robustness allow it to be used in long term studies and screens. However, despite the resemblance to early embryos, the current generation of *Gastruloids* exhibit differences in detail which create the challenge of what it takes to make the similarities more obvious. In this process, engineering will play an important role and help a rational design of tissues and organs. Importantly we feel that our findings suggest that *Gastruloids* could be a useful substitute for embryos in the study of early development.

Materials and Methods:

Cell lines and routine cell culture: AR8::mCherry (Nodal signalling reporter; (Serup et al., 2012)), T/Bra::GFP (Fehling et al., 2003), GATA6::H2B-Venus (Freyer et al., 2015), IBRE4::Cerulean (Serup et al., 2012), *miR-290-mCherry/mir-302-eGFP* (DRC) (Parchem et al., 2014), Nodal::YFP reporter (Papanayotou et al., 2014), Nodal$^{-/-}$ (Camus et al., 2006), Sox17::GFP (Niakan et al., 2010) and TCF/LEF::mCherry (TLC2) (Faunes et al., 2013; Ferrer-Vaquer et al., 2010) were cultured in GMEM supplemented with LIF, foetal bovine serum, Non-Essential Amino Acids, Glutamax, Sodium Pyruvate and β-mercaptoethanol (ESL medium) on gelatinised tissue-culture flasks and passaged every second day as previously described (Faunes et al., 2013; Kalmar et al., 2009; Turner et al., 2014b; Turner et al., 2014a; Turner et al., 2014c). If cells were not being passaged, half the medium in the tissue culture flask was replaced with ESL. All cell lines were routinely tested and confirmed free from mycoplasma. See **table S3** for the cell lines used in this study.

***Gastruloid* culture and application of specific signals:** Aggregates of mouse ESCs were generated using an optimised version of the previously published protocol ((Baillie-Johnson et al., 2015; van den Brink et al., 2014) and supplemental methods). **Table S3** details the number of cells required to generate *Gastruloids* for the cell lines used in this study.

Immunofluorescence, Microscopy and data analysis: *Gastruloids* were fixed, stained with the required antibodies (**table S2**) and imaged by confocal microscopy according to the protocol previously described (Baillie-Johnson et al., 2015). Widefield, single-time point and time-lapse images of *Gastruloids* were acquired using a Zeiss AxioObserver.Z1 (Carl Zeiss, UK) in a humidified CO_2 incubator (5% CO_2, 37°C) with Illumination provided by an LED white-light system (Laser2000, Kettering, UK) and emitted light recorded using a back-illuminated iXon888 Ultra EMCCD (Andor, UK). Images were analysed using FIJI (Schindelin et al., 2012) and plugins therein as previously described (Baillie-Johnson et al., 2015; Preibisch et al., 2009), and the data analysed and plotted as described in the supplemental materials and methods.

***Statistical Analysis**:* Statistical analysis of the *Gastruloids'* normalised fluorescence traces was performed in Matlab (Mathworks, 2016a) and described in the supplemental materials and methods.

Quantitative RT-PCR: *Gastruloids* (*n* = ~64 per time-point) from T/Bra::GFP mouse ESCs, subjected to a Chi or DMSO pulse (between 48 and 72h AA), harvested at 48 or 72h AA, trypsinised, pelleted and RNA extracted using the RNeasy Mini kit (Qiagen, 74104) according to the manufacturer's

instruction as previously described (Turner et al., 2014c). Samples were normalised to the housekeeping gene *PPIA*. The sequences for the primers are described in **table S5**.

Orientation of Gastruloids: To define the AP orientation of Gastruloids, we have assigned the point of T/Bra::GFP expression as the 'Posterior', as the primitive streak, which forms in the posterior of embryo, is the site of T/Bra expression in the embryo (Beddington et al., 1992; Herrmann, 1991; Wilkinson et al., 1990).

At least two biological replicates were performed for each condition.

Acknowledgements: This work is funded by a European Research Council (ERC) Advanced Investigator Award to AMA (DAT, PCH) with the contribution of a BBSRC Project Grant to AMA, an NC3Rs David Sainsbury Fellowship to DAT, Herchel Smith Postdoctoral Fellowship to VT, and an Engineering and Physical Sciences Research Council (EPSRC) Studentship to PB-J. Work in the laboratory of ML was funded by support from Ecole Polytechnique Fédérale de Lausanne (EPFL). Portions of this paper first appeared on the *BioRxiv* pre-print server (Turner et al., 2016b; Turner et al., 2017). We want to thank Pau Rué for assistance with the *Python* code at the project's outset, and Christian Schröter, Tristan Rodriguez, Kat Hadjantonakis and members of the AMA lab for discussions.

Competing Interests: The author declares no competing or financial interests.

Author Contributions: The project was conceived and designed by AMA, DAT and ML. The experiments were performed by: DAT, LAC, PB-J, CRG, MG, PCH; VT assisted with confocal imaging and analysis; the data was analysed by DAT, VT, LA-C, PB-J, CRG, PCH, BS; DAT wrote the FIJI/ImageJ scripts and *Python* code for data analysis; VT devised and performed the statistical analysis for the fluorescence traces; the cell lines were generated by: JC, CG, PS; the paper was written by DAT & AMA with comments from the other authors.

References:

Anderson, K. V. (2000). Finding the genes that direct mammalian development. *Trends in Genetics* **16**, 99–102.

Andoniadou, C. L. and Martinez-Barbera, J. P. (2013). Developmental mechanisms directing early anterior forebrain specification in vertebrates. *Cell. Mol. Life Sci.* **70**, 3739–3752.

Arkell, R. M., Fossat, N. and Tam, P. P. (2013). Wnt signalling in mouse gastrulation and anterior development: new players in the pathway and signal output. *Current Opinion in Genetics & Development*.

Baillie-Johnson, P., van den Brink, S. C., Balayo, T., Turner, D. A. and Martinez Arias, A. (2015). Generation of Aggregates of Mouse Embryonic Stem Cells that Show Symmetry Breaking, Polarization and Emergent Collective Behaviour In Vitro. *J Vis Exp*.

Bauwens, C. L., Peerani, R., Niebruegge, S., Woodhouse, K. A., Kumacheva, E., Husain, M. and Zandstra, P. W. (2008). Control of human embryonic stem cell colony and aggregate size heterogeneity influences differentiation trajectories. *Stem Cells* **26**, 2300–2310.

Beddington, R. S. P., Rashbass, P. and Wilson, V. (1992). Brachyury - a gene affecting mouse gastrulation and early organogenesis. *Dev. Suppl.* 157–165.

Berge, ten, D., Koole, W., Fuerer, C., Fish, M., Eroglu, E. and Nusse, R. (2008). Wnt Signaling Mediates Self-Organization and Axis Formation in Embryoid Bodies. *Cell Stem Cell* **3**, 508–518.

Bertocchini, F. and Stern, C. D. (2002). The hypoblast of the chick embryo positions the primitive streak by antagonizing nodal signaling. *Developmental Cell* **3**, 735–744.

Camus, A., Perea-Gomez, A., Moreau, A. and Collignon, J. (2006). Absence of Nodal signaling promotes precocious neural differentiation in the mouse embryo. *Developmental Biology* **295**, 743–755.

Chambers, I., Silva, J., Colby, D., Nichols, J., Nijmeijer, B., Robertson, M., Vrana, J., Jones, K., Grotewold, L. and Smith, A. (2007). Nanog safeguards pluripotency and mediates germline development. *Nature* **450**, 1230–1234.

Chen, B., Dodge, M. E., Tang, W., Lu, J., Ma, Z., Fan, C.-W., Wei, S., Hao, W., Kilgore, J., Williams, N. S., et al. (2009). Small molecule–mediated disruption of Wnt-dependent signaling in tissue regeneration and cancer. *Nat Chem Biol* **5**, 100–107.

Choi, E., Kraus, M. R.-C., Lemaire, L. A., Yoshimoto, M., Vemula, S., Potter, L. A., Manduchi, E., Stoeckert, C. J., Grapin-Botton, A. and Magnuson, M. A. (2012). Dual lineage-specific expression of Sox17 during mouse embryogenesis. *Stem Cells* **30**, 2297–2308.

Collignon, J., Varlet, I. and Robertson, E. J. (1996). Relationship between asymmetric nodal expression and the direction of embryonic turning. *Nature* **381**, 155–158.

Crease, D. J., Dyson, S. and Gurdon, J. B. (1998). Cooperation between the activin and Wnt pathways in the spatial control of organizer gene expression. *Proceedings of the National Academy of Sciences* **95**, 4398–4403.

Dahle, Ø., Kumar, A. and Kuehn, M. R. (2010). Nodal signaling recruits the histone demethylase Jmjd3 to counteract polycomb-mediated repression at target genes. *Science Signaling* **3**, ra48.

Desbaillets, I., Ziegler, U., Groscurth, P. and Gassmann, M. (2000). Embryoid bodies: an in vitro model of mouse embryogenesis. *Exp. Physiol.* **85**, 645–651.

Dunn, N. R., Vincent, S. D., Oxburgh, L., Robertson, E. J. and Bikoff, E. K. (2004). Combinatorial activities of Smad2 and Smad3 regulate mesoderm formation and patterning in the mouse embryo. *Development* **131**, 1717–1728.

Estarás, C., Benner, C. and Jones, K. A. (2015). SMADs and YAP compete to control elongation of β-catenin:LEF-1-recruited RNAPII during hESC differentiation. *Molecular Cell* **58**, 780–793.

Etoc, F., Metzger, J., Ruzo, A., Kirst, C., Yoney, A., Ozair, M. Z., Brivanlou, A. H. and Siggia, E. D. (2016). A Balance between Secreted Inhibitors and Edge Sensing Controls Gastruloid Self-Organization. *Developmental Cell* **39**, 302–315.

Evans, A. L., Faial, T., Gilchrist, M. J., Down, T., Vallier, L., Pedersen, R. A., Wardle, F. C. and Smith, J. C. (2012). Genomic targets of Brachyury (T) in differentiating mouse embryonic stem cells. *PLoS ONE* **7**, e33346.

Faunes, F., Hayward, P., Descalzo, S. M., Chatterjee, S. S., Balayo, T., Trott, J., Christoforou, A., Ferrer-Vaquer, A., Hadjantonakis, A.-K., Dasgupta, R., et al. (2013). A membrane-associated β-catenin/Oct4 complex correlates with ground-state pluripotency in mouse embryonic stem cells. *Development* **140**, 1171–1183.

Fehling, H. J., Lacaud, G., Kubo, A., Kennedy, M., Robertson, S., Keller, G. and Kouskoff, V. (2003). Tracking mesoderm induction and its specification to the hemangioblast during embryonic stem cell differentiation. *Development* **130**, 4217–4227.

Ferrer-Vaquer, A., Piliszek, A., Tian, G., Aho, R. J., Dufort, D. and Hadjantonakis, A.-K. (2010). A sensitive and bright single-cell resolution live imaging reporter of Wnt/ß-catenin signaling in the mouse. *BMC Dev Biol* **10**, 121.

Fossat, N., Jones, V., García-García, M. J. and Tam, P. P. L. (2012). Modulation of WNT signaling activity is key to the formation of the embryonic head. *Cell Cycle* **11**, 26–32.

Fossat, N., Jones, V., Khoo, P. L., Bogani, D., Hardy, A., Steiner, K., Mukhopadhyay, M., Westphal, H., Nolan, P. M., Arkell, R., et al. (2011). Stringent requirement of a proper level of canonical WNT signalling activity for head formation in mouse embryo. *Development* **138**, 667–676.

Freyer, L., Schröter, C., Saiz, N., Schrode, N., Nowotschin, S., Martinez Arias, A. and Hadjantonakis, A.-K. (2015). A loss-of-function and H2B-Venus transcriptional reporter allele for Gata6 in mice. *BMC Dev Biol* **15**, 38.

Funa, N. S., Schachter, K. A., Lerdrup, M., Ekberg, J., Hess, K., Dietrich, N., Honoré, C., Hansen, K. and Semb, H. (2015). beta-Catenin Regulates Primitive Streak Induction through Collaborative Interactions with SMAD2/ SMAD3 and OCT4. *Stem Cell* **16**, 639–652.

Hamada, H. (2015). Role of physical forces in embryonic development. *Semin Cell Dev Biol* **47-48**, 88–91.

Harrison, S. E., Sozen, B., Christodoulou, N., Kyprianou, C. and Zernicka-Goetz, M. (2017). Assembly of embryonic and extra-embryonic stem cells to mimic embryogenesis in vitro. *Science* eaal1810.

Herrmann, B. G. (1991). Expression pattern of the Brachyury gene in whole-mount TWis/TWis mutant embryos. *Development* **113**, 913–917.

Hiramatsu, R., Matsuoka, T., Kimura-Yoshida, C., Han, S.-W., Mochida, K., Adachi, T., Takayama, S. and Matsuo, I. (2013). External mechanical cues trigger the establishment of the anterior-posterior axis in early mouse embryos. *Developmental Cell* **27**, 131–144.

Huang, S.-M. A., Mishina, Y. M., Liu, S., Cheung, A., Stegmeier, F., Michaud, G. A., Charlat, O., Wiellette, E., Zhang, Y., Wiessner, S., et al. (2009). Tankyrase inhibition stabilizes axin and antagonizes Wnt signalling. *Nature* **461**, 614–620.

Inman, G. J., Nicolás, F. J., Callahan, J. F., Harling, J. D., Gaster, L. M., Reith, A. D., Laping, N. J. and Hill, C. S. (2002). SB-431542 is a potent and specific inhibitor of transforming growth factor-beta superfamily type I activin receptor-like kinase (ALK) receptors ALK4, ALK5, and ALK7. *Mol. Pharmacol.* **62**, 65–74.

Juan, H. and Hamada, H. (2001). Roles of nodal-lefty regulatory loops in embryonic patterning of vertebrates. *Genes to Cells* **6**, 923–930.

Kalmar, T., Lim, C., Hayward, P., Muñoz-Descalzo, S., Nichols, J., Garcia-Ojalvo, J. and Martinez Arias, A. (2009). Regulated Fluctuations in Nanog Expression Mediate Cell Fate Decisions in Embryonic Stem Cells. *Plos Biol* **7**, e1000149.

Kanai-Azuma, M., Kanai, Y., Gad, J. M., Tajima, Y., Taya, C., Kurohmaru, M., Sanai, Y., Yonekawa, H., Yazaki, K., Tam, P. P. L., et al. (2002). Depletion of definitive gut endoderm in Sox17-null mutant mice. *Development* **129**, 2367–2379.

Marcon, L., Diego, X., Sharpe, J. and Müller, P. (2016). High-throughput mathematical analysis identifies Turing networks for patterning with equally diffusing signals. *Elife*.

Marikawa, Y., Tamashiro, D. A. A., Fujita, T. C. and Alarcon, V. B. (2009). Aggregated P19 mouse embryonal carcinoma cells as a simple in vitro model to study the molecular regulations of mesoderm formation and axial elongation morphogenesis. *Genesis* **47**, 93–106.

Martinez Arias, A. and Hayward, P. (2006). Filtering transcriptional noise during development: concepts and mechanisms. *Nat Rev Genet* **7**, 34–44.

Mateus, A. M., Gorfinkiel, N. and Arias, A. M. (2009). Origin and function of fluctuations in cell behaviour and the emergence of patterns. *Semin Cell Dev Biol* **20**, 877–884.

Meinhardt, H. (2006). Primary body axes of vertebrates: generation of a near-Cartesian coordinate system and the role of Spemann-type organizer. *Dev. Dyn.* **235**, 2907–2919.

Merrill, B. J., Pasolli, H. A., Polak, L., Rendl, M., García-García, M. J., Anderson, K. V. and Fuchs, E. (2004). Tcf3: a transcriptional regulator of axis induction in the early embryo. *Development* **131**, 263–274.

Müller, P., Rogers, K. W., Jordan, B. M., Lee, J. S., Robson, D., Ramanathan, S. and Schier, A. F. (2012). Differential diffusivity of Nodal and Lefty underlies a reaction-diffusion patterning system. *Science* **336**, 721–724.

Neely, M. D., Litt, M. J., Tidball, A. M., Li, G. G., Aboud, A. A., Hopkins, C. R., Chamberlin, R., Hong, C. C., Ess, K. C. and Bowman, A. B. (2012). DMH1, a highly selective small molecule BMP inhibitor promotes neurogenesis of hiPSCs: comparison of PAX6 and SOX1 expression during neural induction. *ACS Chem Neurosci* **3**, 482–491.

Niakan, K. K., Ji, H., Eggan, K.12 (2010). Sox17 promotes differentiation in mouse embryonic stem cells by directly regulating extraembryonic gene expression and indirectly antagonizing self-renewal. *Genes & Development* **24**, 312–326.

Papanayotou, C., Benhaddou, A., Camus, A., Perea-Gomez, A., Jouneau, A., Mezger, V., Langa, F., Ott, S., Sabéran-Djoneidi, D. and Collignon, J. (2014). A novel nodal enhancer dependent on pluripotency factors and smad2/3 signaling conditions a regulatory switch during epiblast maturation. *Plos Biol* **12**, e1001890.

Parchem, R. J., Ye, J., Judson, R. L., LaRussa, M. F., Krishnakumar, R., Blelloch, A., Oldham, M. C. and Blelloch, R. (2014). Two miRNA clusters reveal alternative paths in late-stage reprogramming. *Cell Stem Cell* **14**, 617–631.

Perea-Gomez, A., Vella, F. D. J., Shawlot, W., Oulad-Abdelghani, M., Chazaud, C., Meno, C., Pfister, V., Chen, L., Robertson, E., Hamada, H., et al. (2002). Nodal antagonists in the anterior visceral endoderm prevent the formation of multiple primitive streaks. *Developmental Cell* **3**, 745–756.

Petersen, C. P. and Reddien, P. W. (2009). Wnt signaling and the polarity of the primary body axis. *Cell* **139**, 1056–1068.

Pöpperl, H., Schmidt, C., Wilson, V., Hume, C. R., Dodd, J., Krumlauf, R. and Beddington, R. S. P. (1997). Misexpression of Cwnt8C in the mouse induces an ectopic embryonic axis and causes a truncation of the anterior neuroectoderm. *Development* **124**, 2997–3005.

Preibisch, S., Saalfeld, S. and Tomancak, P. (2009). Globally optimal stitching of tiled 3D microscopic image acquisitions. *Bioinformatics* **25**, 1463–1465.

Riechmann, V. and Ephrussi, A. (2001). Axis formation during Drosophila oogenesis. *Current Opinion in Genetics & Development*.

Rivera-Pérez, J. A. and Hadjantonakis, A.-K. (2015). The Dynamics of Morphogenesis in the Early Mouse Embryo. *Cold Spring Harbor Perspectives in Biology* **7**.

Rivera-Pérez, J. A. and Magnuson, T. (2005). Primitive streak formation in mice is preceded by localized activation of Brachyury and Wnt3. *Developmental Biology* **288**, 363–371.

Rossant, J. and Tam, P. P. L. (2009). Blastocyst lineage formation, early embryonic asymmetries and axis patterning in the mouse. *Development* **136**, 701–713.

Roth, S. and Lynch, J. A. (2009). Symmetry Breaking During Drosophila Oogenesis. *Cold Spring Harbor Perspectives in Biology* **1**, a001891–a001891.

Sasai, Y., Eiraku, M. and Suga, H. (2012). In vitro organogenesis in three dimensions: self-organising stem cells. *Development*.

Saund, R. S., Kanai-Azuma, M., Kanai, Y., Kim, I., Lucero, M. T. and Saijoh, Y. (2012). Gut endoderm is involved in the transfer of left-right asymmetry from the node to the lateral plate mesoderm in the mouse embryo. *Development* **139**, 2426–2435.

Schindelin, J., Arganda-Carreras, I., Frise, E., Kaynig, V., Longair, M., Pietzsch, T., Preibisch, S., Rueden, C., Saalfeld, S. and Schmid, B. (2012). Fiji: an open-source platform for biological-image analysis. *Nature Methods* **9**, 676–682.

Serup, P., Gustavsen, C., Klein, T., Potter, L. A., Lin, R., Mullapudi, N., Wandzioch, E., Hines, A., Davis, A., Bruun, C., et al. (2012). Partial promoter substitutions generating transcriptional sentinels of diverse signaling pathways in embryonic stem cells and mice. *Dis Model Mech* **5**, 956–966.

Simunovic, M. and Brivanlou, A. H. (2017). Embryoids, organoids and gastruloids: new approaches to understanding embryogenesis. *Development* **144**, 976–985.

Skromne, I. and Stern, C. D. (2001). Interactions between Wnt and Vg1 signalling pathways initiate primitive streak formation in the chick embryo. *Development* **128**, 2915–2927.

St Johnston, D. (2002). The Art and Design of Genetic Screens: Drosophila Melanogaster. *Nat Rev Genet* **3**, 176–188.

Steinbeisser, H., De Robertis, E. M., Ku, M., Kessler, D. S. and Melton, D. A. (1993). Xenopus axis formation: induction of goosecoid by injected Xwnt-8 and activin mRNAs. *Development* **118**, 499–507.

Stern, C. D. (2006). Evolution of the mechanisms that establish the embryonic axes. *Current Opinion in Genetics & Development* **16**, 413–418.

Takaoka, K. and Hamada, H. (2012). Cell fate decisions and axis determination in the early mouse embryo. *Development* **139**, 3–14.

Tam, P. P. L. and Gad, J. M. (2004). Gastrulation in the Mouse Embryo. In *Gastrulation: From Cells to Embryo* (ed. Stern, C. D., pp. 233–262. New York: Cold Spring Harbor Laboratory Press.

Tam, P. P. L. and Loebel, D. A. F. (2007). Gene function in mouse embryogenesis: get set for gastrulation. *Nat Rev Genet* **8**, 368–381.

Tortelote, G. G. and Hernández-Hernández, J. M. (2012). Wnt3 function in the epiblast is required for the maintenance but not the initiation of gastrulation in mice. *Developmental Biology*.

Turner, D. A., Alonso-Crisostomo, L., Girgin, M., Baillie-Johnson, P., Glodowski, C. R., Hayward, P. C., Collignon, J., Gustavsen, C., Serup, P., Steventon, B., et al. (2017). Gastruloids develop the three body axes in the absence of extraembryonic tissues and spatially localised signalling. *BioRxiv*.

Turner, D. A., Baillie-Johnson, P. and Martinez Arias, A. (2016a). Organoids and the genetically encoded self-assembly of embryonic stem cells. *Bioessays* **38**, 181–191.

Turner, D. A., Glodowski, C. R., Alonso-Crisostomo, L., Baillie-Johnson, Hayward, P. C., Collignon, J., Gustavsen, C., Serup, P., Schröter, C. and Martinez Arias, A. (2016b). Interactions between Nodal and Wnt signalling Drive Robust Symmetry-Breaking and Axial Organisation in Gastruloids (Embryonic Organoids). *BioRxiv* 1–31.

Turner, D. A., Hayward, P. C., Baillie-Johnson, P., Rué, P., Broome, R., Faunes, F. and Martinez Arias, A. (2014a). Wnt/β-catenin and FGF signalling direct the specification and maintenance of a neuromesodermal axial progenitor in ensembles of mouse embryonic stem cells. *Development* **141**, 4243–4253.

Turner, D. A., Rué, P., Mackenzie, J. P., Davies, E. and Martinez Arias, A. (2014b). Brachyury cooperates with Wnt/β-Catenin signalling to elicit Primitive Streak like behaviour in differentiating mouse ES cells. *BMC Biology* **12**, 63.

Turner, D. A., Trott, J., Hayward, P., Rué, P. and Martinez Arias, A. (2014c). An interplay between extracellular signalling and the dynamics of the exit from pluripotency drives cell fate decisions in mouse ES cells. *Biology Open* **3**, 614–626.

van den Brink, S. C., Baillie-Johnson, P., Balayo, T., Hadjantonakis, A.-K., Nowotschin, S., Turner, D. A. and Martinez Arias, A. (2014). Symmetry breaking, germ layer specification and axial organisation in aggregates of mouse embryonic stem cells. *Development* **141**, 4231–4242.

Warmflash, A., Sorre, B., Etoc, F., Siggia, E. D. and Brivanlou, A. H. (2014). A method to recapitulate early embryonic spatial patterning in human embryonic stem cells. *Nature Methods* **11**, 847–854.

Wilkinson, D. G., Bhatt, S. and Herrmann, B. G. (1990). Expression pattern of the mouse T gene and its role in mesoderm formation. *Nature* **343**, 657–659.

Yamamoto, M., Saijoh, Y., Perea-Gomez, A., Shawlot, W., Behringer, R. R., Ang, S.-L., Hamada, H. and Meno, C. (2004). Nodal antagonists regulate formation of the anteroposterior axis of the mouse embryo. *Nature* **428**, 387–392.

Ying, Q.-L., Stavridis, M., Griffiths, D., Li, M. and Smith, A. (2003). Conversion of embryonic stem cells into neuroectodermal precursors in adherent monoculture. *Nat Biotechnol* **21**, 183–186.

Yoon, Y., Huang, T., Tortelote, G. G., Wakamiya, M., Hadjantonakis, A.-K., Behringer, R. R. and Rivera-Pérez, J. A. (2015). Extra-embryonic Wnt3 regulates the establishment of the primitive streak in mice. *Developmental Biology*.

Zhao, T., Gan, Q., Stokes, A., Lassiter, R. N. T., Wang, Y., Chan, J., Han, J. X., Pleasure, D. E., Epstein, J. A. and Zhou, C. J. (2014). β-catenin regulates Pax3 and Cdx2 for caudal neural tube closure and elongation. *Development* **141**, 148–157.

Figures

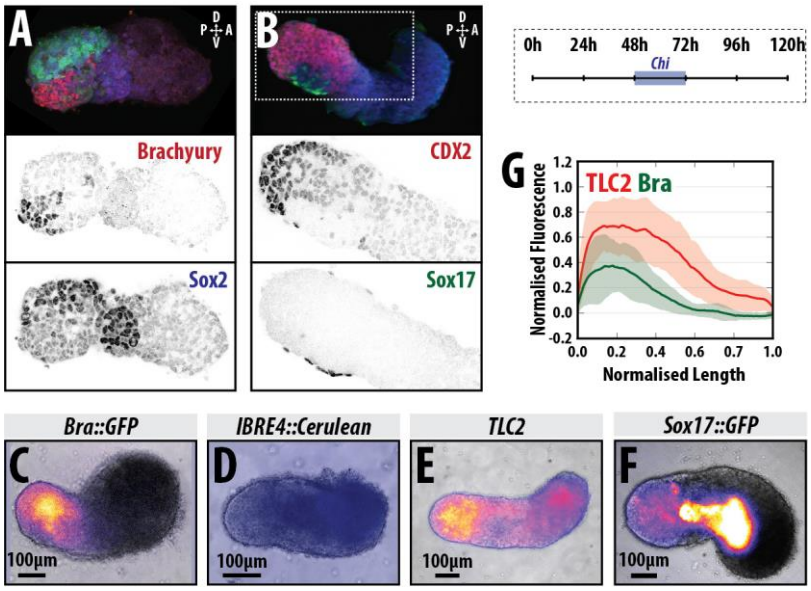

Fig. 1. ***Axial organisation of Gastruloids.*** Sox1::GFP (**A**) and Nodal::YFP reporter (**B**) *Gastruloids* pulsed with Chi (48-72hAA) and stained with Hoechst and anti-GFP with either (**A**) T/Bra (red) and Sox2 (Blue) or (**B**) CDX2 (red) and Sox17 (green) at 120h AA; hoechst is not shown in (**A**); staining representative of at least three replicate experiments; 3D projections are displayed. *Gastruloids* formed from Bra::GFP (**C**), BMP (IBRE4::Cerulean; **D**), Wnt/β-Catenin (TLC2; **E**) and Sox17::GFP (**F**) reporter lines following a 48-72h Chi pulse. (**E**) Quantification of reporter expression for the TLC2 (red) and Bra::GFP (green) *Gastruloids* in a posterior to anterior direction. Stimulation results in activation of the TLC2 reporter with highest expression at the posterior pole. Schematic for the stimulation regime shown top right.

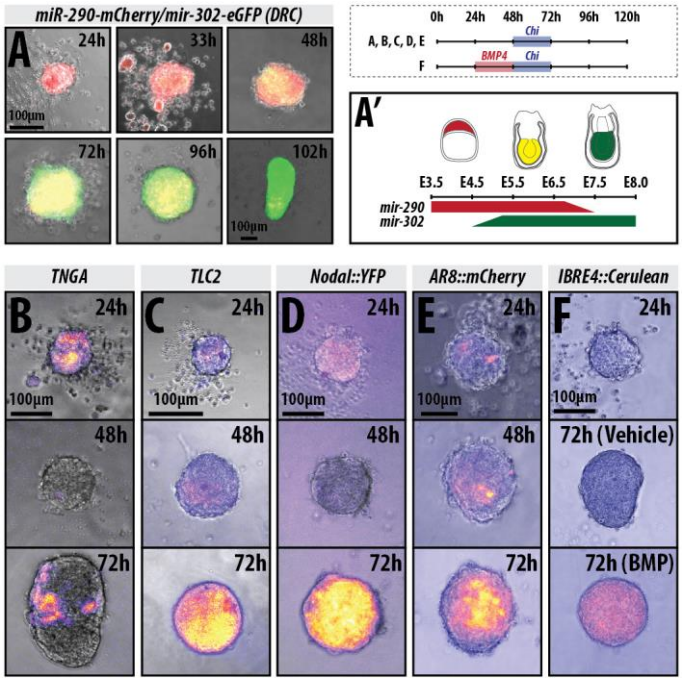

Fig. 2. ***Gastruloids progress through stages similar to the early embryonic to late epiblast.*** (**A**) *mir-290-mCherry/mir-302-eGFP* (DRC) *Gastruloids* imaged by widefield microscopy for 102h (n = 6 for 24-48h and 8 for 72-120h). The colour changes schematic is shown in (**A'**), part adapted from (Parchem et al., 2014) and (Turner et al., 2016b). (**B**) TNGA (n = 21), (**C**) TLC2 (24 & 48h n = 84; 72h n = 42), (**D**) Nodal::YFP (Nodal expression; n = 24 & 48h n = 84; 72h n = 42), (**E**) AR8::mCherry (Nodal signalling; n = 14), (**F**) IBRE4::Cerulean (BMP reporter; 24h n = 70; 48 & 72h n = 14). Schematic for the stimulation regime shown top right.

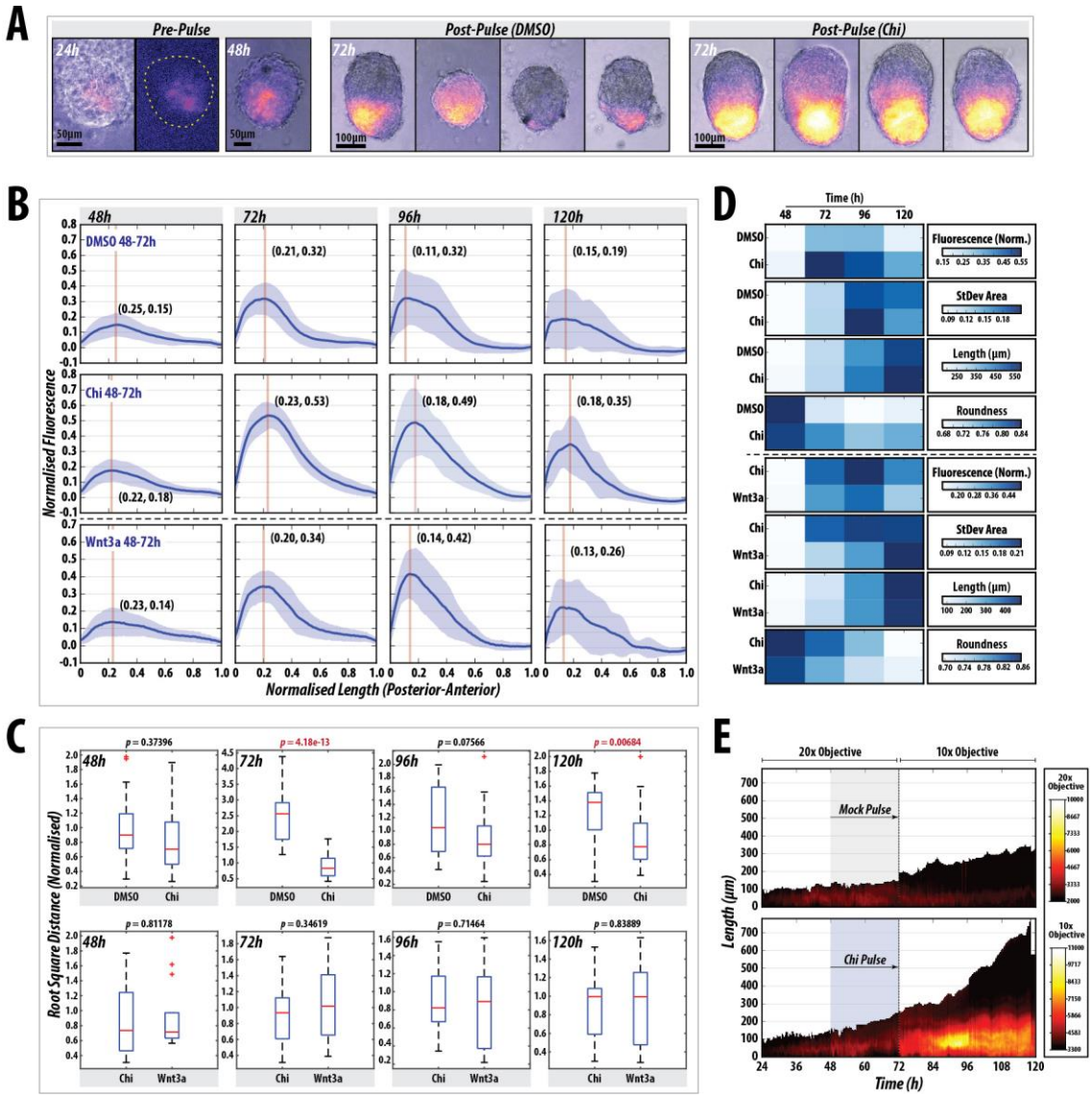

Fig. 3. ***Wnt/β-Catenin signalling stabilises and enhances spontaneous symmetry-breaking and polarisation events in Gastruloids.*** (**A**) T/Bra::GFP expression in *Gastruloids* at 24 and 48h prior to the Chi pulse (left), and examples (i-iv) of *Gastruloids* following a DMSO or Chi pulse (*n* = 28). Chi stimulation increases the robustness of the response and reproducibility of the phenotype. (**B**) Quantification of T/Bra::GFP reporter expression in individual *Gastruloids* over time following DMSO (*n = 28*), Chi (*n = 28*) or Wnt3A (*n = 14*). The maximum length of each *Gastruloid* is rescaled to 1 unit and the fluorescence is normalised to the maximum fluorescence from the Chi condition. Wnt3A condition is from a different replicate (indicated by hashed horizontal line). Vertical line in each plot marks the peak max and the corresponding coordinates denote the position of this value. (**C**) Statistical analysis of the indicated treatments showing the normalised root square displacement as a measure of the heterogeneity for each condition within each time-point, and the indicated *p* values as assessed by non-paired Student's t-test. (**D**) Heat maps indicating the

average fluorescence (fluorescence norm.), the average area taken up by the standard deviation (StDev Area), average length and the roundness of the *Gastruloids* in the indicated conditions and time-points from the traces in **B** (**fig. S2** and Materials and Methods). (**E**) Live imaging of a *Gastruloid* subjected to a pulse of DMSO (top) or Chi (bottom) between 48 and 72h AA (*n* = 21/condition). *Gastruloid* length indicated by the ordinate (posterior = 0µm), time on the abscissa and the fluorescence intensity in colour. Early time-points (24-72h AA) imaged with a higher power objective. Scale-bar as indicated.

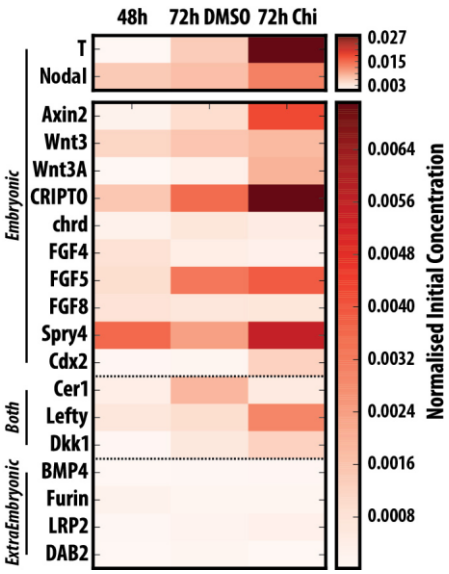

Fig. 4. ***Gastruloids do not express genes associated with extraembryonic tissues and progressively activate posterior markers.*** Quantitative PCR analysis of *Gastruloids* at 24, 48 and 72h AA for genes associated with the Epiblast, Extraembryonic tissues or those expressed in both tissues (*n* = ~64 *Gastrluoids* per time-point). Gastruloids display a more differentiated phenotype over time with little detectable expression genes associated with the extraembryonic tissues.

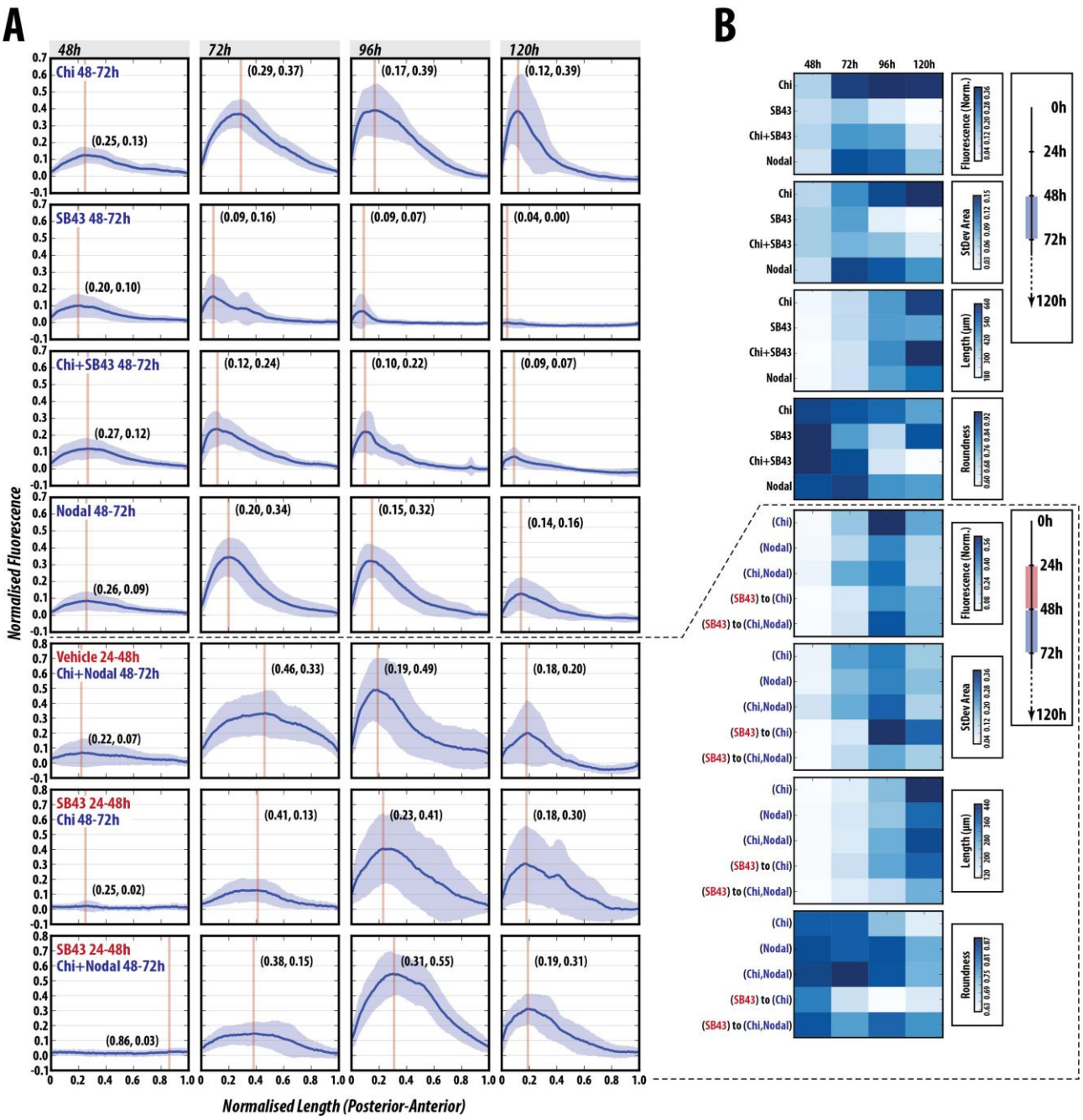

Fig. 5. ***Nodal signalling absolutely required for T/Bra induction and correct patterning.*** (**A**) *Gastruloids* stimulated with Chi, SB43, Chi + SB43 or Nodal alone between 48 and 72h AA (*n* = 13, 14, 14, 14 respectively), or subjected to either vehicle or SB43 pre-treatment (24-48h AA) prior to a Chi, Nodal or Chi+Nodal pulse (48-72h AA; *n* = 14 per condition). Normalised fluorescence traces shown per condition with corresponding shape descriptors as heatmaps (**B**). SB43 treatment blocks the expression of Bra::GFP and cannot be rescued by Chi co-stimulation. Inhibition of Nodal signalling has a positive influence on axial length and elongation morphology suggesting that Nodal modulates axial extension (see **fig. S5 and S6** for further details and statistical analysis).

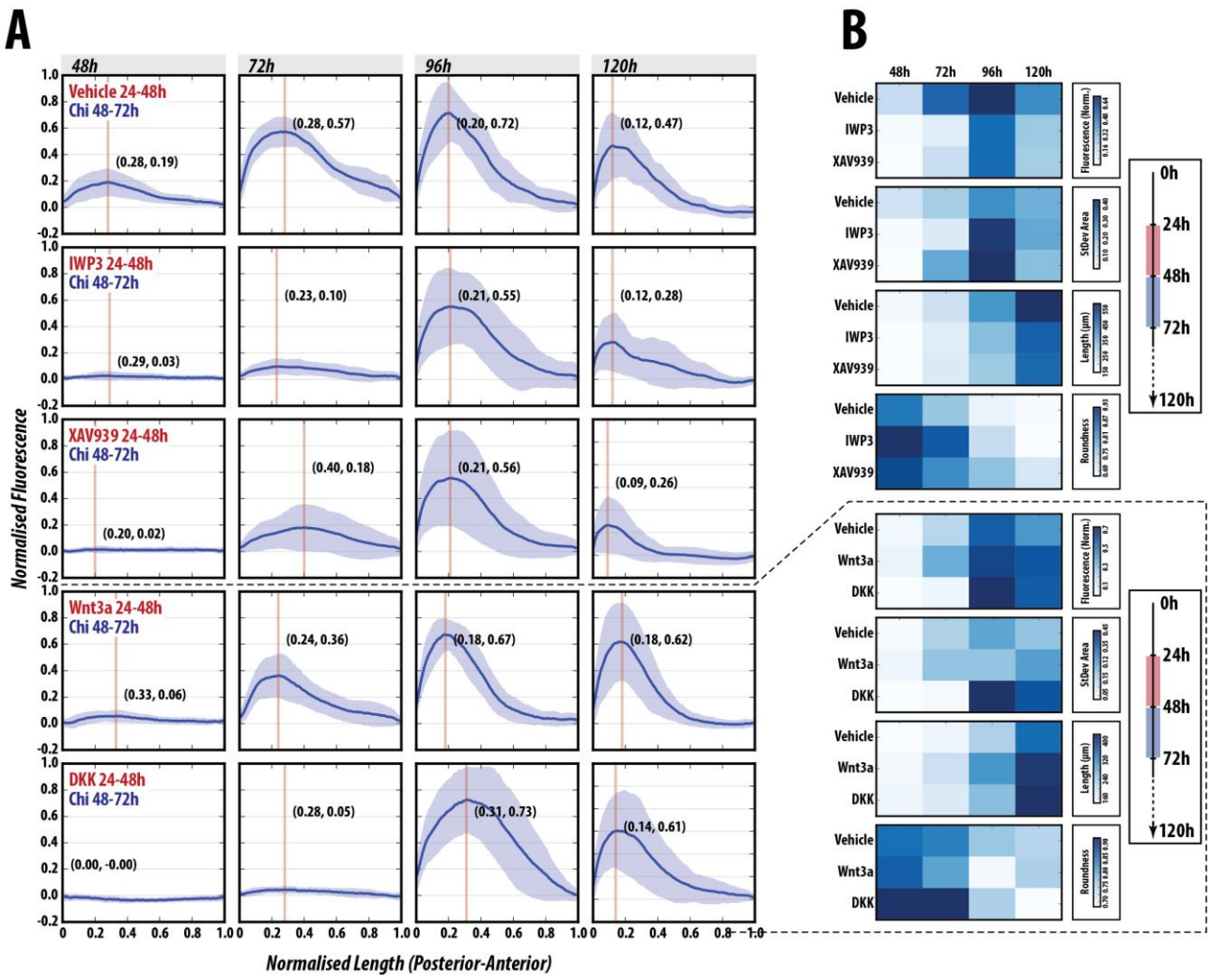

Fig. 6. ***Wnt/β-Catenin inhibition delays but does not inhibit Bra::GFP expression.*** Bra::GRP *Gastruloids* stimulated with a pulse of Chi (48-72h AA) following pre-treatment with vehicle IWP2, XAV939, DKK or Wnt3a (*n* = 14 per condition). Fluorescence traces (**A**) and heatmaps of the data (**B**) are shown. Blocking secretion of Wnt proteins with IWP2 effectively abolishes Bra::GFP expression until 96h AA, whereby highly heterogeneous expression is observed. Interestingly, the pulse of Chi can partially rescue Bra::GFP expression at 72h following XAV939 pre-treatment, indicating the requirement for wnt protein secretion in maintenance of expression. Wnt3a pre-treatment reduces the heterogeneity of the response, better defines the pole of expression and maintains high Bra expression for longer than controls (see **fig. S7 and S8** for further details and statistical analysis).

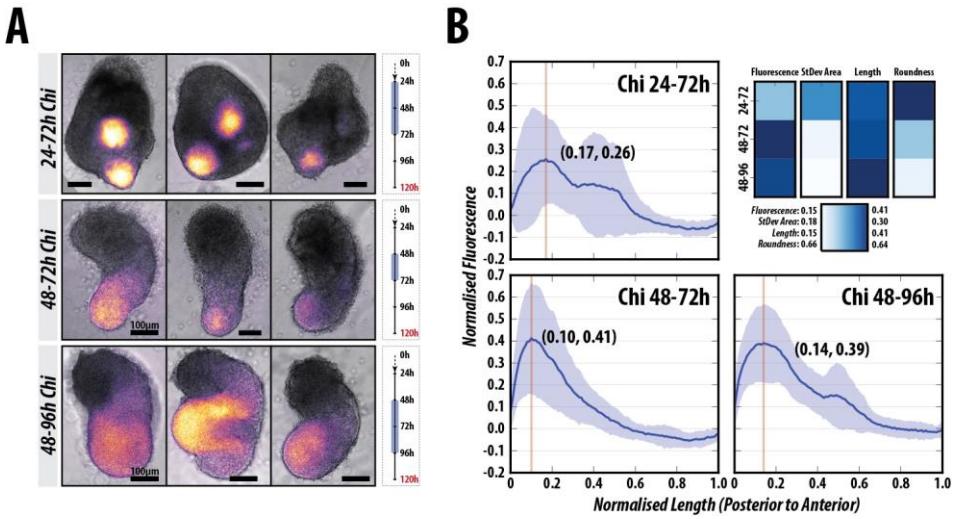

Fig. 7. ***Wnt/β-Catenin signalling between 48-72h AA is essential for the correct position and expression of T/Bra.*** (**A**) Examples of the morphology and expression of T/Bra::GFP *Gastruloids* stimulated with Chi between 24-72h (top; *n* = 14), 48-72h (middle, *n* = 14) and 48-96h (bottom, *n* = 13) AA and (**B**) the corresponding fluorescence and shape-descriptor quantification. Multiple poles of expression and stunted elongations are observed when Chi is applied between 24-72h AA whereas longer, later stimulation (48-96h) results wider *Gastruloids* and less well defined T/Bra::GFP expression, compared with the 48-72h control (refer to **fig. S9** for further details and statistical analysis).

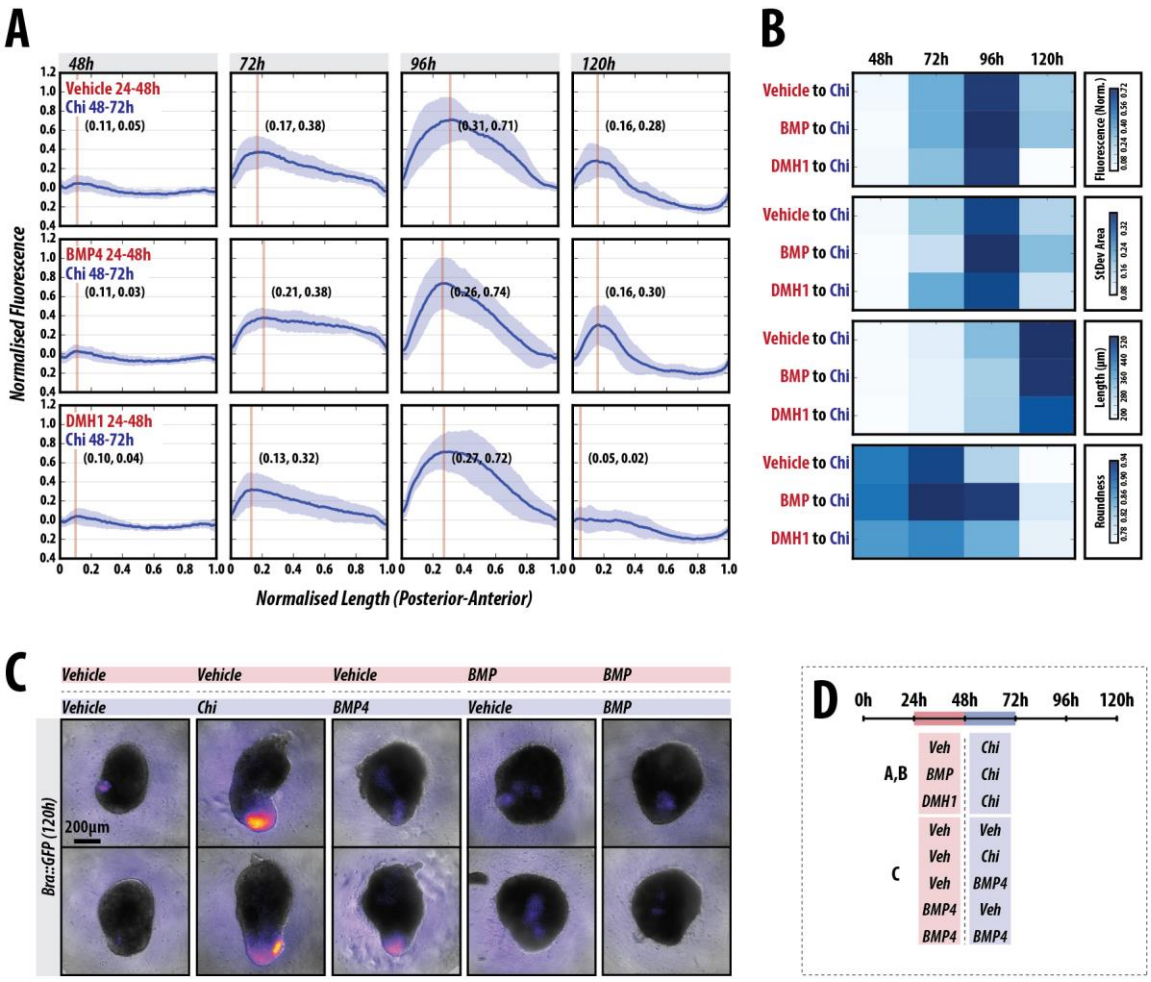

Fig. 8. ***BMP signalling is dispensable for early Gastruloid patterning.*** (**A**) T/Bra::GFP *Gastruloids* stimulated with Chi (48-72h) AA following a 24h pulse of either vehicle (top), BMP4 (middle) or DMH1 (bottom; *n* = 12, 13 and 13 at 120h respectively), an inhibitor of BMP signalling between 24 and 48h AA. Normalised fluorescence traces shown per condition (**A**) with corresponding fluorescence and shape descriptor quantification (**B**). Inhibition of BMP signalling by DMH1 or activation by BMP4 (24-48h AA) does not alter the initial patterning of *Gastruloids*, BMP treatment at this time has minimal effect on the subsequent patterning. (**C**) *Gastruloids* imaged at 120h by widefield microscopy following 24-48h (pink horizontal box) Vehicle or BMP4 stimulation followed by either Vehicle, Chi or BMP4 as indicated (blue horizontal box) between 48-72h AA (*n* = 16 per condition); see (**D**) for stimulation schematic. BMP4 is unable to substitute for Chi in terms of the elongation and patterning of Bra, and its sustained expression over time (refer to **fig. S10** for further details and statistical analysis). Scale bar in **C** represents 200µm.

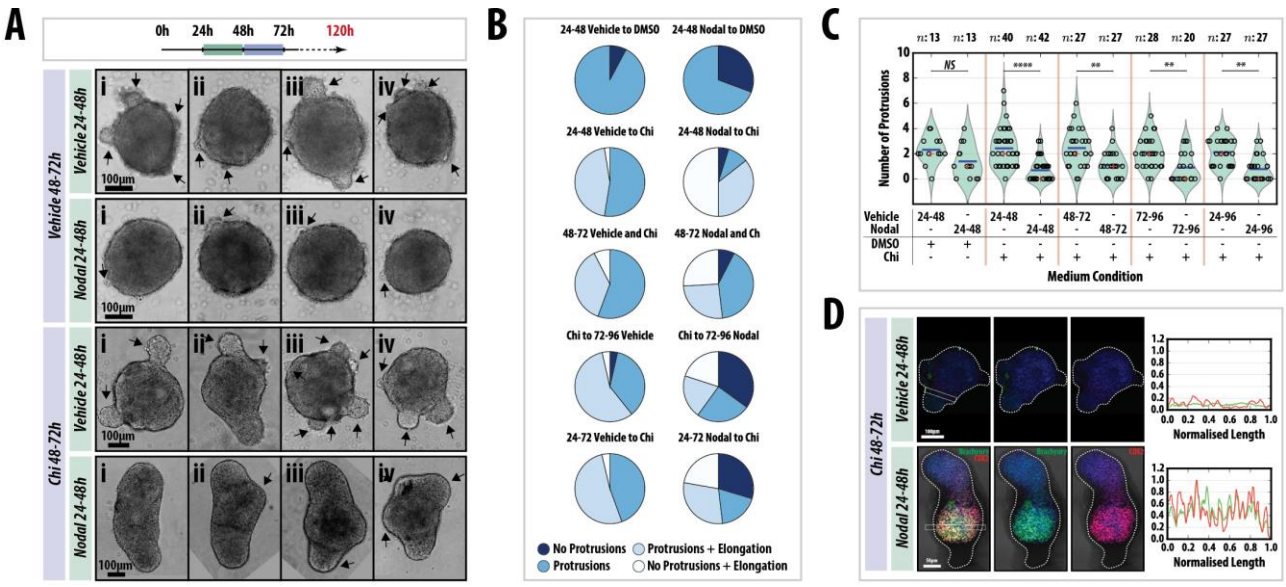

Fig. 9. ***Tight temporal regulation of Nodal signalling is required for axial elongation and proper Axial patterning.*** (**A**) Nodal$^{-/-}$ *Gastruloids* pulsed with either DMSO or Chi (48-72h AA) following a pulse of the vehicle or 100ng/ml Nodal (24-48h) and (**B**) the quantification of morphology. Nodal pre-stimulation suppresses protrusions; Chi stimulation enhances an elongated phenotype but does not suppress protrusions. The wild-type phenotype can be rescued if Chi treated *Gastruloids* have been previously exposed to Nodal. Addition of Nodal at different time-points is not able to rescue the elongations (left and **fig. S11**). (**C**) The number of protrusions in each condition. Significance determined following Mann-Whitney U test with Bonferroni adjustment. (**D**) Immunofluorescence of Nodal$^{-/-}$ *Gastruloids* treated as indicated and stained at 120h with Hoechst (blue), Brachyury (Green) and CDX2 (Red). Nodal addition rescues axial patterning. Later addition of Nodal has less of an effect on the patterning (see **fig. S11**). Sample sizes (*n*) shown above part C.

Supplemental Materials and Methods

Immunofluorescence, Microscopy and data analysis: *Gastruloids* were fixed and stained for as required according to the protocol previously described (Baillie-Johnson et al., 2015). Hoechst3342 was used to mark the nuclei (see **table S2** for the antibodies used and their dilutions). Confocal z-stacks of Gastruloids were generated using an LSM700 (Zeiss) on a Zeiss Axiovert 200 M using a 40× EC Plan-NeoFluar 1.3 NA DIC oil-immersion objective. Hoechst3342, Alexa-488, -568 and -633 were sequentially excited with 405, 488, 555 and 639 nm diode lasers respectively as previously described (Turner et al., 2014). Data capture was carried out using Zen2010 v6 (Carl Zeiss Microscopy Ltd, Cambridge UK). The z-stacks were acquired for at least 4 *Gastruloids* per condition with a z-interval of 0.5µm. Images were analysed using the ImageJ image processing package FIJI (Schindelin et al., 2012).

Widefield, single-time point images of *Gastruloids* were acquired using a Zeiss AxioObserver.Z1 (Carl Zeiss, UK) in a humidified CO_2 incubator (5% CO_2, 37°C) with a 20x LD Plan-Neofluar 0.4 NA Ph2 objective with the correction collar set to image through plastic. Illumination was provided by an LED white-light system (Laser2000, Kettering, UK) in combination with filter cubes GFP-1828A-ZHE (Semrock, NY, USA), YFP-2427B-ZHE (Semrock, NY, USA) and Filter Set 45 (Carl Zeiss Microscopy Ltd. Cambridge, UK) used for GFP, YFP and RFP respectively, and emitted light recorded using a back-illuminated iXon888 Ultra EMCCD (Andor, UK). Images were analysed using FIJI (Schindelin et al., 2012) and plugins therein as previously described (Baillie-Johnson et al., 2015) and when required, images were stitched using the 'Pairwise Stitching' plugin in FIJI (Preibisch et al., 2009). Briefly, the fluorescence intensity was measured by a line of interest (LOI) drawn from the posterior to anterior region of the *Gastruloid* with the LOI width set to half the diameter of a typical *Gastruloid* at 48h (100px with the 20x objective). The background for each position was measured and subtracted from the fluorescence for each *Gastruloid*. Shape-descriptors were generated by converting brightfield images of Gastruloids to binary images and measuring them by particle detection in FIJI.

Fluorescence levels were normalised to the maximum obtained in following Chi stimulation, and the maximum length of each *Gastruloid* was rescaled 1 unit. Average fluorescence traces of *Gastruloids* ±S.D. are shown in the main figures, and the raw data and individual traces in the supplemental data. For live imaging experiments, each well of a 96-well plate containing individual *Gastruloids* were imaged as described above using both the 20x (24-72h) and the 10x (72-96h) objectives, and images captured every 20 min for a maximum of 96h (120h AA). All images were analysed in FIJI (Schindelin et al., 2012) using the LOI interpolator (Soroldoni et al., 2014) with the LOI set as described above.

Data processing and graph plotting was performed in the Jupyter IPython notebook environment (Kluyver et al., 2016; Perez and Granger, 2007) using the following principle modules: Matplotlib (Hunter, 2007; McDougall et al., 2016), NumPy & SciPy (Oliphant, 2007; Terrel et al., 2015a; Terrel et al., 2015b), *tifffile* (Silvester, 2015), Statsmodels (Fulton et al., 2014) and Pandas (Van den Bossche et al., 2015). All code is freely available upon request.

Statistical Analysis: Statistical analysis of the normalised fluorescence traces was performed in Matlab (Mathworks, 2016a) . Let $f_{c,i}(x)$ denote the signal intensity profile for T/Bra expression over the normalized length of the i^{th} *Gastruloid* in condition c; x denotes the coordinate along the normalized length of the i^{th} *Gastruloid* where $x = 0$ denotes the posterior end and $x = 1$ denotes

the anterior end. $\mu_0(x)$ and $\sigma_0(x)$ denote the mean and standard deviation, respectively, of the signal intensity profile for T/Bra expression over the normalised length of the control *Gastruloids*. We define a measure of assessing differences between intensity profiles, of a *Gastruloid* in a given condition and the control *Gastruloids*, similar to the root-mean-square deviation used to measure differences between values of an estimator and the values observed. We call this measure the *Normalised Root Square Distance* (η) and for the i^{th} *Gastruloid* in condition *c* it is defined as follows:

$$\eta_{c,i} = \sqrt{\sum_{j=1}^{N} \frac{(f_{c,i}(x_j) - \mu_0(x_j))^2}{\sigma_0^2(x_j)}}$$

where N denotes the maximum number of points (typically 100) defining the normalised length of the *Gastruloid*. As a physical interpretation of this measure, it can be seen that $\eta_{c,i} = 0$ means that the signal intensity profile for the i^{th} *Gastruloid* in condition *c* is identical to the mean intensity profile of the control *Gastruloids*. $\eta_{c,i} \leq 1$ means that the signal intensity profile for the i^{th} *Gastruloid* in condition *c* is within the standard deviation around the mean intensity profile of the control *Gastruloids*, thereby implying that the *Gastruloid* in condition *c* is similar to the control. Significance between treatments within each time-point was determined using a non-paired Student's t-test.

Gastruloid culture and application of specific signals: Aggregates of mouse ESCs were generated using an optimised version of the previously described protocol (Baillie-Johnson et al., 2015; van den Brink et al., 2014). Mouse ESCs harvested from tissue-culture flasks were centrifuged and washed twice in warm PBS. After the final wash, the pellet was resuspended in 3ml warm N2B27 and cell concentration determined using a Moxi™ Z automated cell counter with curve-fitting (Orflo Technologies). The number of cells required to generate *Gastruloids* of ~150µm in diameter by 48h (optimised for each cell line, ~300 cells; **table S3**) was then plated in 40µl droplets of N2B27 in round-bottomed low-adhesion 96-well plates. Counting cells after washing in PBS in this way instead of prior to the washes (as described previously (Baillie-Johnson et al., 2015; van den Brink et al., 2014)) results in the number of cells required for *Gastruloid* formation being ~100 fewer than previously described as fewer are lost during washing. See **table S3** for the number of cells required for each cell line.

In experiments which required the addition of specific factors to *Gastruloids* on the second day of aggregation (24-48h), 20µl medium was carefully removed with a multichannel pipette, and 20µl of N2B27 containing twice the concentration of the required factors was added. This method was preferable to the addition of smaller volumes containing higher concentrations of agonist/antagonists, as the data from these experiments showed more variation between *Gastruloids* (DAT, PB-J, AMA unpublished). Control experiments showed that replacement of half the medium at this stage did not significantly alter the ability of *Gastruloids* to respond to signals on the third day (DAT, PB-J, AMA unpublished). The next day, 150µl fresh N2B27 was added to each of the wells with a multichannel pipette and left for no more than 30 min to wash the *Gastruloids*; a time delay ensured that sample loss was prevented. Following washing, 150µl N2B27 containing the required factors was then applied. The small molecules used in this study and their concentrations are described in **table S4**.

Supplemental Movies:

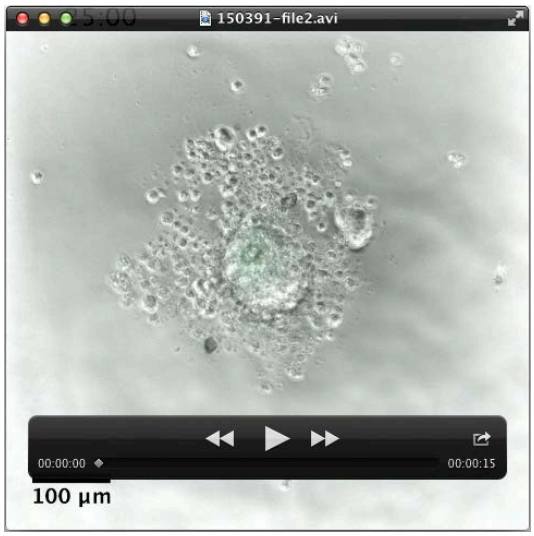

Movie 1. ***T/Bra::GFP expression in Gastruloids following DMSO treatment (48-72h AA).*** Gastruloids made from T/Bra::GFP mESCs stimulated with a mock pulse of DMSO and imaged by wide-field microscopy from 24h to 120h AA every 20 min. The 20x objective was used between 24 and 72h, followed by the 10x objective from 72h to the end of the experiment. Quantification of both the length and fluorescence as a function of time can be seen in **Fig. 3D** (top).

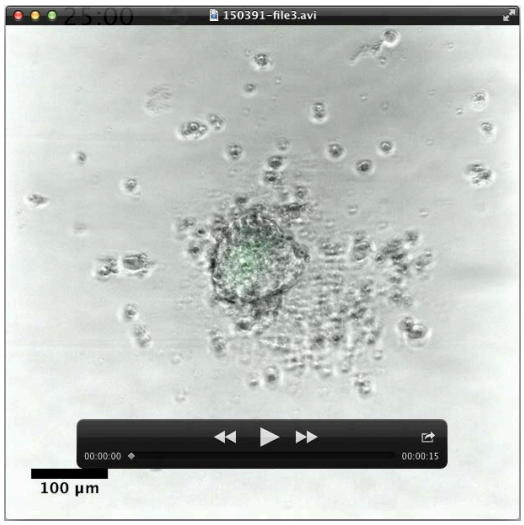

Movie 2. ***T/Bra::GFP expression in Gastruloids following Chi treatment (48-72h AA).*** Gastruloids made from T/Bra::GFP mESCs stimulated with a pulse of Chi and imaged by wide-field microscopy from 24h to 120h AA every 20 min. The 20x objective was used between 24 and 72h, followed by the 10x objective from 72h to the end of the experiment. Quantification of both the length and fluorescence as a function of time can be seen in **Fig. 3D** (bottom).

Supplemental Tables:

Tables S1-S5

Table S1. Expression phenotype of T/Bra::GFP mESCs. The proportion of T/Bra::GFP *Gastruloids* not expressing the reporter (No Expression) or displaying either Polarised or Ubiquitous expression at 24, 48 and 72h AA followed by a pulse of DMSO or Chi (72h). The standard deviation is shown in brackets and the number of *Gastruloids* analysed are shown.

	Condition	No Expression	Polarised	Ubiquitous	Spherical	Ovoid	Elongated	*n*
24h	N2B27	26.8 (21.5)	62.5 (16.1)	10.7 (15.2)	100.0 (0.0)	0.0 (0.0)	0.0 (0.0)	112
48h		23.7 (13.2)	74.1 (11.8)	2.2 (3.4)	67.0 (9.4)	33.0 (9.4)	0.0 (0.0)	140
72h	DMSO	3.6 (-)	89.3 (-)	7.1 (-)	10.7 (-)	85.7 (-)	3.6 (-)	28
	Chi	0.0 (-)	91.2 (11.7)	8.8 (11.7)	23.3 (18.2)	52.9 (18.1)	23.8 (26.3)	82

Table S2. Antibodies and their concentrations used for *Gastruloid* immunofluorescence with the associated supplier details.

		Species	Dilution	Cat. Number	Supplier
Primary	Brachyury	Goat	1:200	sc-17743	Santa Cruz Biotechnologies
	CDX2	Rabbit	1:200	MA5-14494	ThermoFisher
	GFP	Chicken	1:2000	A11122	Molecular Probes
	Nanog	Mouse	1:300	14-5761-80	e-Biosciences
	Sox2	Rabbit	1:200	AB5603	Millipore
	Sox17	Goat	1:200	AF1924	R&D Systems
Secondary	Goat-A633	Donkey	1:500	A21082	Molecular Probes
	Mouse-A568	Donkey	1:500	A10037	Molecular Probes
	Rabbit-A488	Donkey	1:500	A21206	Molecular Probes
	Hoechst3342	n/a	1:1000	H3570	Invitrogen (ThermoFisher)

Table S3. Cell lines used and numbers of cells required for *Gastruloid* culture. The average diameter of the *Gastruloids* at 48h AA is indicated with the standard deviation and the number of *Gastruloids* measured. ND: not determined.

Cell line	Reference	Cells/40µl	48h diameter (µm)
AR8::mCherry	(Serup et al., 2012)	450	182.7 ±17.3 (*n* = 83)
T/Bra::GFP	(Fehling et al., 2003)	300	161.0 ±26.2 (*n* = 222)
miR-290-mCherry/mir-302-eGFP (DRC)	(Parchem et al., 2014)	300-400	N.D.
GATA6::H2B-Venus	(Freyer et al., 2015)	300	154.2 ± (*n* = 10)
IBRE4-TA-Cerulean	(Serup et al., 2012)	300	152.6 ±12.2 (*n* = 39)
Nodal::YFP	(Papanayotou et al., 2014)	400	138.7 ±16.1 (*n* = 124)
Nodal$^{-/-}$ (FC-15)	(Camus et al., 2006)	300	181.6 ±23.7 (*n* = 251)
Sox17::GFP	(Niakan et al., 2010)	400	N.D.
TCF/LEF::mCherry (TLC2)	(Faunes et al., 2013; Ferrer-Vaquer et al., 2010)	200-300	194.9 ±20.7 (n = 56)

Table S4. Concentrations of Small molecules and recombinant proteins used in this study, and the associated supplier details.

	Reference	[Working]	[Stock]	Cat. Number	Supplier
CHI99201	(Ring et al., 2003)	3µM	10mM	4423	Tocris
DMH1	(Neely et al., 2012)	500nM	5mM	HY-12273	MedChem Express
IWP2	(Chen et al., 2009)	1µM	5mM	04-0034	Stemgent
SB431542	(Inman et al., 2002)	10µM	100mM	1614	Tocris
XAV939	(Huang et al., 2009)	1µM	10mM	HY-15147	MedChem Express
BMP4	-	1ng/ml	100µg/ml	314-BP	R&D Systems
DKK	-	200ng/ml	100µg/ml	5897-DK	
Nodal	-	1µg/ml	50µg/ml	1315-ND-025	
Wnt3a	-	100ng/ml	40µg/ml	1324-WN-002	

Table S5. Primer Sequences used for qRT-PCR.

Gene	Forward Sequence	Reverse Sequence
Axin2	CTAGACTACGGCCATCAGGAA	GCTGGCAGACAGGACATACA
Bmp4	CTCAAGGGAGTGGAGATTGG	ATGCTTGGGACTACGTTTGG
Cer1	GGAAACGCCATAAGTCTCCA	AGGGTCAGAATTTGCCATTG
Chordin	GTGCCTCTGCTCTGCTTCTT	AGGAGTTCGCATGGATATGG
Dkk1	CCATTCTGGCCAACTCTTTC	CATTCCCTCCCTTCCAATAAC
Fgf4	GGCCACTCCACAGAGATAGG	ACTTGGGCTCAAGCAGTAGG
Fgf5	GCTCAATGATCAGAAGGAGGA	TCAGCTGGTCTTGAATGAGG
Fgf8	AGGACTGCGTATTCACAGAGAT	CATGTACCAGCCCTCGTACT
Lefty1	AGGGTGCAGACCTGTAGCTG	GGAAGCAAAGAGCACACACA
Nodal	AGCCACTGTCCAGTTCTCCAG	GTGTCTGCCAAGCATACATCTC
Noggin	CCCATCATTTCCGAGTGTAAG	CTCGCTAGAGGGTGGTGAAA
ppia	TTACCCATCAAACCATTCCTTCTG	AACCCAAAGAACTTCAGTGAGAGC
SPRY4	ATGGTGGATGTCGATCCTGT	GGAGGGGGAGCTACAGAGAC
T/Bra	CTGGGAGCTCAGTTCTTTCG	GTCCACGAGGCTATGAGGAG
Wnt3	CTAATGCTGGCTTGACGAGG	ACATGGTAGAGAGTGCAGGC
Wnt3a	CATACAGGAGTGTGCCTGGA	AATCCAGTGGTGGGTGGATA

Supplementary Figures:

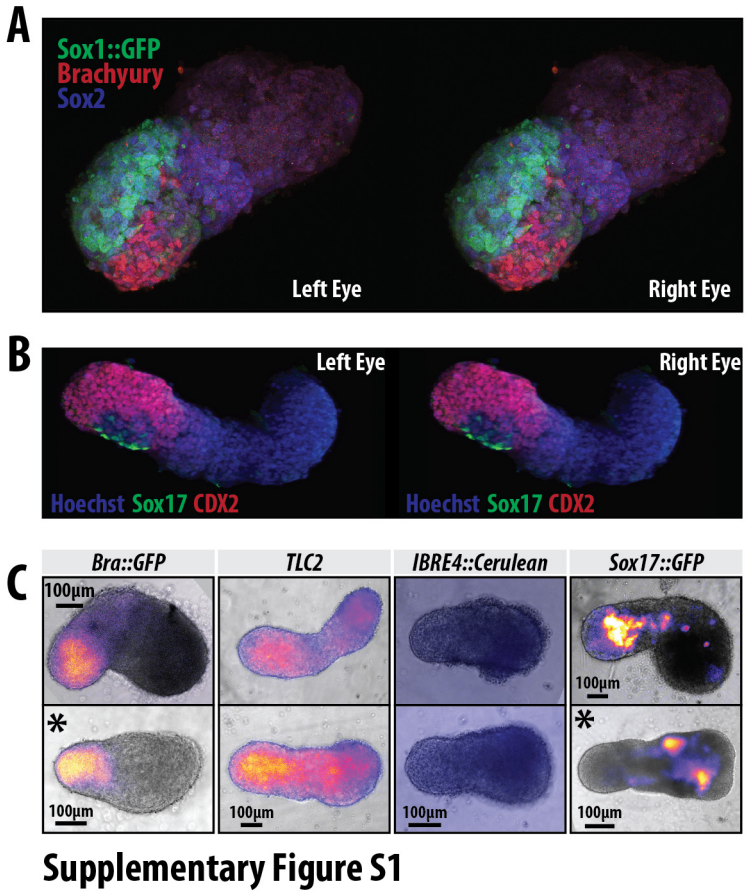

Supplementary Figure S1

Fig. S1. ***Expression of axial markers in Gastruloids.*** (**A,B**) Stereo images of *Gastruloids* from Nodal::YFP (**A**) and Sox1::GFP (**B**) mESCs stained for anti YFP (green) and either CDX2 (**A**) or T/Bra (**B**) (red) at 120h AA. (**C**) Further examples of *Gastruloids* from the indicated cell lines at 120h AA (see **Fig. 1C-F**). Asterisks represent *Gastruloids* from a different replicate experiment.

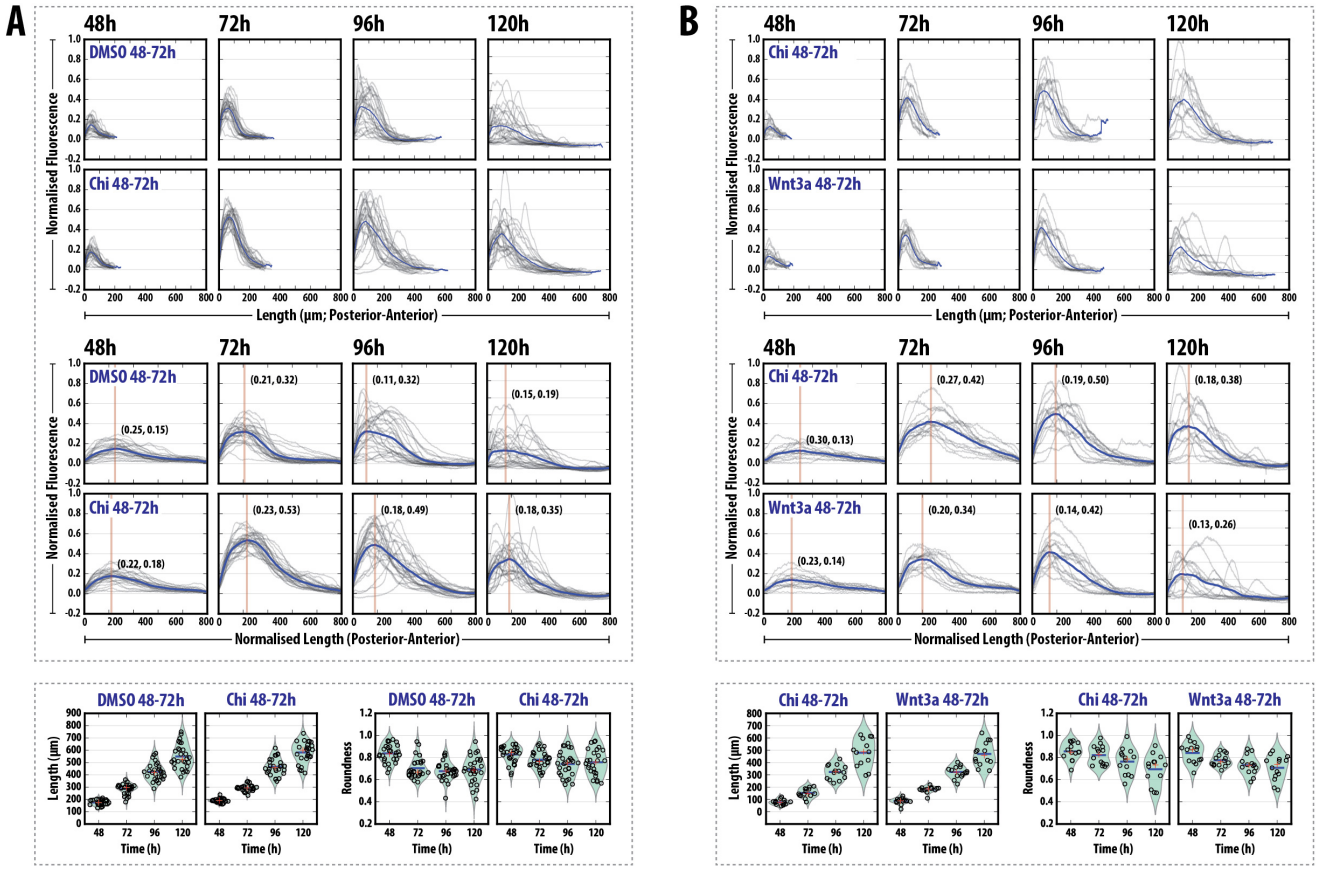

Supplementary Figure S2

Fig. S2. ***Quantification of T/Bra::GFP Gastruloid Fluorescence***. (**A,B**) Expression of the T/Bra::GFP reporter at the indicated time-points (DMSO or Chi (**A**) and Chi or Wnt3a (**B**) stimulation) prior to length normalisation (top) and following normalisation of the length to from 0 to 1 (middle). The bottom panel in each shows the length and roundness of the *Gastruloids* in the indicated conditions.

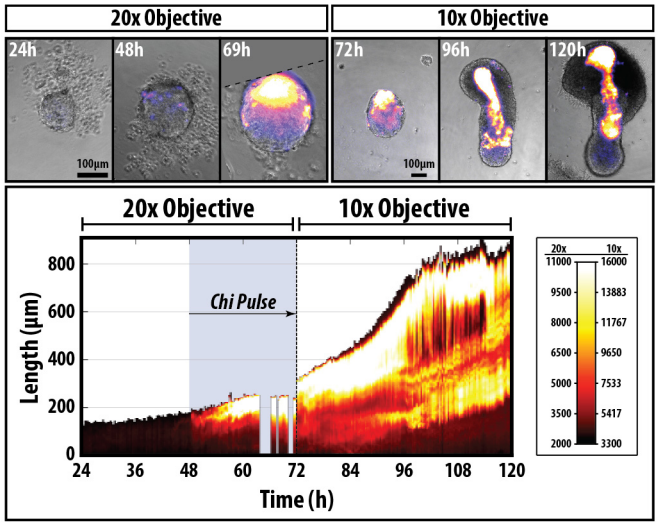

Supplementary Figure S3

Fig. S3. ***Sox17::GFP is expressed anterior to the elongating region of the Gastruloids at 120h AA*****.** *Gastruloids* made from Sox17::GFP mESCs were grown in standard conditions (see materials and methods), pulsed with Chi between 48 and 72h AA and imaged by widefield microscopy continuously for 96h with a time-interval of 20 min. Top row displays still images from the time-lapse experiment using the 20x objective (24h, 48h, 69h) and the 10x objective (72, 96, 120h; *n* = 21). Quantification of the length and fluorescence along the 'mid-line' of the *Gastruloid* every 20 min (bottom row; see materials and methods in main text and supplemental for explanation of quantification). Colour map represents the fluorescence and the time of Chi addition indicated. Gaps in the quantification are due to the *Gastruloid* leaving the field of view, an example of which is indicated at the 69h time-point (top row) with the hashed line representing the edge of the field of view. The posterior of the *Gastruloid* is orientated towards the base of the figures, as time-lapse imaging revealed the Sox17::GFP negative region was absent from the elongating, posterior region. Scale bar indicates 100µm in all images.

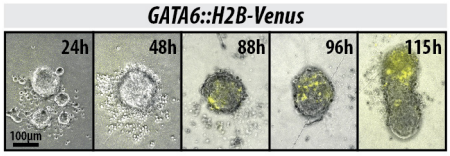

Supplementary Figure S4

Fig. S4. ***Expression of GATA6::H2BVenus in Gastruloids over time.*** *Gastruloids* made from GATA6::H2B-Venus mESCs were grown in standard conditions and imaged by widefield microscopy continuously for 115h with a time-interval of 20 min (*n* = 9). GATA6 expression is apparent at approximately 88h AA and becomes restricted to the anterior region of the *Gastruloid* (as judged by morphology).

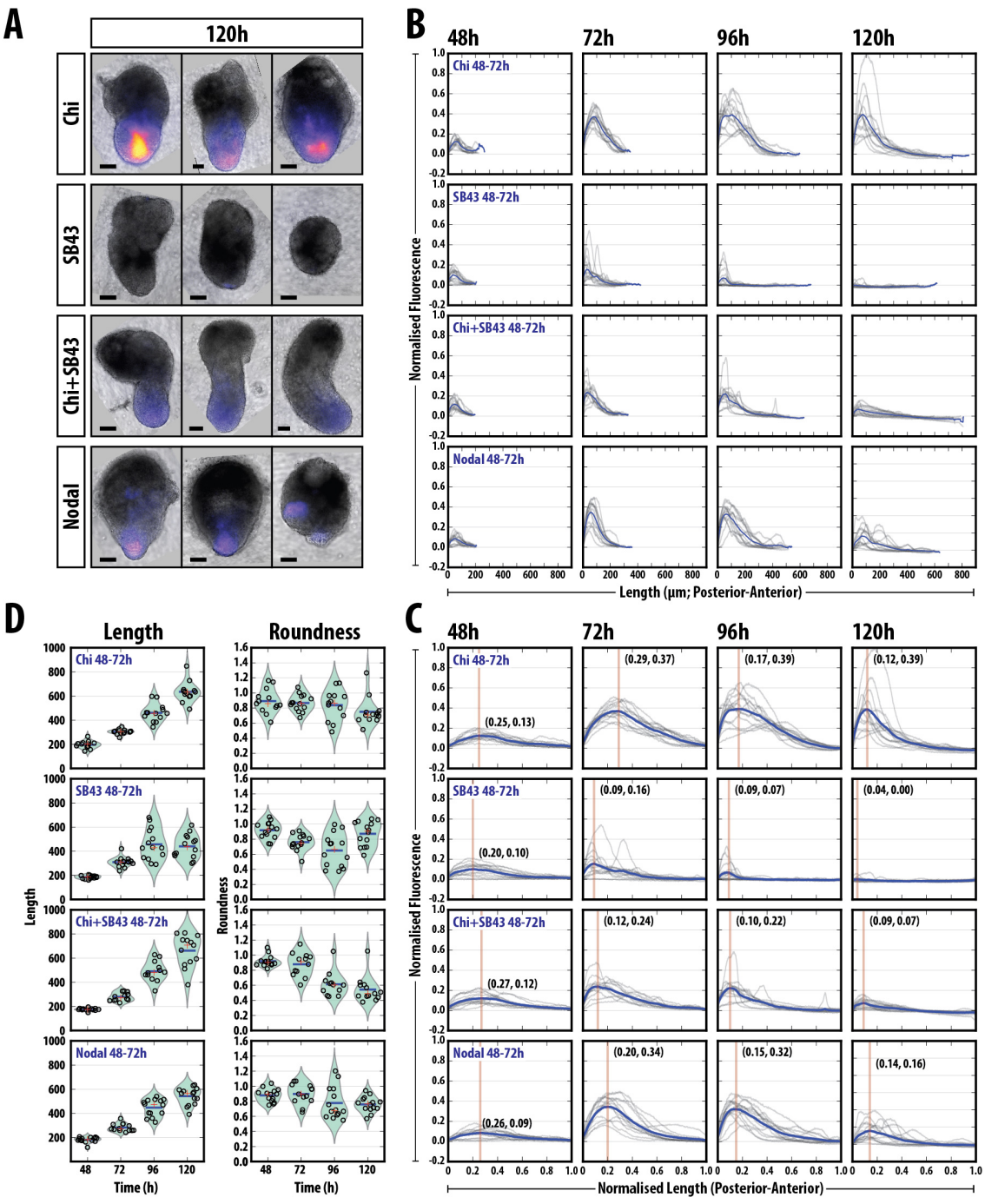

Supplementary Figure S5

Fig. S5. ***Quantifying the Effect of modulating Nodal signalling in Gastruloids (#1).*** (**A**) examples of T/Bra::GFP reporter expression in *Gastruloids* treated as indicated. (**B, C, D**) Quantification of the reporter expression at the indicated time-points prior to length normalisation (**B**) and following normalisation of the length from 0 and 1 (**C**). The length and roundness of the Gastruloids in the indicated conditions (**D**). (**E**) Statistical analysis of the normalised fluorescence traces showing (**upper panel**) the *normalised root square distance* as a measure of the heterogeneity within each condition of the *Gastruloids* in the indicated conditions (see supplemental materials and methods), and (**lower panel**) the *significance matrix* showing the pairwise *p* values between individual treatments per time-point. Significance determined by non-paired Student's t-test; *p*-values highlighted in red indicate $p < 0.05$. Vertical line and coordinates in **C** correspond to the location and position of the peak maximum. Scale bar indicates 100 μm.

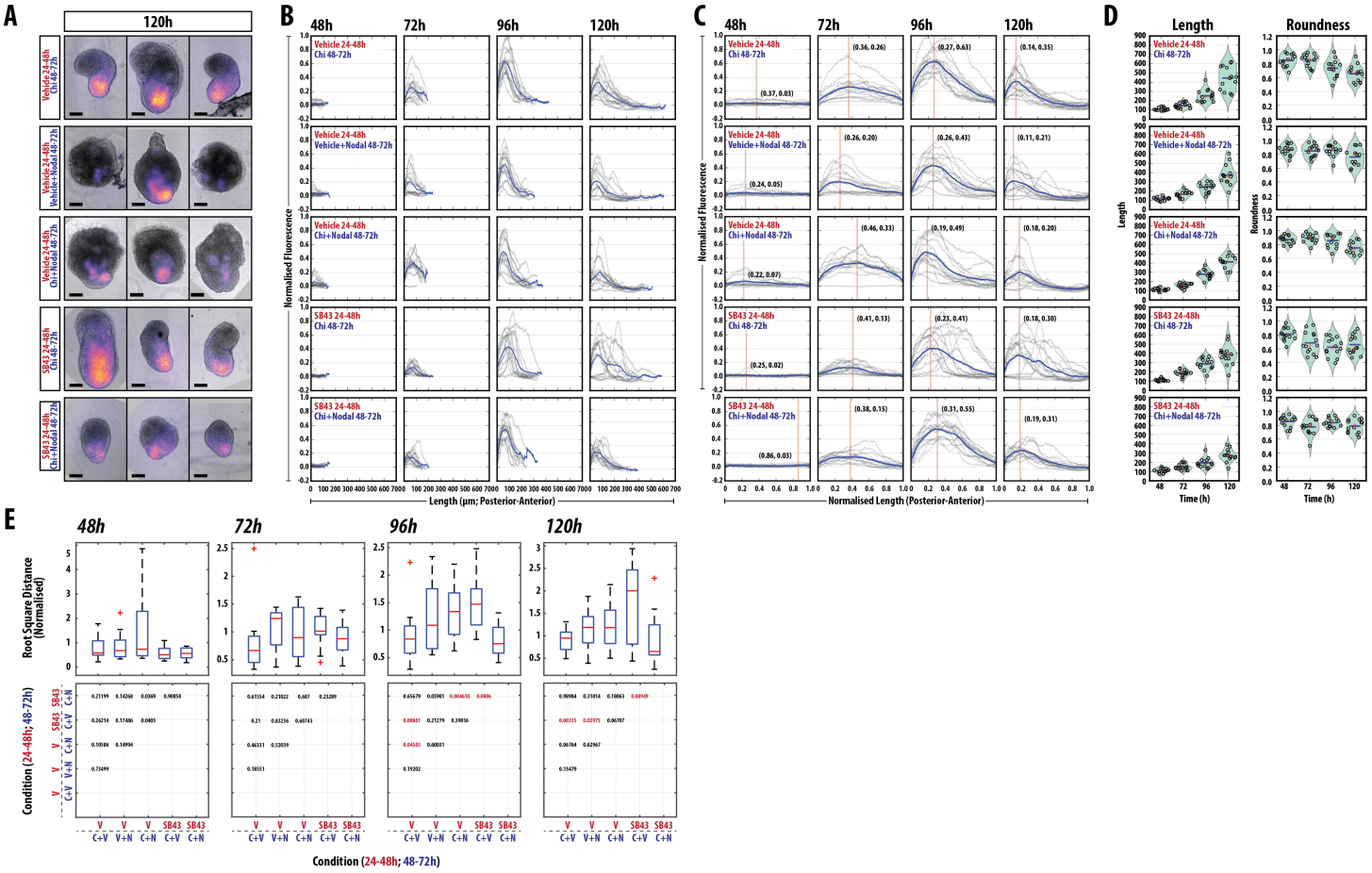

Supplementary Figure S6

Fig. S6. ***Quantifying the Effect of modulating Nodal signalling in Gastruloids (#2).*** (**A**) examples of T/Bra::GFP reporter expression in *Gastruloids* treated as indicated. (**B, C, D**) Quantification of the reporter expression prior to length normalisation (**B**) and following normalisation of the length from 0 and 1 (**C**). The length and roundness of the Gastruloids in the indicated conditions (**D**). (**E**) Statistical analysis of the normalised fluorescence traces showing (**upper panel**) the *normalised root square distance* as a measure of the heterogeneity within each condition of the *Gastruloids* in the indicated conditions (see supplemental materials and methods), and (**lower panel**) the *significance matrix* showing the pairwise *p* values between individual treatments per time-point. Significance determined by non-paired Student's t-test; *p*-values highlighted in red indicate $p < 0.05$. Vertical line and coordinates in C correspond to the location and position of the peak maximum. Scale bar indicates 100 µm.

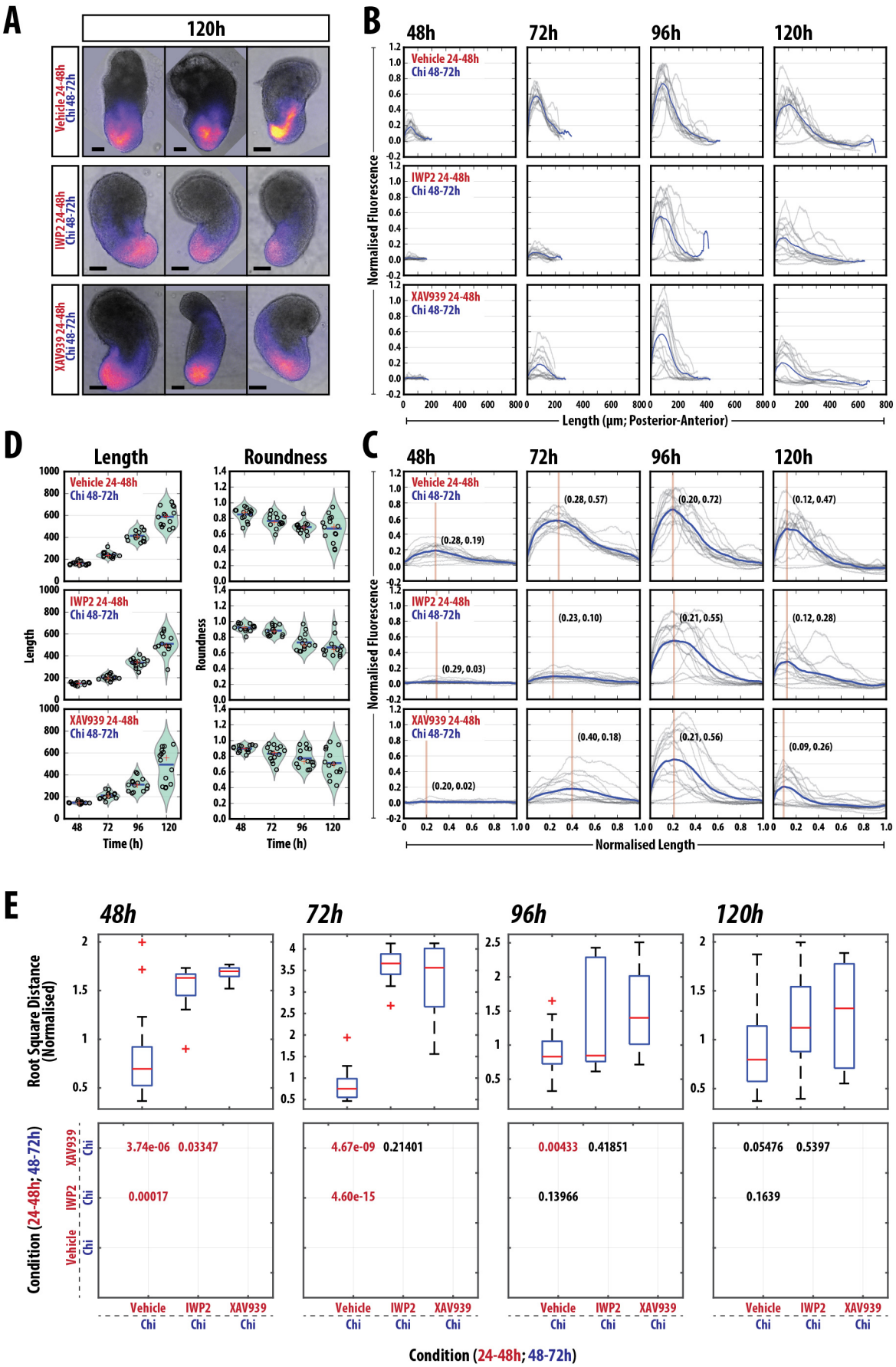

Supplementary Figure S7

Fig. S7. ***Quantifying the Effect of modulating Wnt/β-Catenin signalling in Gastruloids (#1).*** (**A**) examples of T/Bra::GFP reporter expression in *Gastruloids* treated as indicated. (**B, C, D**) Quantification of the reporter expression prior to length normalisation (**B**) and following normalisation of the length from 0 and 1 (**C**). The length and roundness of the Gastruloids in the indicated conditions (**D**). (**E**) Statistical analysis of the normalised fluorescence traces showing (**upper panel**) the *normalised root square distance* as a measure of the heterogeneity within each condition of the *Gastruloids* in the indicated conditions (see supplemental materials and methods), and (**lower panel**) the *significance matrix* showing the pairwise *p* values between individual treatments per time-point. Significance determined by non-paired Student's t-test; *p*-values highlighted in red indicate $p < 0.05$. Vertical line and coordinates in C correspond to the location and position of the peak maximum. Scale bar indicates 100 µm.

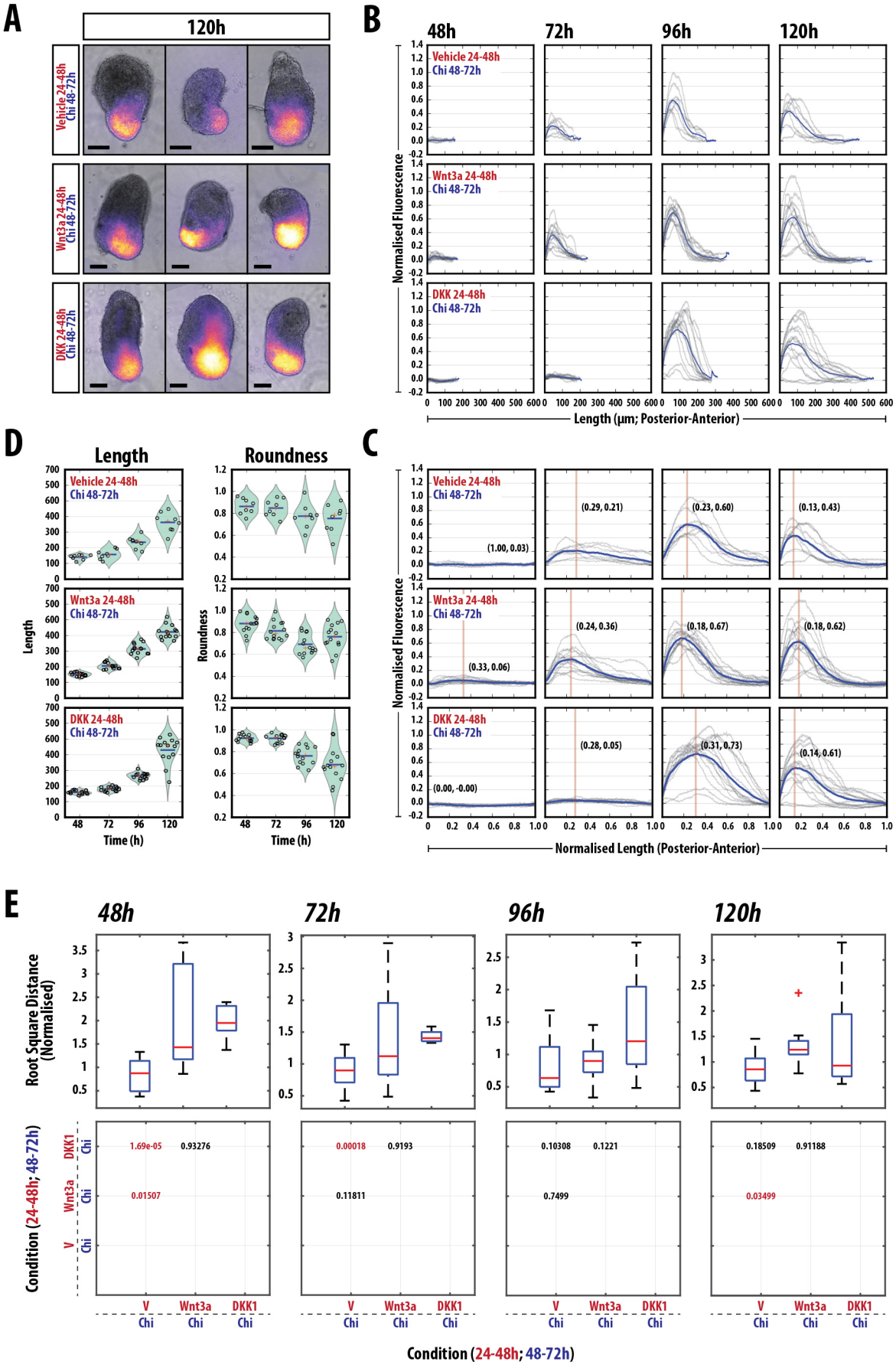

Supplementary Figure S8

Fig. S8. ***Quantifying the Effect of modulating Wnt/β-Catenin signalling in Gastruloids (#2).*** (**A**) examples of T/Bra::GFP reporter expression in *Gastruloids* treated as indicated. (**B, C, D**) Quantification of the reporter expression prior to length normalisation (**B**) and following normalisation of the length from 0 and 1 (**C**). The length and roundness of the Gastruloids in the indicated conditions (**D**). (**E**) Statistical analysis of the normalised fluorescence traces showing (**upper panel**) the *normalised root square distance* as a measure of the heterogeneity within each condition of the *Gastruloids* in the indicated conditions (see supplemental materials and methods), and (**lower panel**) the *significance matrix* showing the pairwise *p* values between individual treatments per time-point. Significance determined by non-paired Student's t-test; *p*-values highlighted in red indicate $p < 0.05$. Vertical line and coordinates in C correspond to the location and position of the peak maximum. Scale bar indicates 100 µm.

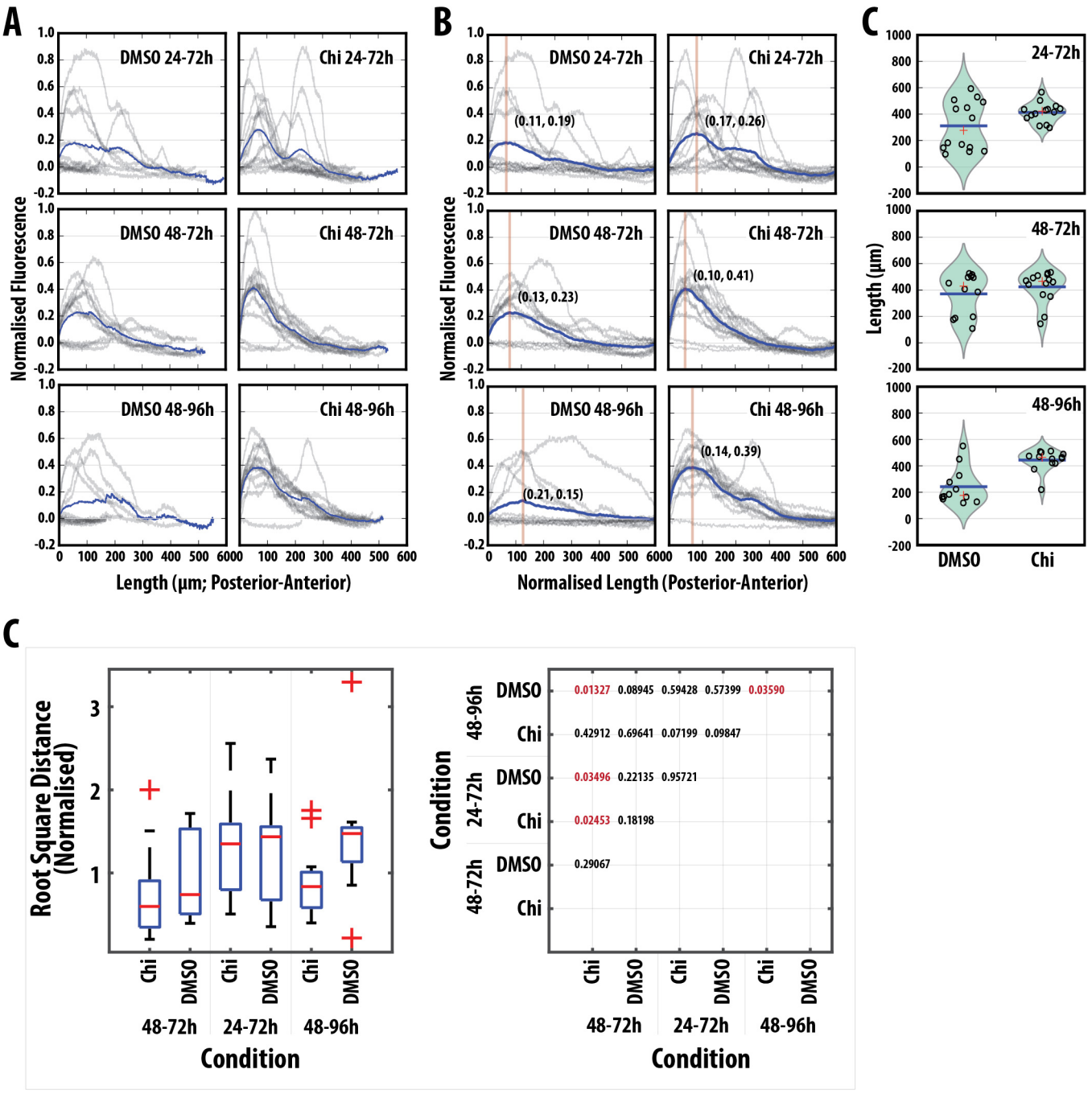

Supplementary Figure S9

Fig. S9. ***Quantifying the Effect of modulating the time of Wnt/β-Catenin signalling in Gastruloids.*** (**A,B**) Quantification of the reporter expression prior to length normalisation (**A**) and following normalisation of the length from 0 and 1 (**B**). The length and roundness of the Gastruloids in the indicated conditions (**C**). (**D**) Statistical analysis of the normalised fluorescence traces showing (**upper panel**) the *normalised root square distance* as a measure of the heterogeneity within each condition of the *Gastruloids* in the indicated conditions (see supplemental materials and methods), and (**lower panel**) the *significance matrix* showing the pairwise *p* values between individual treatments per time-point. Significance determined by non-paired Student's t-test; *p*-values highlighted in red indicate $p < 0.05$. Vertical line and coordinates in **B** correspond to the location and position of the peak maximum.

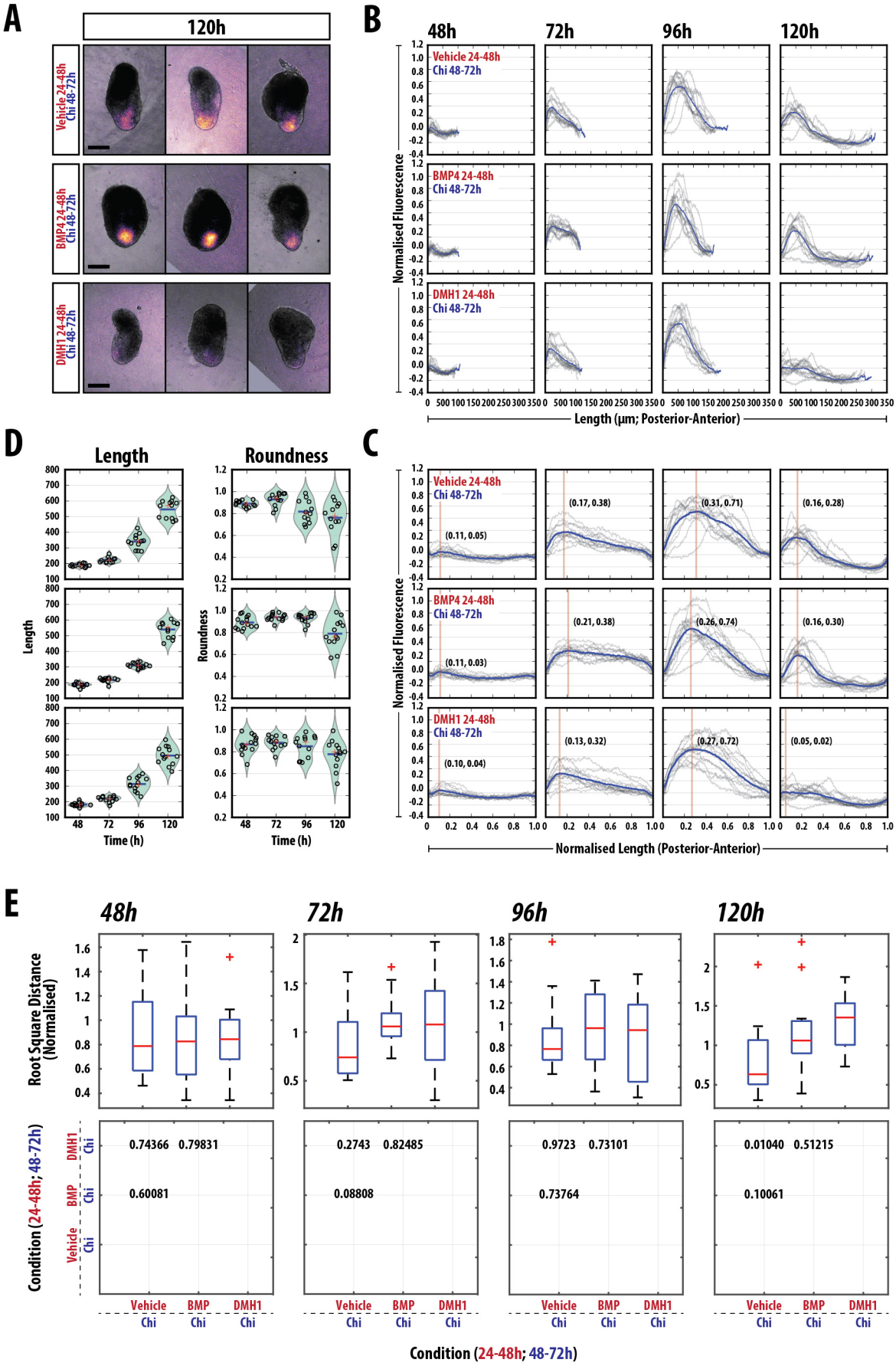

Supplementary Figure S10

Fig. S10. ***Quantifying the Effect of modulating BMP signalling in Gastruloids.*** (**A**) examples of T/Bra::GFP reporter expression in *Gastruloids* treated as indicated. (**B, C, D**) Quantification of the reporter expression prior to length normalisation (**B**) and following normalisation of the length from 0 and 1 (**C**). The length and roundness of the Gastruloids in the indicated conditions (**D**). (**E**) Statistical analysis of the normalised fluorescence traces showing (**upper panel**) the *normalised root square distance* as a measure of the heterogeneity within each condition of the *Gastruloids* in the indicated conditions (see supplemental materials and methods), and (**lower panel**) the *significance matrix* showing pairwise *p* values between individual treatments per time-point. Significance determined by non-paired Student's t-test; *p*-values highlighted in red indicate $p < 0.05$. Vertical line and coordinates in C correspond to the location and position of the peak maximum. Scale bar indicates 100 μm.

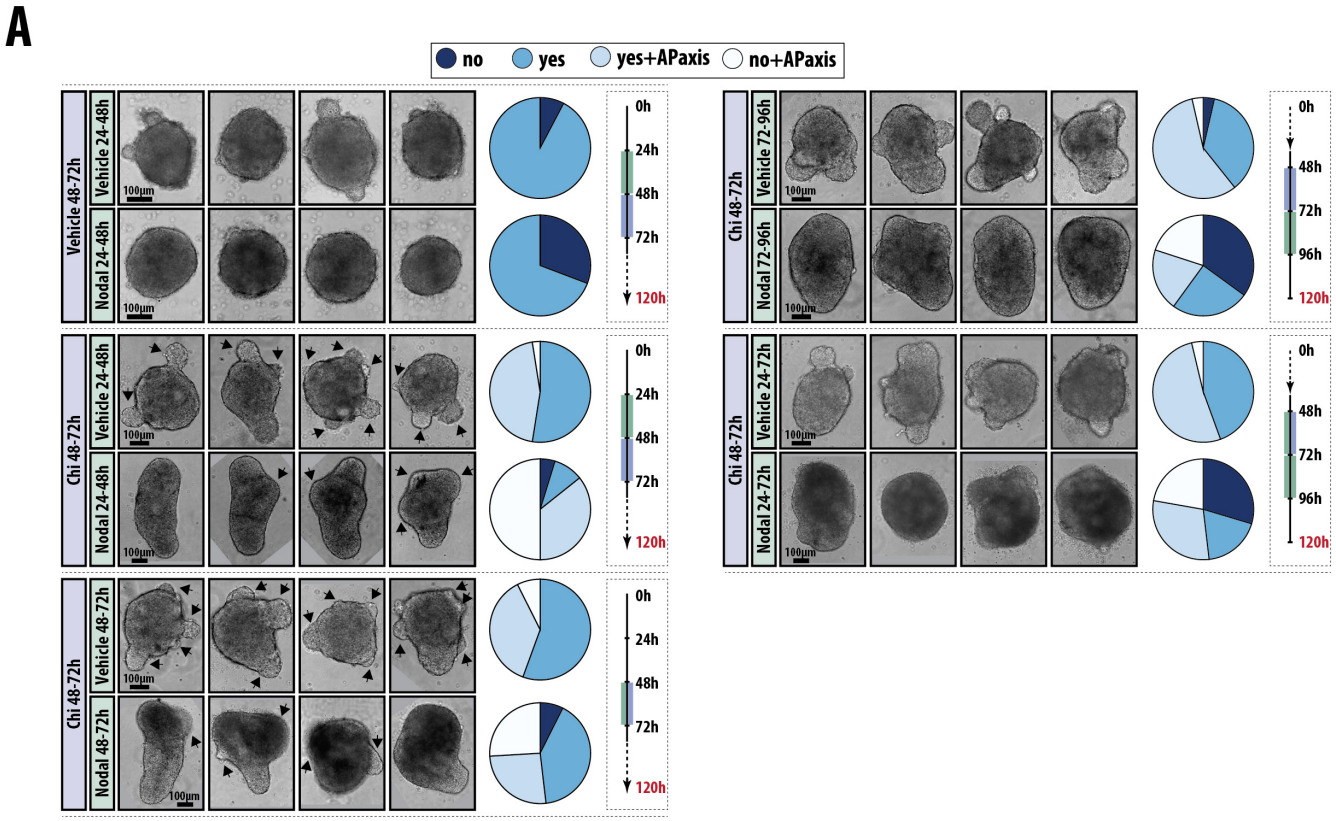

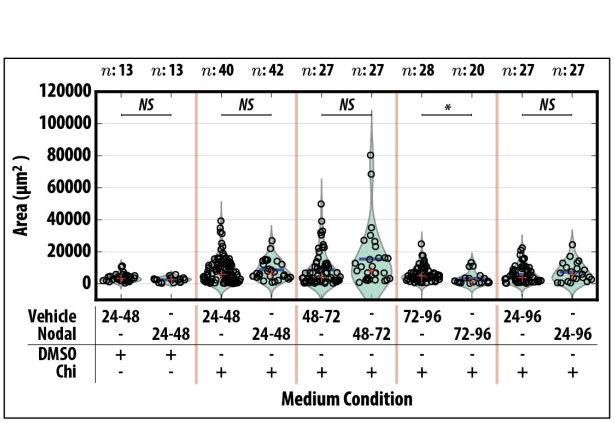

Supplementary Figure S11

Fig. S11. ***Modulation of Nodal signalling in Nodal mutants***. (**A**) Examples of *Gastruloids* treated with Chi between 48 and 72h with a 24h pulse of either vehicle or Nodal at the indicated time-points (24-48h, 48-72h, 72-96h and 24-72h AA). Pie charts indicated the proportion which do not show protrusions ('no'), show protrusions ('yes'), show protrusions with a defined AP axis ('yes+APaxis') or don't show protrusions but still have a defined AP axis ('no+APaxis'). The schematic for the time-course is indicated on the right of the panel. (**B**) Quantification of the area of the protrusions in the indicated experimental conditions. Significance determined following Mann-Whitney U test followed by Bonferroni adjustment, comparing selected columns. Asterisk indicates $p < 0.05$.

References from Supplemental Material

Baillie-Johnson, P., van den Brink, S. C., Balayo, T., Turner, D. A. and Martinez Arias, A. (2015). Generation of Aggregates of Mouse Embryonic Stem Cells that Show Symmetry Breaking, Polarization and Emergent Collective Behaviour In Vitro. *J Vis Exp*.

Camus, A., Perea-Gomez, A., Moreau, A. and Collignon, J. (2006). Absence of Nodal signaling promotes precocious neural differentiation in the mouse embryo. *Developmental Biology* **295**, 743–755.

Chen, B., Dodge, M. E., Tang, W., Lu, J., Ma, Z., Fan, C.-W., Wei, S., Hao, W., Kilgore, J., Williams, N. S., et al. (2009). Small molecule–mediated disruption of Wnt-dependent signaling in tissue regeneration and cancer. *Nat Chem Biol* **5**, 100–107.

Faunes, F., Hayward, P., Descalzo, S. M., Chatterjee, S. S., Balayo, T., Trott, J., Christoforou, A., Ferrer-Vaquer, A., Hadjantonakis, A.-K., Dasgupta, R., et al. (2013). A membrane-associated β-catenin/Oct4 complex correlates with ground-state pluripotency in mouse embryonic stem cells. *Development* **140**, 1171–1183.

Fehling, H. J., Lacaud, G., Kubo, A., Kennedy, M., Robertson, S., Keller, G. and Kouskoff, V. (2003). Tracking mesoderm induction and its specification to the hemangioblast during embryonic stem cell differentiation. *Development* **130**, 4217–4227.

Ferrer-Vaquer, A., Piliszek, A., Tian, G., Aho, R. J., Dufort, D. and Hadjantonakis, A.-K. (2010). A sensitive and bright single-cell resolution live imaging reporter of Wnt/ß-catenin signaling in the mouse. *BMC Dev Biol* **10**, 121.

Freyer, L., Schröter, C., Saiz, N., Schrode, N., Nowotschin, S., Martinez Arias, A. and Hadjantonakis, A.-K. (2015). A loss-of-function and H2B-Venus transcriptional reporter allele for Gata6 in mice. *BMC Dev Biol* **15**, 38.

Fulton, C., Perktold, J., Seabold, S., Gommers, R., Arel-Bundock, V. and McKinney, W. (2014). Statsmodels. BSD.

Huang, S.-M. A., Mishina, Y. M., Liu, S., Cheung, A., Stegmeier, F., Michaud, G. A., Charlat, O., Wiellette, E., Zhang, Y., Wiessner, S., et al. (2009). Tankyrase inhibition stabilizes axin and antagonizes Wnt signalling. *Nature* **461**, 614–620.

Hunter, J. D. (2007). Matplotlib: A 2D Graphics Environment. *Comput. Sci. Eng.* **9**, 90–95.

Inman, G. J., Nicolás, F. J., Callahan, J. F., Harling, J. D., Gaster, L. M., Reith, A. D., Laping, N. J. and Hill, C. S. (2002). SB-431542 is a potent and specific inhibitor of transforming growth factor-beta superfamily type I activin receptor-like kinase (ALK) receptors ALK4, ALK5, and ALK7. *Mol. Pharmacol.* **62**, 65–74.

Kluyver, T., Ragan-Kelley, B., Pérez, F., Granger, B., Bussonnier, M., Frederic, J., Kelley, K., Hamrick, J., Grout, J., Corlay, S., et al. (2016). *Jupyter Notebooks—a publishing format for reproducible computational workflows*. (eds. Loizides, F. and Schmidt, C. Positioning and Power in Academic Publishing: Players, Agents and Agendas.

McDougall, D., Firing, E., Perez, F., Thomas, I., Ivanov, P., Nielsen, J. H., Seppänen, J. K., Kniazev,

N., Droettboom, M., Fitzpatrick, M., et al. (2016). Matplotlib.

Neely, M. D., Litt, M. J., Tidball, A. M., Li, G. G., Aboud, A. A., Hopkins, C. R., Chamberlin, R., Hong, C. C., Ess, K. C. and Bowman, A. B. (2012). DMH1, a highly selective small molecule BMP inhibitor promotes neurogenesis of hiPSCs: comparison of PAX6 and SOX1 expression during neural induction. *ACS Chem Neurosci* **3**, 482–491.

Niakan, K. K., Ji, H., Eggan, K.12 (2010). Sox17 promotes differentiation in mouse embryonic stem cells by directly regulating extraembryonic gene expression and indirectly antagonizing self-renewal. *Genes & Development* **24**, 312–326.

Oliphant, T. E. (2007). Python for Scientific Computing. *Comput. Sci. Eng.* **9**, 10–20.

Papanayotou, C., Benhaddou, A., Camus, A., Perea-Gomez, A., Jouneau, A., Mezger, V., Langa, F., Ott, S., Sabéran-Djoneidi, D. and Collignon, J. (2014). A novel nodal enhancer dependent on pluripotency factors and smad2/3 signaling conditions a regulatory switch during epiblast maturation. *Plos Biol* **12**, e1001890.

Parchem, R. J., Ye, J., Judson, R. L., LaRussa, M. F., Krishnakumar, R., Blelloch, A., Oldham, M. C. and Blelloch, R. (2014). Two miRNA clusters reveal alternative paths in late-stage reprogramming. *Cell Stem Cell* **14**, 617–631.

Perez, F. and Granger, B. E. (2007). IPython: A System for Interactive Scientific Computing. *Comput. Sci. Eng.* **9**, 21–29.

Preibisch, S., Saalfeld, S. and Tomancak, P. (2009). Globally optimal stitching of tiled 3D microscopic image acquisitions. *Bioinformatics* **25**, 1463–1465.

Ring, D. B., Johnson, K. W., Henriksen, E. J., Nuss, J. M., Goff, D., Kinnick, T. R., Ma, S. T., Reeder, J. W., Samuels, I., Slabiak, T., et al. (2003). Selective Glycogen Synthase Kinase 3 Inhibitors Potentiate Insulin Activation of Glucose Transport and Utilization In Vitro and In Vivo. *Diabetes* **52**, 588–595.

Schindelin, J., Arganda-Carreras, I., Frise, E., Kaynig, V., Longair, M., Pietzsch, T., Preibisch, S., Rueden, C., Saalfeld, S. and Schmid, B. (2012). Fiji: an open-source platform for biological-image analysis. *Nature Methods* **9**, 676–682.

Serup, P., Gustavsen, C., Klein, T., Potter, L. A., Lin, R., Mullapudi, N., Wandzioch, E., Hines, A., Davis, A., Bruun, C., et al. (2012). Partial promoter substitutions generating transcriptional sentinels of diverse signaling pathways in embryonic stem cells and mice. *Dis Model Mech* **5**, 956–966.

Silvester, S. (2015). Tifffile. BSD.

Soroldoni, D., Jörg, D. J., Morelli, L. G., Richmond, D. L., Schindelin, J., Jülicher, F. and Oates, A. C. (2014). Genetic oscillations. A Doppler effect in embryonic pattern formation. *Science* **345**, 222–225.

Terrel, A. R., Harris, C., Cournapeau, D., Jamie, Wiebe, M., Smith, N. J., Pitrou, A., Virtanen, P., Gommers, R., Kern, R., et al. (2015a). NumPy. BSD.

Terrel, A. R., Harris, C., Cournapeau, D., Laxalde, D., Burovski, E., Moore, E., Pedregosa, F.,

Varoquax, G., Henriksen, I., Jamie, et al. (2015b). SciPy. BSD.

Turner, D. A., Rué, P., Mackenzie, J. P., Davies, E. and Martinez Arias, A. (2014). Brachyury cooperates with Wnt/β-Catenin signalling to elicit Primitive Streak like behaviour in differentiating mouse ES cells. *BMC Biology* **12**, 63.

Van den Bossche, J., Hoyer, S. and McKinney, W. (2015). Pandas. BSD.

van den Brink, S. C., Baillie-Johnson, P., Balayo, T., Hadjantonakis, A.-K., Nowotschin, S., Turner, D. A. and Martinez Arias, A. (2014). Symmetry breaking, germ layer specification and axial organisation in aggregates of mouse embryonic stem cells. *Development* **141**, 4231–4242.

Supplemental Materials and Methods

Immunofluorescence, Microscopy and data analysis: *Gastruloids* were fixed and stained for as required according to the protocol previously described (Baillie-Johnson et al., 2015). Hoechst3342 was used to mark the nuclei (see **table S2** for the antibodies used and their dilutions). Confocal z-stacks of Gastruloids were generated using an LSM700 (Zeiss) on a Zeiss Axiovert 200 M using a 40× EC Plan-NeoFluar 1.3 NA DIC oil-immersion objective. Hoechst3342, Alexa-488, -568 and -633 were sequentially excited with 405, 488, 555 and 639 nm diode lasers respectively as previously described (Turner et al., 2014). Data capture was carried out using Zen2010 v6 (Carl Zeiss Microscopy Ltd, Cambridge UK). The z-stacks were acquired for at least 4 *Gastruloids* per condition with a z-interval of 0.5µm. Images were analysed using the ImageJ image processing package FIJI (Schindelin et al., 2012).

Widefield, single-time point images of *Gastruloids* were acquired using a Zeiss AxioObserver.Z1 (Carl Zeiss, UK) in a humidified CO_2 incubator (5% CO_2, 37°C) with a 20x LD Plan-Neofluar 0.4 NA Ph2 objective with the correction collar set to image through plastic. Illumination was provided by an LED white-light system (Laser2000, Kettering, UK) in combination with filter cubes GFP-1828A-ZHE (Semrock, NY, USA), YFP-2427B-ZHE (Semrock, NY, USA) and Filter Set 45 (Carl Zeiss Microscopy Ltd. Cambridge, UK) used for GFP, YFP and RFP respectively, and emitted light recorded using a back-illuminated iXon888 Ultra EMCCD (Andor, UK). Images were analysed using FIJI (Schindelin et al., 2012) and plugins therein as previously described (Baillie-Johnson et al., 2015) and when required, images were stitched using the 'Pairwise Stitching' plugin in FIJI (Preibisch et al., 2009). Briefly, the fluorescence intensity was measured by a line of interest (LOI) drawn from the posterior to anterior region of the *Gastruloid* with the LOI width set to half the diameter of a typical *Gastruloid* at 48h (100px with the 20x objective). The background for each position was measured and subtracted from the fluorescence for each *Gastruloid*. Shape-descriptors were generated by converting brightfield images of Gastruloids to binary images and measuring them by particle detection in FIJI.

Fluorescence levels were normalised to the maximum obtained in following Chi stimulation, and the maximum length of each *Gastruloid* was rescaled 1 unit. Average fluorescence traces of *Gastruloids* ±S.D. are shown in the main figures, and the raw data and individual traces in the supplemental data. For live imaging experiments, each well of a 96-well plate containing individual *Gastruloids* were imaged as described above using both the 20x (24-72h) and the 10x (72-96h) objectives, and images captured every 20 min for a maximum of 96h (120h AA). All images were analysed in FIJI (Schindelin et al., 2012) using the LOI interpolator (Soroldoni et al., 2014) with the LOI set as described above.

Data processing and graph plotting was performed in the Jupyter IPython notebook environment (Kluyver et al., 2016; Perez and Granger, 2007) using the following principle modules: Matplotlib (Hunter, 2007; McDougall et al., 2016), NumPy & SciPy (Oliphant, 2007; Terrel et al., 2015a; Terrel et al., 2015b), *tifffile* (Silvester, 2015), Statsmodels (Fulton et al., 2014) and Pandas (Van den Bossche et al., 2015). All code is freely available upon request.

Statistical Analysis: Statistical analysis of the normalised fluorescence traces was performed in Matlab (Mathworks, 2016a) . Let $f_{c,i}(x)$ denote the signal intensity profile for T/Bra expression over the normalized length of the i^{th} *Gastruloid* in condition c; x denotes the coordinate along the normalized length of the i^{th} *Gastruloid* where $x = 0$ denotes the posterior end and $x = 1$ denotes

the anterior end. $\mu_0(x)$ and $\sigma_0(x)$ denote the mean and standard deviation, respectively, of the signal intensity profile for T/Bra expression over the normalised length of the control *Gastruloids*. We define a measure of assessing differences between intensity profiles, of a *Gastruloid* in a given condition and the control *Gastruloids*, similar to the root-mean-square deviation used to measure differences between values of an estimator and the values observed. We call this measure the *Normalised Root Square Distance* (η) and for the i^{th} *Gastruloid* in condition *c* it is defined as follows:

$$\eta_{c,i} = \sqrt{\sum_{j=1}^{N} \frac{(f_{c,i}(x_j) - \mu_0(x_j))^2}{\sigma_0^2(x_j)}}$$

where N denotes the maximum number of points (typically 100) defining the normalised length of the *Gastruloid*. As a physical interpretation of this measure, it can be seen that $\eta_{c,i} = 0$ means that the signal intensity profile for the i^{th} *Gastruloid* in condition *c* is identical to the mean intensity profile of the control *Gastruloids*. $\eta_{c,i} \leq 1$ means that the signal intensity profile for the i^{th} *Gastruloid* in condition *c* is within the standard deviation around the mean intensity profile of the control *Gastruloids*, thereby implying that the *Gastruloid* in condition *c* is similar to the control. Significance between treatments within each time-point was determined using a non-paired Student's t-test.

Gastruloid culture and application of specific signals: Aggregates of mouse ESCs were generated using an optimised version of the previously described protocol (Baillie-Johnson et al., 2015; van den Brink et al., 2014). Mouse ESCs harvested from tissue-culture flasks were centrifuged and washed twice in warm PBS. After the final wash, the pellet was resuspended in 3ml warm N2B27 and cell concentration determined using a Moxi™ Z automated cell counter with curve-fitting (Orflo Technologies). The number of cells required to generate *Gastruloids* of ~150µm in diameter by 48h (optimised for each cell line, ~300 cells; **table S3**) was then plated in 40µl droplets of N2B27 in round-bottomed low-adhesion 96-well plates. Counting cells after washing in PBS in this way instead of prior to the washes (as described previously (Baillie-Johnson et al., 2015; van den Brink et al., 2014)) results in the number of cells required for *Gastruloid* formation being ~100 fewer than previously described as fewer are lost during washing. See **table S3** for the number of cells required for each cell line.

In experiments which required the addition of specific factors to *Gastruloids* on the second day of aggregation (24-48h), 20µl medium was carefully removed with a multichannel pipette, and 20µl of N2B27 containing twice the concentration of the required factors was added. This method was preferable to the addition of smaller volumes containing higher concentrations of agonist/antagonists, as the data from these experiments showed more variation between *Gastruloids* (DAT, PB-J, AMA unpublished). Control experiments showed that replacement of half the medium at this stage did not significantly alter the ability of *Gastruloids* to respond to signals on the third day (DAT, PB-J, AMA unpublished). The next day, 150µl fresh N2B27 was added to each of the wells with a multichannel pipette and left for no more than 30 min to wash the *Gastruloids*; a time delay ensured that sample loss was prevented. Following washing, 150µl N2B27 containing the required factors was then applied. The small molecules used in this study and their concentrations are described in **table S4**.

Supplemental Movies

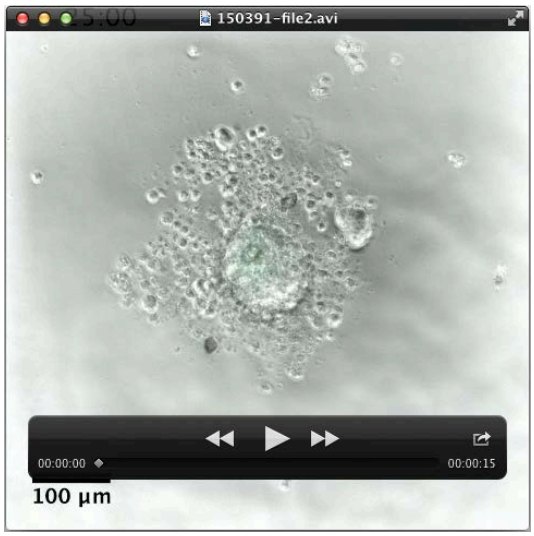

Movie 1. ***T/Bra::GFP expression in Gastruloids following DMSO treatment (48-72h AA).*** Gastruloids made from T/Bra::GFP mESCs stimulated with a mock pulse of DMSO and imaged by wide-field microscopy from 24h to 120h AA every 20 min. The 20x objective was used between 24 and 72h, followed by the 10x objective from 72h to the end of the experiment. Quantification of both the length and fluorescence as a function of time can be seen in **Fig. 3D** (top).

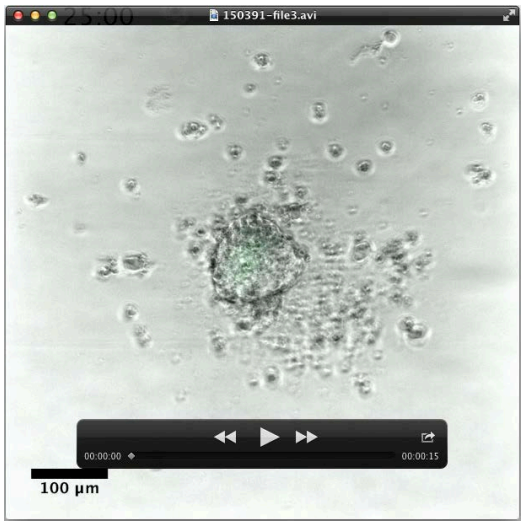

Movie 2. ***T/Bra::GFP expression in Gastruloids following Chi treatment (48-72h AA).*** Gastruloids made from T/Bra::GFP mESCs stimulated with a pulse of Chi and imaged by wide-field microscopy from 24h to 120h AA every 20 min. The 20x objective was used between 24 and 72h, followed by the 10x objective from 72h to the end of the experiment. Quantification of both the length and fluorescence as a function of time can be seen in **Fig. 3D** (bottom).

Supplemental Tables

Tables S1-S5

Table S1. Expression phenotype of T/Bra::GFP mESCs. The proportion of T/Bra::GFP *Gastruloids* not expressing the reporter (No Expression) or displaying either Polarised or Ubiquitous expression at 24, 48 and 72h AA followed by a pulse of DMSO or Chi (72h). The standard deviation is shown in brackets and the number of *Gastruloids* analysed are shown.

	Condition	No Expression	Polarised	Ubiquitous	Spherical	Ovoid	Elongated	*n*
24h	N2B27	26.8 (21.5)	62.5 (16.1)	10.7 (15.2)	100.0 (0.0)	0.0 (0.0)	0.0 (0.0)	112
48h		23.7 (13.2)	74.1 (11.8)	2.2 (3.4)	67.0 (9.4)	33.0 (9.4)	0.0 (0.0)	140
72h	DMSO	3.6 (-)	89.3 (-)	7.1 (-)	10.7 (-)	85.7 (-)	3.6 (-)	28
	Chi	0.0 (-)	91.2 (11.7)	8.8 (11.7)	23.3 (18.2)	52.9 (18.1)	23.8 (26.3)	82

Table S2. Antibodies and their concentrations used for *Gastruloid* immunofluorescence with the associated supplier details.

		Species	Dilution	Cat. Number	Supplier
Primary	Brachyury	Goat	1:200	sc-17743	Santa Cruz Biotechnologies
	CDX2	Rabbit	1:200	MA5-14494	ThermoFisher
	GFP	Chicken	1:2000	A11122	Molecular Probes
	Nanog	Mouse	1:300	14-5761-80	e-Biosciences
	Sox2	Rabbit	1:200	AB5603	Millipore
	Sox17	Goat	1:200	AF1924	R&D Systems
Secondary	Goat-A633	Donkey	1:500	A21082	Molecular Probes
	Mouse-A568	Donkey	1:500	A10037	Molecular Probes
	Rabbit-A488	Donkey	1:500	A21206	Molecular Probes
	Hoechst3342	n/a	1:1000	H3570	Invitrogen (ThermoFisher)

Table S3. Cell lines used and numbers of cells required for *Gastruloid* culture. The average diameter of the *Gastruloids* at 48h AA is indicated with the standard deviation and the number of *Gastruloids* measured. ND: not determined.

Cell line	Reference	Cells/40µl	48h diameter (µm)
AR8::mCherry	(Serup et al., 2012)	450	182.7 ±17.3 (*n* = 83)
T/Bra::GFP	(Fehling et al., 2003)	300	161.0 ±26.2 (*n* = 222)
miR-290-mCherry/mir-302-eGFP (DRC)	(Parchem et al., 2014)	300-400	N.D.
GATA6::H2B-Venus	(Freyer et al., 2015)	300	154.2 ± (*n* = 10)
IBRE4-TA-Cerulean	(Serup et al., 2012)	300	152.6 ±12.2 (*n* = 39)
Nodal::YFP	(Papanayotou et al., 2014)	400	138.7 ±16.1 (*n* = 124)
Nodal$^{-/-}$ (FC-15)	(Camus et al., 2006)	300	181.6 ±23.7 (*n* = 251)
Sox17::GFP	(Niakan et al., 2010)	400	N.D.
TCF/LEF::mCherry (TLC2)	(Faunes et al., 2013; Ferrer-Vaquer et al., 2010)	200-300	194.9 ±20.7 (n = 56)

Table S4. Concentrations of Small molecules and recombinant proteins used in this study, and the associated supplier details.

	Reference	[Working]	[Stock]	Cat. Number	Supplier
CHIR99201	(Ring et al., 2003)	3µM	10mM	4423	Tocris
DMH1	(Neely et al., 2012)	500nM	5mM	HY-12273	MedChem Express
IWP2	(Chen et al., 2009)	1µM	5mM	04-0034	Stemgent
SB431542	(Inman et al., 2002)	10µM	100mM	1614	Tocris
XAV939	(Huang et al., 2009)	1µM	10mM	HY-15147	MedChem Express
BMP4	-	1ng/ml	100µg/ml	314-BP	R&D Systems
DKK	-	200ng/ml	100µg/ml	5897-DK	
Nodal	-	1µg/ml	50µg/ml	1315-ND-025	
Wnt3a	-	100ng/ml	40µg/ml	1324-WN-002	

Table S5. Primer Sequences used for qRT-PCR.

Gene	Forward sequence	Reverse sequence
Axin2	CTAGACTACGGCCATCAGGAA	GCTGGCAGACAGGACATACA
Bmp4	CTCAAGGGAGTGGAGATTGG	ATGCTTGGGACTACGTTTGG
CDX2	TCCTGCTGACTGCTTTCTGA	CCCTTCCTGATTTGTGGAGA
Cer1	GGAAACGCCATAAGTCTCCA	AGGGTCAGAATTTGCCATTG
Chordin	GTGCCTCTGCTCTGCTTCTT	AGGAGTTCGCATGGATATGG
Cripto	CTGTCTGCCATAGCCTGAGTT	TACCTGCCTTTGCCTGATTT
Dab2	AAGCCACAATCATGGACAAA	CACAACTTGGCAGGAACAAA
Dkk1	CCATTCTGGCCAACTCTTTC	CATTCCCTCCCTTCCAATAAC
Fgf4	GGCCACTCCACAGAGATAGG	ACTTGGGCTCAAGCAGTAGG
Fgf5	GCTCAATGATCAGAAGGAGGA	TCAGCTGGTCTTGAATGAGG
Fgf8	AGGACTGCGTATTCACAGAGAT	CATGTACCAGCCCTCGTACT
Furin	CTTCAGCTTGGATCACTTGG	TTAGAAAGGGCTTGGTGGTG
Lefty1	AGGGTGCAGACCTGTAGCTG	GGAAGCAAAGAGCACACACA
LRP2	CTGTATGTCCCGGCTCTTCT	CACCCTTCCATTCATTCGTT
Nodal	AGCCACTGTCCAGTTCTCCAG	GTGTCTGCCAAGCATACATCTC
ppia	TTACCCATCAAACCATTCCTTCTG	AACCCAAAGAACTTCAGTGAGAGC
SPRY4	ATGGTGGATGTCGATCCTGT	GGAGGGGGAGCTACAGAGAC
T/Bra	CTGGGAGCTCAGTTCTTTCG	GTCCACGAGGCTATGAGGAG
Wnt3	CTAATGCTGGCTTGACGAGG	ACATGGTAGAGAGTGCAGGC
Wnt3a	CATACAGGAGTGTGCCTGGA	AATCCAGTGGTGGGTGGATA

Supplementary Figures

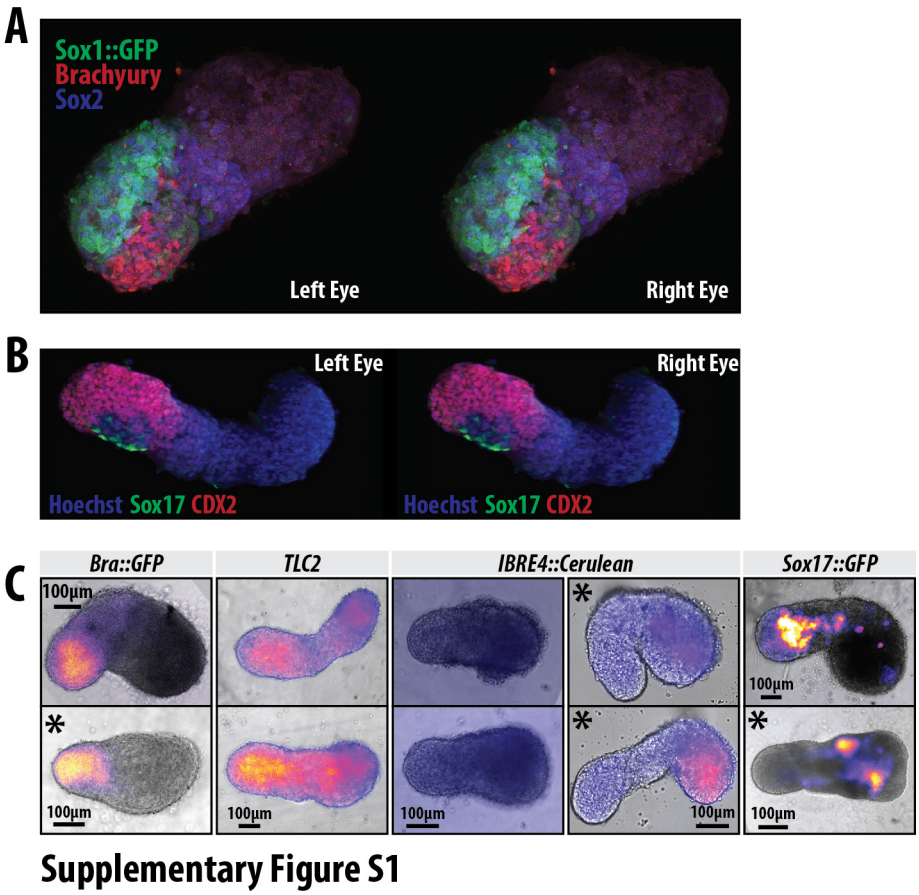

Supplementary Figure S1

Fig. S1. ***Expression of axial markers in Gastruloids.*** (**A,B**) Stereo images of *Gastruloids* from Nodal::YFP (**A**) and Sox1::GFP (**B**) mESCs stained for anti YFP (green) and either CDX2 (**A**) or T/Bra (**B**) (red) at 120h AA. (**C**) Further examples of *Gastruloids* from the indicated cell lines at 120h AA (see **Fig. 1C-F**). Asterisks represent *Gastruloids* from a different replicate experiment.

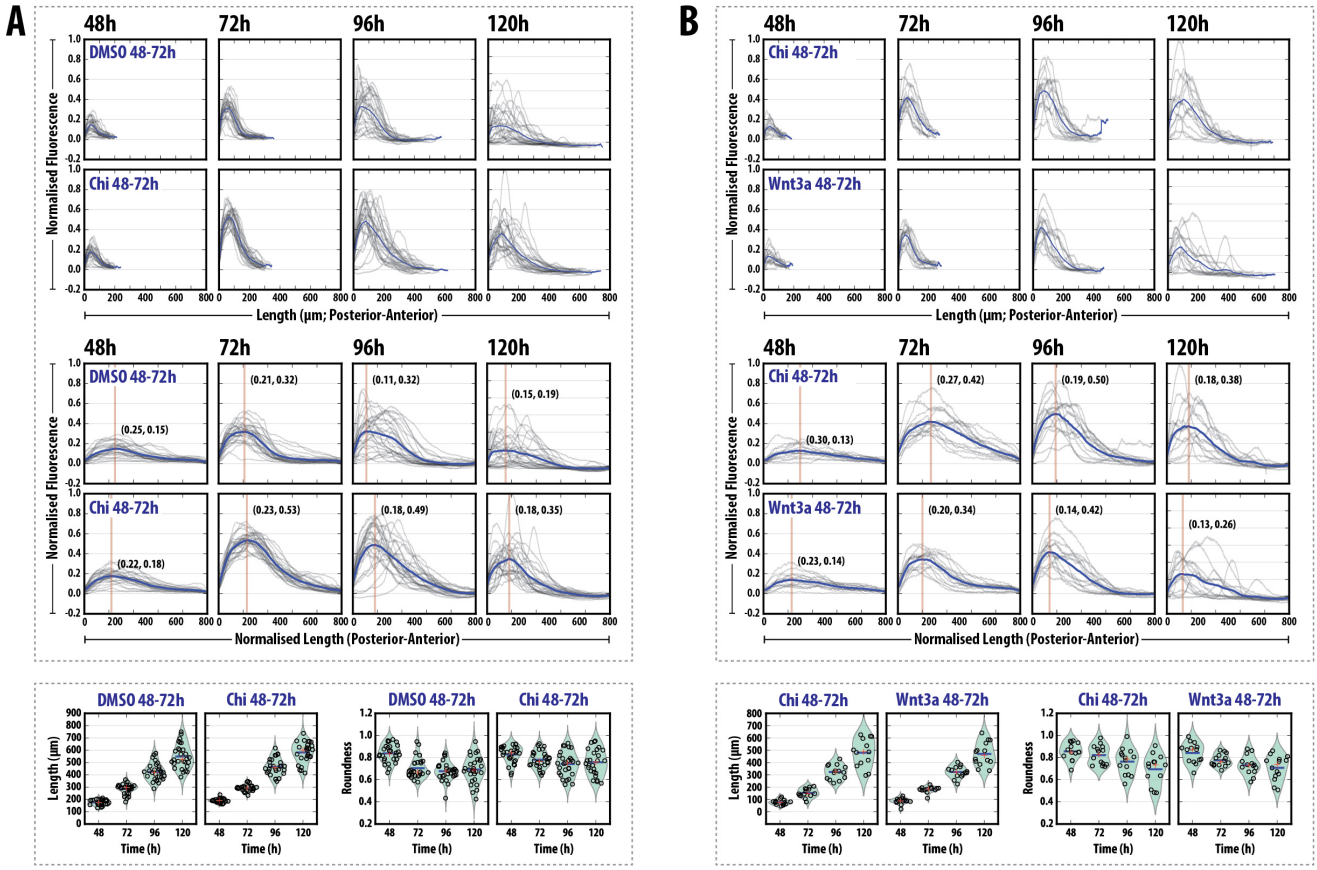

Supplementary Figure S2

Fig. S2. ***Quantification of T/Bra::GFP Gastruloid Fluorescence***. (**A,B**) Expression of the T/Bra::GFP reporter at the indicated time-points (DMSO or Chi (**A**) and Chi or Wnt3a (**B**) stimulation) prior to length normalisation (top) and following normalisation of the length to from 0 to 1 (middle). The bottom panel in each shows the length and roundness of the *Gastruloids* in the indicated conditions.

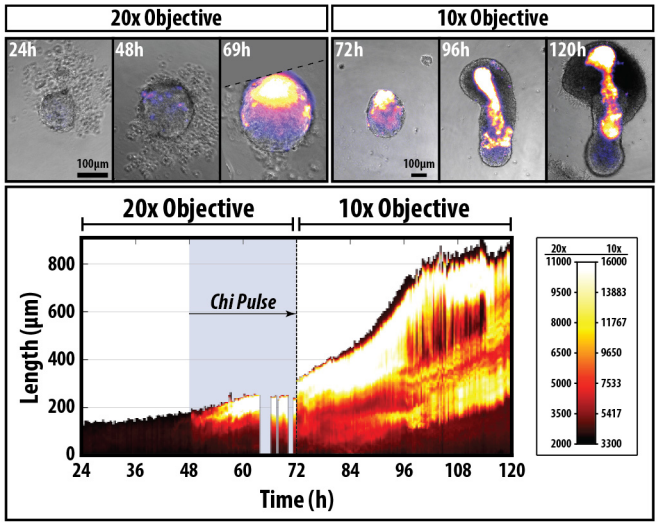

Supplementary Figure S3

Fig. S3. ***Sox17::GFP is expressed anterior to the elongating region of the Gastruloids at 120h AA*****.** *Gastruloids* made from Sox17::GFP mESCs were grown in standard conditions (see materials and methods), pulsed with Chi between 48 and 72h AA and imaged by widefield microscopy continuously for 96h with a time-interval of 20 min. Top row displays still images from the time-lapse experiment using the 20x objective (24h, 48h, 69h) and the 10x objective (72, 96, 120h; *n* = 21). Quantification of the length and fluorescence along the 'mid-line' of the *Gastruloid* every 20 min (bottom row; see materials and methods in main text and supplemental for explanation of quantification). Colour map represents the fluorescence and the time of Chi addition indicated. Gaps in the quantification are due to the *Gastruloid* leaving the field of view, an example of which is indicated at the 69h time-point (top row) with the hashed line representing the edge of the field of view. The posterior of the *Gastruloid* is orientated towards the base of the figures, as time-lapse imaging revealed the Sox17::GFP negative region was absent from the elongating, posterior region. Scale bar indicates 100µm in all images.

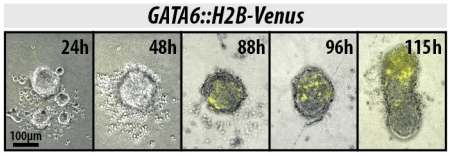

Supplementary Figure S4

Fig. S4. ***Expression of GATA6::H2BVenus in Gastruloids over time.*** *Gastruloids* made from GATA6::H2B-Venus mESCs were grown in standard conditions and imaged by widefield microscopy continuously for 115h with a time-interval of 20 min (*n* = 9). GATA6 expression is apparent at approximately 88h AA and becomes restricted to the anterior region of the *Gastruloid* (as judged by morphology).

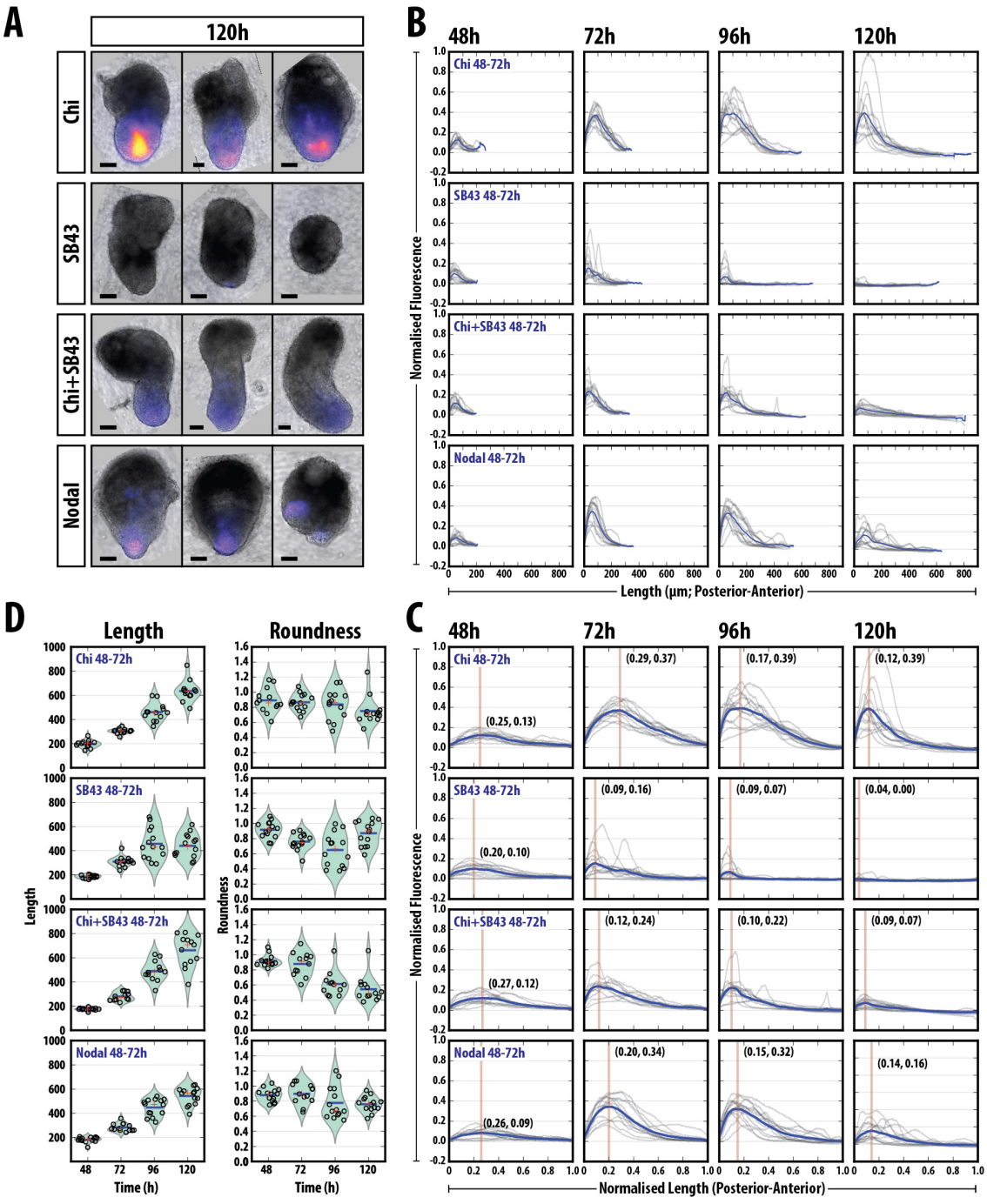

Supplementary Figure S5

Fig. S5. ***Quantifying the Effect of modulating Nodal signalling in Gastruloids (#1).*** (**A**) examples of T/Bra::GFP reporter expression in *Gastruloids* treated as indicated. (**B, C, D**) Quantification of the reporter expression at the indicated time-points prior to length normalisation (**B**) and following normalisation of the length from 0 and 1 (**C**). The length and roundness of the Gastruloids in the indicated conditions (**D**). (**E**) Statistical analysis of the normalised fluorescence traces showing (**upper panel**) the *normalised root square distance* as a measure of the heterogeneity within each condition of the *Gastruloids* in the indicated conditions (see supplemental materials and methods), and (**lower panel**) the *significance matrix* showing the pairwise *p* values between individual treatments per time-point. Significance determined by non-paired Student's t-test; *p*-values highlighted in red indicate $p < 0.05$. Vertical line and coordinates in **C** correspond to the location and position of the peak maximum. Scale bar indicates 100 µm.

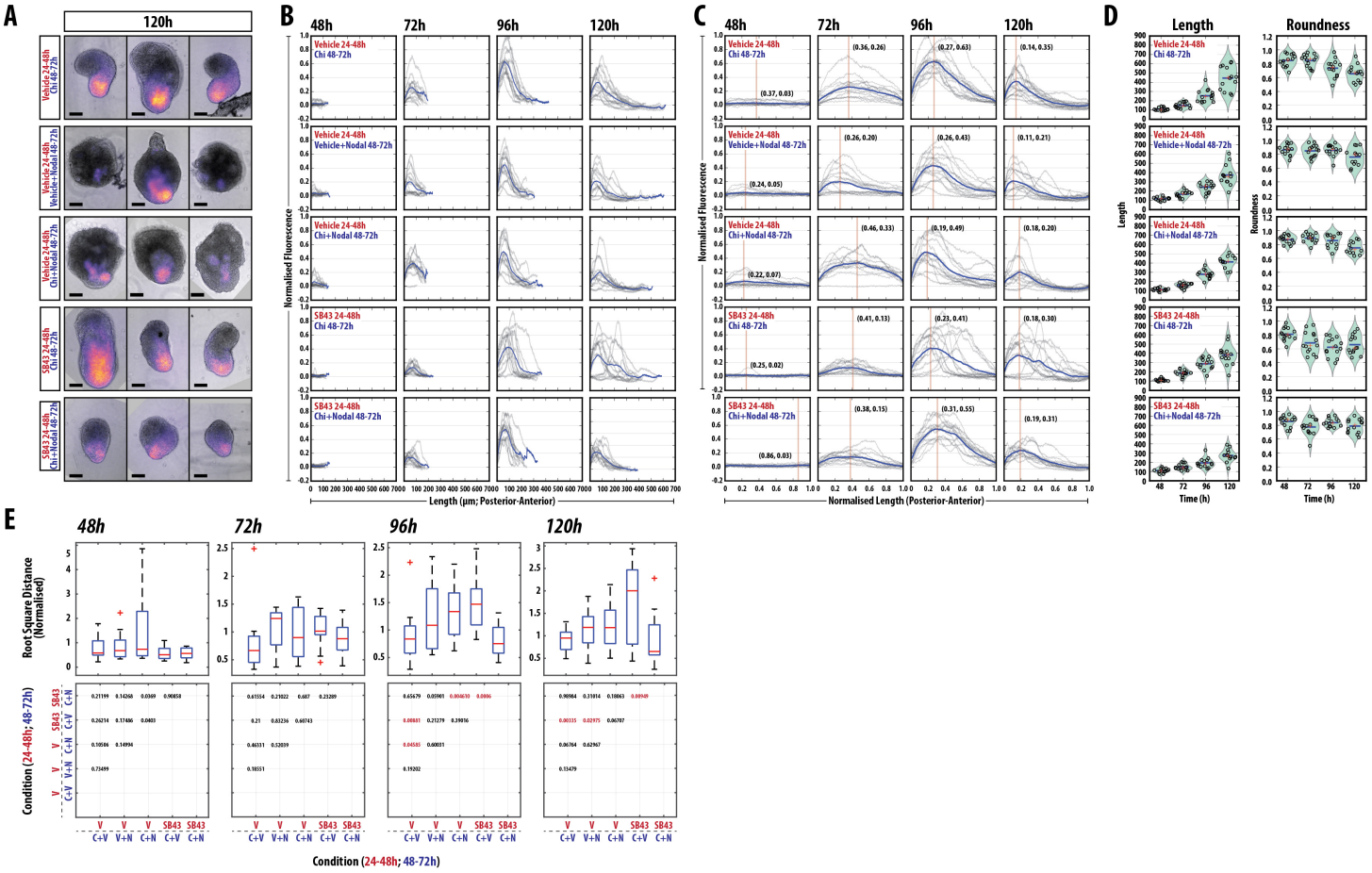

Supplementary Figure S6

Fig. S6. ***Quantifying the Effect of modulating Nodal signalling in Gastruloids (#2).*** (**A**) examples of T/Bra::GFP reporter expression in *Gastruloids* treated as indicated. (**B, C, D**) Quantification of the reporter expression prior to length normalisation (**B**) and following normalisation of the length from 0 and 1 (**C**). The length and roundness of the Gastruloids in the indicated conditions (**D**). (**E**) Statistical analysis of the normalised fluorescence traces showing (**upper panel**) the *normalised root square distance* as a measure of the heterogeneity within each condition of the *Gastruloids* in the indicated conditions (see supplemental materials and methods), and (**lower panel**) the *significance matrix* showing the pairwise *p* values between individual treatments per time-point. Significance determined by non-paired Student's t-test; *p*-values highlighted in red indicate $p < 0.05$. Vertical line and coordinates in C correspond to the location and position of the peak maximum. Scale bar indicates 100 µm.

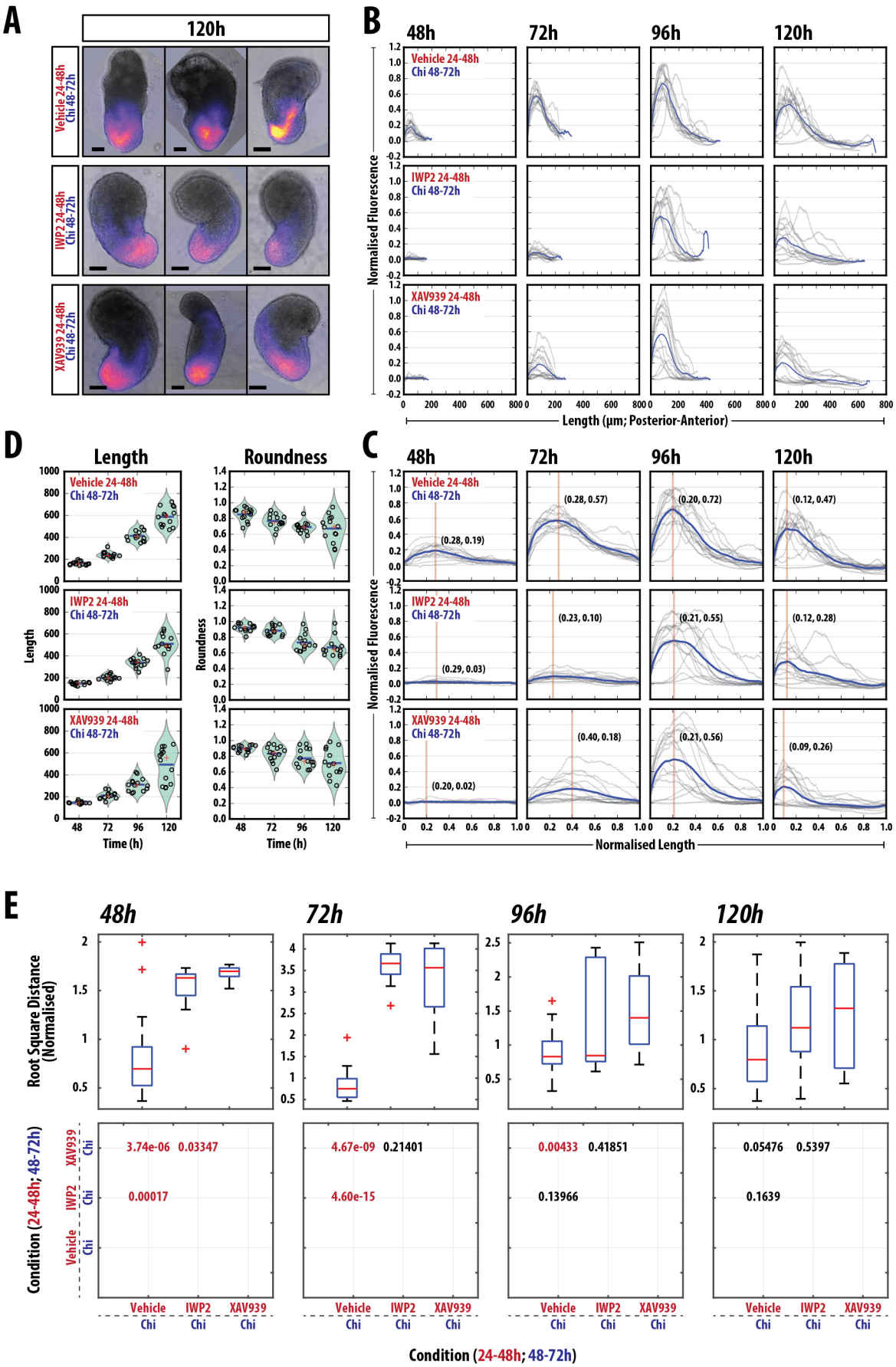

Supplementary Figure S7

Fig. S7. ***Quantifying the Effect of modulating Wnt/β-Catenin signalling in Gastruloids (#1).*** (**A**) examples of T/Bra::GFP reporter expression in *Gastruloids* treated as indicated. (**B, C, D**) Quantification of the reporter expression prior to length normalisation (**B**) and following normalisation of the length from 0 and 1 (**C**). The length and roundness of the Gastruloids in the indicated conditions (**D**). (**E**) Statistical analysis of the normalised fluorescence traces showing (**upper panel**) the *normalised root square distance* as a measure of the heterogeneity within each condition of the *Gastruloids* in the indicated conditions (see supplemental materials and methods), and (**lower panel**) the *significance matrix* showing the pairwise *p* values between individual treatments per time-point. Significance determined by non-paired Student's t-test; *p*-values highlighted in red indicate $p < 0.05$. Vertical line and coordinates in C correspond to the location and position of the peak maximum. Scale bar indicates 100 µm.

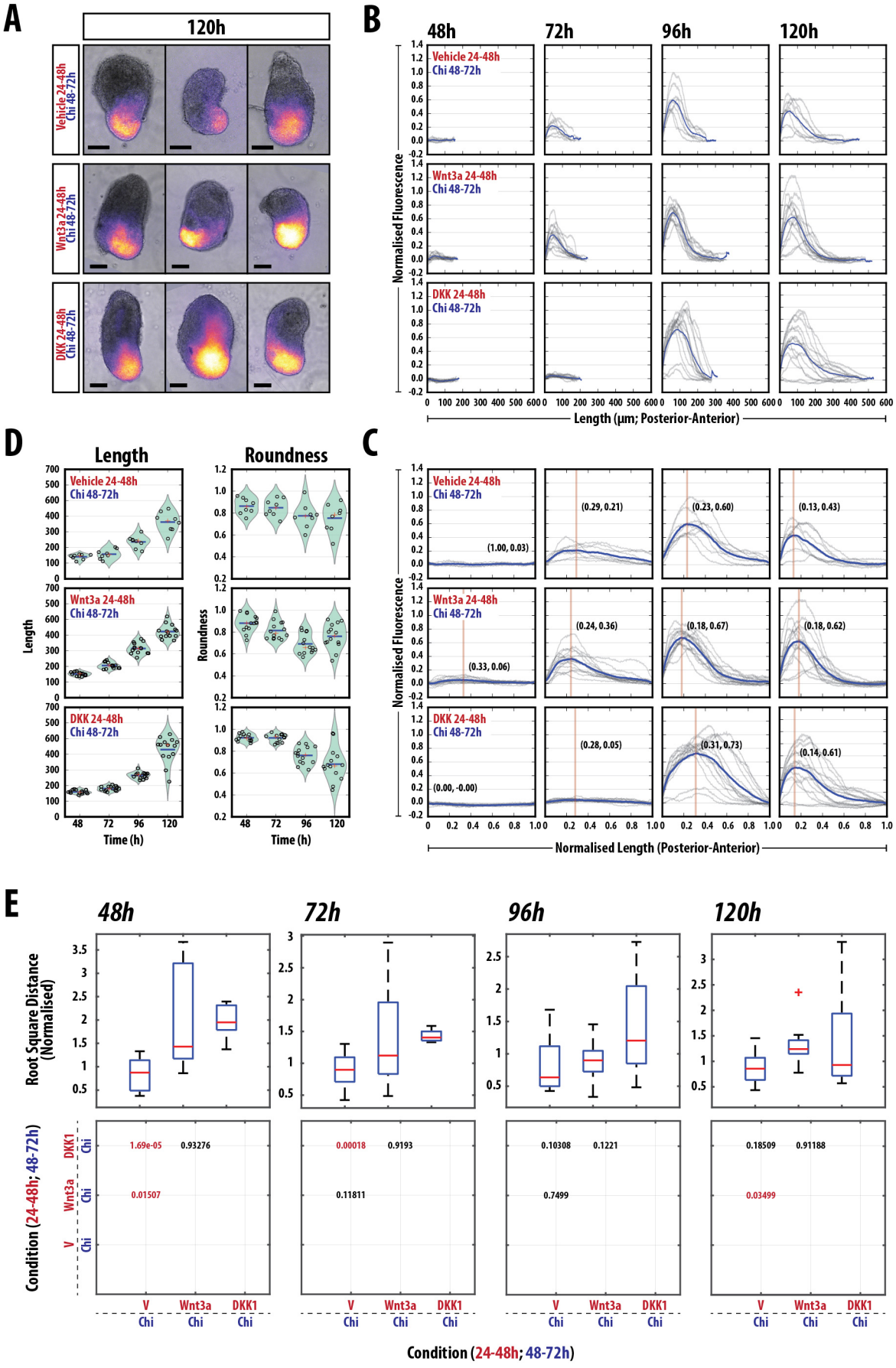

Supplementary Figure S8

Fig. S8. ***Quantifying the Effect of modulating Wnt/β-Catenin signalling in Gastruloids (#2).*** (**A**) examples of T/Bra::GFP reporter expression in *Gastruloids* treated as indicated. (**B, C, D**) Quantification of the reporter expression prior to length normalisation (**B**) and following normalisation of the length from 0 and 1 (**C**). The length and roundness of the Gastruloids in the indicated conditions (**D**). (**E**) Statistical analysis of the normalised fluorescence traces showing (**upper panel**) the *normalised root square distance* as a measure of the heterogeneity within each condition of the *Gastruloids* in the indicated conditions (see supplemental materials and methods), and (**lower panel**) the *significance matrix* showing the pairwise *p* values between individual treatments per time-point. Significance determined by non-paired Student's t-test; *p*-values highlighted in red indicate $p < 0.05$. Vertical line and coordinates in C correspond to the location and position of the peak maximum. Scale bar indicates 100 µm.

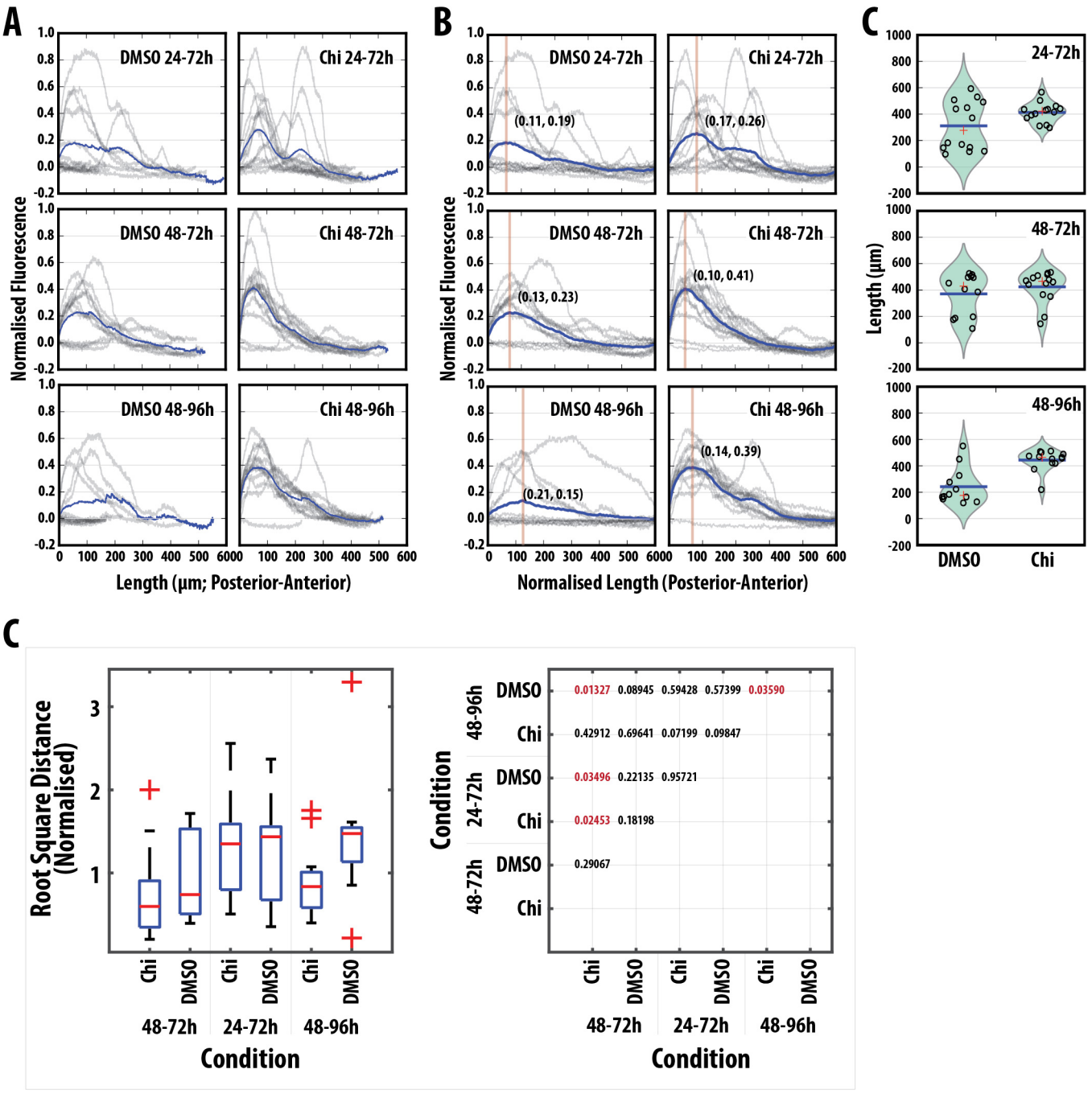

Supplementary Figure S9

Fig. S9. ***Quantifying the Effect of modulating the time of Wnt/β-Catenin signalling in Gastruloids.*** (**A,B**) Quantification of the reporter expression prior to length normalisation (**A**) and following normalisation of the length from 0 and 1 (**B**). The length and roundness of the Gastruloids in the indicated conditions (**C**). (**D**) Statistical analysis of the normalised fluorescence traces showing (**upper panel**) the *normalised root square distance* as a measure of the heterogeneity within each condition of the *Gastruloids* in the indicated conditions (see supplemental materials and methods), and (**lower panel**) the *significance matrix* showing the pairwise *p* values between individual treatments per time-point. Significance determined by non-paired Student's t-test; *p*-values highlighted in red indicate $p < 0.05$. Vertical line and coordinates in **B** correspond to the location and position of the peak maximum.

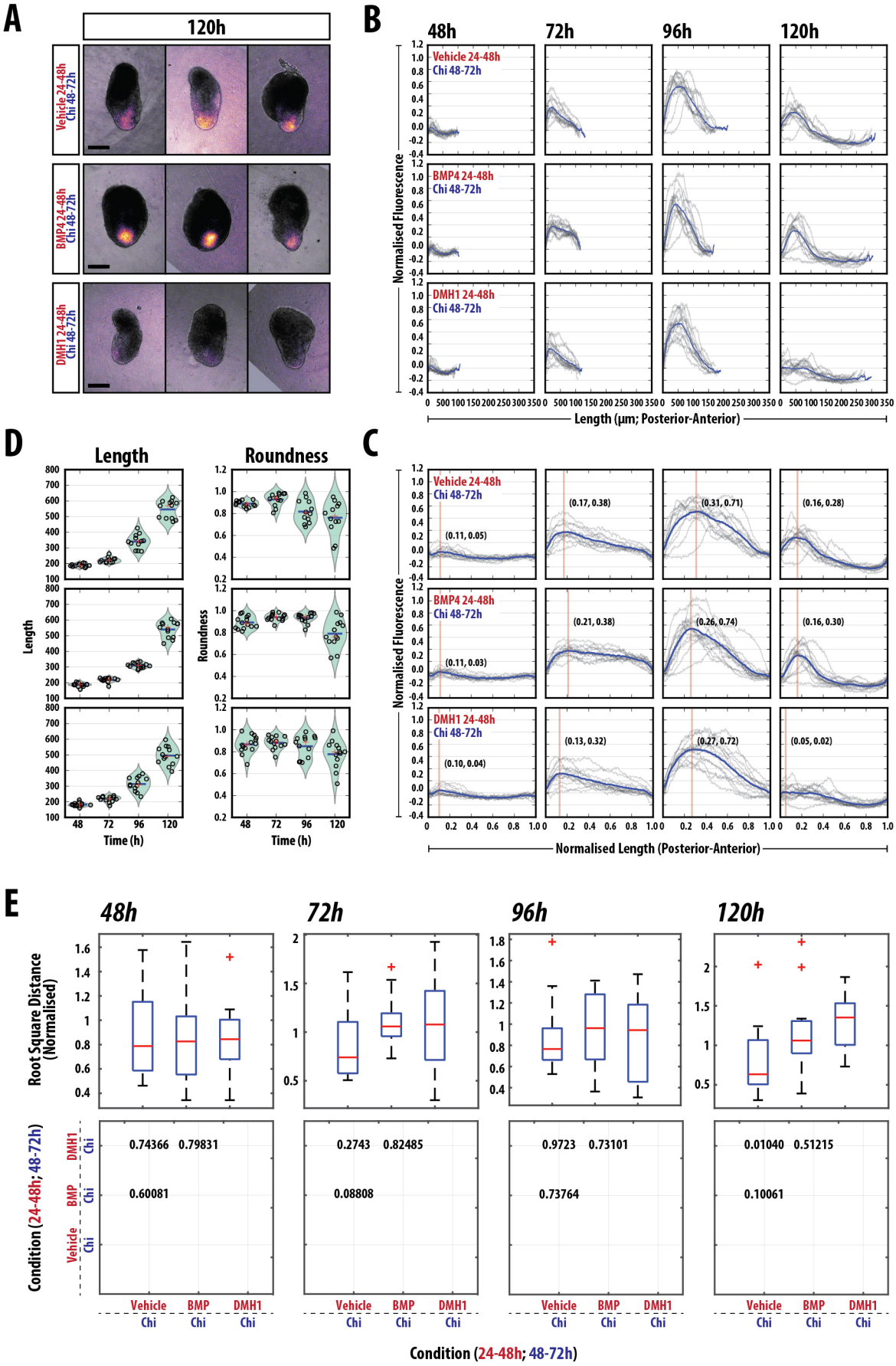

Supplementary Figure S10

Fig. S10. ***Quantifying the Effect of modulating BMP signalling in Gastruloids.*** (**A**) examples of T/Bra::GFP reporter expression in *Gastruloids* treated as indicated. (**B, C, D**) Quantification of the reporter expression prior to length normalisation (**B**) and following normalisation of the length from 0 and 1 (**C**). The length and roundness of the Gastruloids in the indicated conditions (**D**). (**E**) Statistical analysis of the normalised fluorescence traces showing (**upper panel**) the *normalised root square distance* as a measure of the heterogeneity within each condition of the *Gastruloids* in the indicated conditions (see supplemental materials and methods), and (**lower panel**) the *significance matrix* showing pairwise *p* values between individual treatments per time-point. Significance determined by non-paired Student's t-test; *p*-values highlighted in red indicate $p < 0.05$. Vertical line and coordinates in C correspond to the location and position of the peak maximum. Scale bar indicates 100 μm.

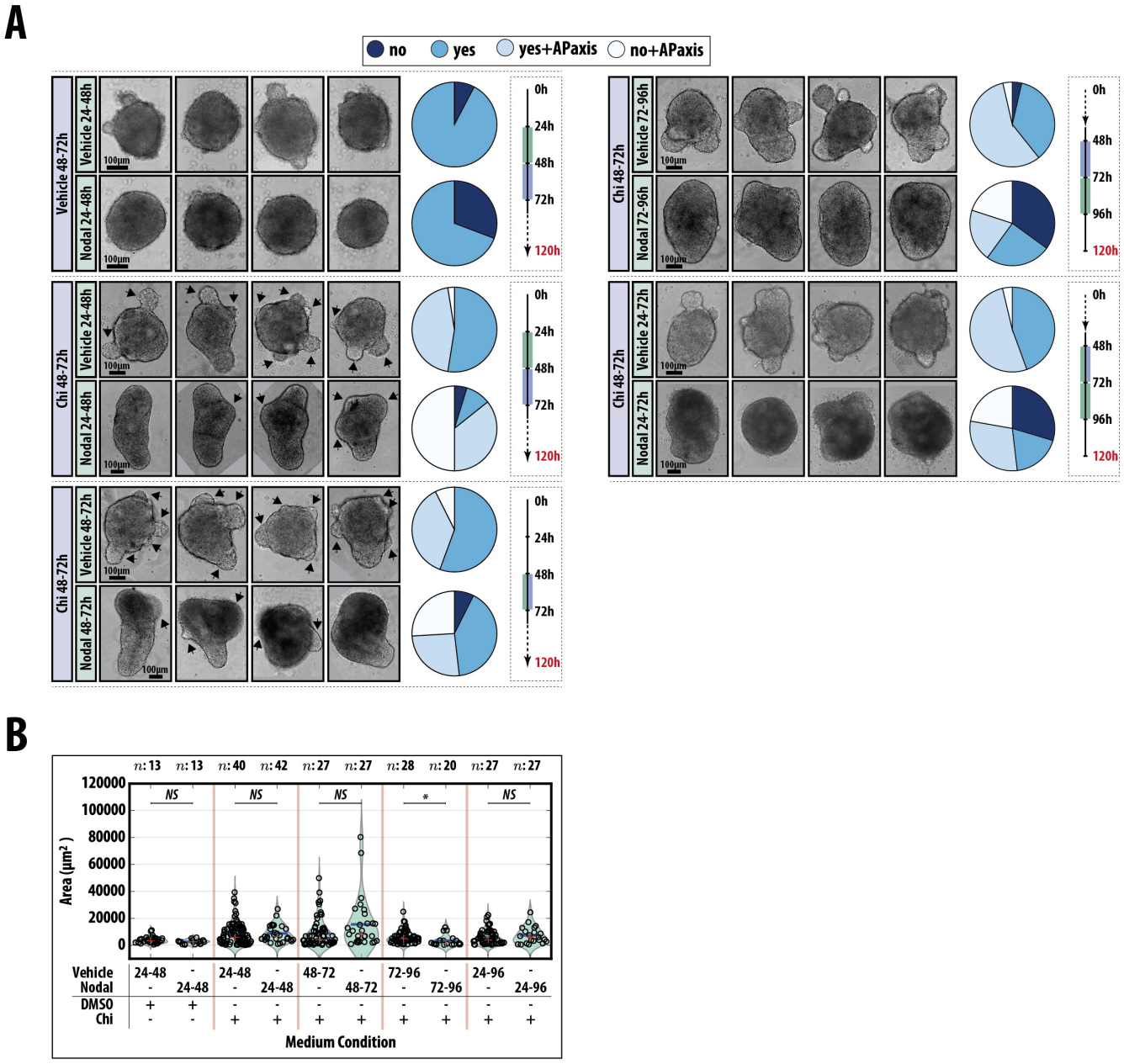

Supplementary Figure S11

Fig. S11. ***Modulation of Nodal signalling in Nodal mutants***. (**A**) Examples of *Gastruloids* treated with Chi between 48 and 72h with a 24h pulse of either vehicle or Nodal at the indicated time-points (24-48h, 48-72h, 72-96h and 24-72h AA). Pie charts indicated the proportion which do not show protrusions ('no'), show protrusions ('yes'), show protrusions with a defined AP axis ('yes+APaxis') or don't show protrusions but still have a defined AP axis ('no+APaxis'). The schematic for the time-course is indicated on the right of the panel. (**B**) Quantification of the area of the protrusions in the indicated experimental conditions. Significance determined following Mann-Whitney U test followed by Bonferroni adjustment, comparing selected columns. Asterisk indicates $p < 0.05$.

References from Supplemental Material

Baillie-Johnson, P., van den Brink, S. C., Balayo, T., Turner, D. A. and Martinez Arias, A. (2015). Generation of Aggregates of Mouse Embryonic Stem Cells that Show Symmetry Breaking, Polarization and Emergent Collective Behaviour In Vitro. *J Vis Exp*.

Camus, A., Perea-Gomez, A., Moreau, A. and Collignon, J. (2006). Absence of Nodal signaling promotes precocious neural differentiation in the mouse embryo. *Developmental Biology* **295**, 743–755.

Chen, B., Dodge, M. E., Tang, W., Lu, J., Ma, Z., Fan, C.-W., Wei, S., Hao, W., Kilgore, J., Williams, N. S., et al. (2009). Small molecule–mediated disruption of Wnt-dependent signaling in tissue regeneration and cancer. *Nat Chem Biol* **5**, 100–107.

Faunes, F., Hayward, P., Descalzo, S. M., Chatterjee, S. S., Balayo, T., Trott, J., Christoforou, A., Ferrer-Vaquer, A., Hadjantonakis, A.-K., Dasgupta, R., et al. (2013). A membrane-associated β-catenin/Oct4 complex correlates with ground-state pluripotency in mouse embryonic stem cells. *Development* **140**, 1171–1183.

Fehling, H. J., Lacaud, G., Kubo, A., Kennedy, M., Robertson, S., Keller, G. and Kouskoff, V. (2003). Tracking mesoderm induction and its specification to the hemangioblast during embryonic stem cell differentiation. *Development* **130**, 4217–4227.

Ferrer-Vaquer, A., Piliszek, A., Tian, G., Aho, R. J., Dufort, D. and Hadjantonakis, A.-K. (2010). A sensitive and bright single-cell resolution live imaging reporter of Wnt/ß-catenin signaling in the mouse. *BMC Dev Biol* **10**, 121.

Freyer, L., Schröter, C., Saiz, N., Schrode, N., Nowotschin, S., Martinez Arias, A. and Hadjantonakis, A.-K. (2015). A loss-of-function and H2B-Venus transcriptional reporter allele for Gata6 in mice. *BMC Dev Biol* **15**, 38.

Fulton, C., Perktold, J., Seabold, S., Gommers, R., Arel-Bundock, V. and McKinney, W. (2014). Statsmodels. BSD.

Huang, S.-M. A., Mishina, Y. M., Liu, S., Cheung, A., Stegmeier, F., Michaud, G. A., Charlat, O., Wiellette, E., Zhang, Y., Wiessner, S., et al. (2009). Tankyrase inhibition stabilizes axin and antagonizes Wnt signalling. *Nature* **461**, 614–620.

Hunter, J. D. (2007). Matplotlib: A 2D Graphics Environment. *Comput. Sci. Eng.* **9**, 90–95.

Inman, G. J., Nicolás, F. J., Callahan, J. F., Harling, J. D., Gaster, L. M., Reith, A. D., Laping, N. J. and Hill, C. S. (2002). SB-431542 is a potent and specific inhibitor of transforming growth factor-beta superfamily type I activin receptor-like kinase (ALK) receptors ALK4, ALK5, and ALK7. *Mol. Pharmacol.* **62**, 65–74.

Kluyver, T., Ragan-Kelley, B., Pérez, F., Granger, B., Bussonnier, M., Frederic, J., Kelley, K., Hamrick, J., Grout, J., Corlay, S., et al. (2016). *Jupyter Notebooks—a publishing format for reproducible computational workflows*. (eds. Loizides, F. and Schmidt, C. Positioning and Power in Academic Publishing: Players, Agents and Agendas.

McDougall, D., Firing, E., Perez, F., Thomas, I., Ivanov, P., Nielsen, J. H., Seppänen, J. K., Kniazev,

N., Droettboom, M., Fitzpatrick, M., et al. (2016). Matplotlib.

Neely, M. D., Litt, M. J., Tidball, A. M., Li, G. G., Aboud, A. A., Hopkins, C. R., Chamberlin, R., Hong, C. C., Ess, K. C. and Bowman, A. B. (2012). DMH1, a highly selective small molecule BMP inhibitor promotes neurogenesis of hiPSCs: comparison of PAX6 and SOX1 expression during neural induction. *ACS Chem Neurosci* **3**, 482–491.

Niakan, K. K., Ji, H., Eggan, K.12 (2010). Sox17 promotes differentiation in mouse embryonic stem cells by directly regulating extraembryonic gene expression and indirectly antagonizing self-renewal. *Genes & Development* **24**, 312–326.

Oliphant, T. E. (2007). Python for Scientific Computing. *Comput. Sci. Eng.* **9**, 10–20.

Papanayotou, C., Benhaddou, A., Camus, A., Perea-Gomez, A., Jouneau, A., Mezger, V., Langa, F., Ott, S., Sabéran-Djoneidi, D. and Collignon, J. (2014). A novel nodal enhancer dependent on pluripotency factors and smad2/3 signaling conditions a regulatory switch during epiblast maturation. *Plos Biol* **12**, e1001890.

Parchem, R. J., Ye, J., Judson, R. L., LaRussa, M. F., Krishnakumar, R., Blelloch, A., Oldham, M. C. and Blelloch, R. (2014). Two miRNA clusters reveal alternative paths in late-stage reprogramming. *Cell Stem Cell* **14**, 617–631.

Perez, F. and Granger, B. E. (2007). IPython: A System for Interactive Scientific Computing. *Comput. Sci. Eng.* **9**, 21–29.

Preibisch, S., Saalfeld, S. and Tomancak, P. (2009). Globally optimal stitching of tiled 3D microscopic image acquisitions. *Bioinformatics* **25**, 1463–1465.

Ring, D. B., Johnson, K. W., Henriksen, E. J., Nuss, J. M., Goff, D., Kinnick, T. R., Ma, S. T., Reeder, J. W., Samuels, I., Slabiak, T., et al. (2003). Selective Glycogen Synthase Kinase 3 Inhibitors Potentiate Insulin Activation of Glucose Transport and Utilization In Vitro and In Vivo. *Diabetes* **52**, 588–595.

Schindelin, J., Arganda-Carreras, I., Frise, E., Kaynig, V., Longair, M., Pietzsch, T., Preibisch, S., Rueden, C., Saalfeld, S. and Schmid, B. (2012). Fiji: an open-source platform for biological-image analysis. *Nature Methods* **9**, 676–682.

Serup, P., Gustavsen, C., Klein, T., Potter, L. A., Lin, R., Mullapudi, N., Wandzioch, E., Hines, A., Davis, A., Bruun, C., et al. (2012). Partial promoter substitutions generating transcriptional sentinels of diverse signaling pathways in embryonic stem cells and mice. *Dis Model Mech* **5**, 956–966.

Silvester, S. (2015). Tifffile. BSD.

Soroldoni, D., Jörg, D. J., Morelli, L. G., Richmond, D. L., Schindelin, J., Jülicher, F. and Oates, A. C. (2014). Genetic oscillations. A Doppler effect in embryonic pattern formation. *Science* **345**, 222–225.

Terrel, A. R., Harris, C., Cournapeau, D., Jamie, Wiebe, M., Smith, N. J., Pitrou, A., Virtanen, P., Gommers, R., Kern, R., et al. (2015a). NumPy. BSD.

Terrel, A. R., Harris, C., Cournapeau, D., Laxalde, D., Burovski, E., Moore, E., Pedregosa, F.,

Varoquax, G., Henriksen, I., Jamie, et al. (2015b). SciPy. BSD.

Turner, D. A., Rué, P., Mackenzie, J. P., Davies, E. and Martinez Arias, A. (2014). Brachyury cooperates with Wnt/β-Catenin signalling to elicit Primitive Streak like behaviour in differentiating mouse ES cells. *BMC Biology* **12**, 63.

Van den Bossche, J., Hoyer, S. and McKinney, W. (2015). Pandas. BSD.

van den Brink, S. C., Baillie-Johnson, P., Balayo, T., Hadjantonakis, A.-K., Nowotschin, S., Turner, D. A. and Martinez Arias, A. (2014). Symmetry breaking, germ layer specification and axial organisation in aggregates of mouse embryonic stem cells. *Development* **141**, 4231–4242.